University of South Florida

Digital Commons @ University of South Florida

USF Tampa Graduate Theses and Dissertations

USF Graduate Theses and Dissertations

March 2022

Defining the role of Oxidized Mitochondrial DNA in Myelodysplastic Syndromes

Grace Anne Ward
University of South Florida

Follow this and additional works at: https://digitalcommons.usf.edu/etd

Part of the Cell Biology Commons, Molecular Biology Commons, and the Oncology Commons

Scholar Commons Citation

Defining the role of Oxidized Mitochondrial DNA in Myelodysplastic Syndromes

by

Grace Anne Ward

A dissertation submitted in partial fulfillment
of the requirements for the degree of
Doctor of Philosophy
Department of Cell Biology, Microbiology, and Molecular Biology
College of Arts and Sciences
University of South Florida

Major Professor: Kenneth Wright, Ph.D.
John Cleveland, Ph.D.
Eric Padron, M.D.
Eric Lau. Ph.D.
Guillermo Garcia-Manero, M.D.

Date of Approval:
February 8, 2022

Keywords: DAMP, inflammasome, pyroptosis, Toll-like Receptor 9, bone marrow failure, caspase-1

Dedication

To my husband: Mike Steel. To my family and friends: Cindy, Dan, Kyle Ward. Ali Turk,

Sara and Chelsea Carle, Natalia Sumi, Erinn Sonntag, Grant Joslin, and Dr. Leigh Ruth.

Acknowledgments

This work was done during a lab shut down, a change in advisors, and a global pandemic; this dissertation would not have been possible without the amazing support of my colleagues. Dr. Alan List laid the foundation for the research and continued to be a supportive mentor even when his own career was uncertain; I am proud to have worked in your lab.

Thank you to my committee members, Dr. Eric Padron, Dr. Eric Lau, and Dr. John Cleveland. I appreciate all your insight, guidance, and support during this journey. Dr. Ken Wright for being my academic mentor and for taking me in. To Dr. Guillermo Garcia-Manero, I am honored with the chance to learn from a leader in MDS, and a distinguished physician/scientist. I am appreciative of your welcoming and kind nature.

Dr. Erika Eksioglu who welcomed me and my projects and helped me grow during a difficult time. Drs. Nicole Vincelette and Seongseok Yun who have always cared for me as a person and a scientist. Amy McLemore has taught me to look for the beauty in your surroundings and that happiness is not a given, but a goal that we must strive for with gratitude and positivity. Ben Meyer, my buddy, who always believed me and helped me feel less alone which is the most wonderful gift a grad student can receive. Alexandra Calescibetta, 'Ann Alex you perfect sunflower', you make every group of misfits feel like the coolest team. Robert "Trey" Dalton, a kindred anxious spirit. Nghi Lam, a lovely friend a nerd. Alexis Onimus, who appreciates my sarcasm and dark

humor. Amy Aldrich, forever thoughtful and kind. Hsin-An "Richard" Hou, thank you for bringing such positivity and energy to every situation.

Table of Contents

List of Figures

List of Tables

Abstract

Myelodysplastic Syndromes (MDS) are heterogeneous bone marrow (BM) failure malignancies characterized by constitutive innate immune activation, NLRP3 inflammasome (IFM) driven pyroptotic cell death, and the induction of interferon-stimulated genes (ISG). MDS often diagnostically resembles other hematologic disorders, as such, additional tools are needed for the discrimination from overlapping disorders. We observed that oxidized mitochondrial DNA (ox-mtDNA) is released upon cytolysis. We hypothesize that levels of ox-mtDNA are high in MDS, allowing us to use it as a diagnostic biomarker; and that cell free ox-mtDNA is contributing to feedforward BM failure.

ROC/AUC analysis demonstrated that ox-mtDNA is a sensitive and specific biomarker for MDS compared to healthy donors (AUC=0.964), and other hematological malignancies excluding CLL (AUC=0.893). Ox-mtDNA positively and significantly correlated with levels of known alarmins S100A9, S100A8, and ASC specks demonstrating utility as a biomarker for the magnitude of medullary pyroptosis in MDS.

Toll-like receptor 9 (TLR9) is an endosomal, DNA sensing pattern recognition receptor that activates the IFM and ISG response through MyDDosome signaling. We found that MDS hematopoietic stem cells have increased TLR9 cell surface expression, which is induced by exposure to ox-mtDNA. We observed ox-mtDNA treatment phenocopies MDS via caspase-1 and IL-1β cleavage, ASC specks, LDH release, and activation of ISGs. We next assessed whether IFM activation by ox-mtDNA is TLR9-

dependent and found that TLR9-KO cells were no longer responsive to ox-mtDNA while TLR9 overexpression induced sensitization to ox-mtDNA. We evaluated the impact of ox-mtDNA on hematopoietic colony forming capacity (CFC) and found that normal BM CFC was diminished by ox-mtDNA and rescued by TLR9 lentiviral knockdown. Upon chemical inhibition of the TLR9 pathway, including a competitive TLR9-IgG sponge, we observed significantly decreased inflammasome and restored CFC of MDS primary samples.

We conclude that MDS BM cells have TLR9 on the plasma membrane which primes them for response to ox-mtDNA released by neighboring pyroptotic cells. Our research shows that ox-mtDNA is a novel alarmin that activated the IFM via TLR9 and provides an index of pyroptosis in MDS. Blocking TLR9 activation may provide a novel therapeutic strategy for MDS and suppression of inflammatory BM failure.

Chapter 1: Myelodysplastic Syndromes

Introduction to MDS

Myelodysplastic Syndromes (MDS) are a group of chronic malignant failure diseases and one of the major types of acquired bone marrow failure. As one of the most common clonal hematological disorders, MDS is characterized by cytopenia and ineffective hematopoiesis leading to frequent need for blood transfusions in lower risk disease and, over time, progression towards Acute Myeloid Leukemia (AML) (Garcia-Manero, Chien, & Montalban-Bravo, 2020). This rare and chronic malignant disease, historically referred to as 'pre-leukemia', is often difficult to diagnose due to low initial symptom burden which can hamper timely and effective treatment. Currently, MDS diagnosis is a composite profile based upon bone marrow biopsy, cytogenetics, blast count, blood smear, and level of cytopenia which makes diagnosis inaccurate as several other hematologic disorders are morphologically similar to MDS (Cogle, 2015). Thus, effective diagnosis requires a high level of pathology expertise, often external laboratory testing, and is inefficient and expensive (Glauser et al., 2013). Better diagnostic tools and novel treatments are imperative not only for MDS patients but also other bone marrow failure syndromes and inflammatory diseases.

Disease characteristics and diagnosis criteria

MDS is characterized by peripheral blood cytopenias and cytologic dysplasia (Mohammad, 2018; Tanaka & Bejar, 2019) with anemia remaining the principal management challenge which presents in approximately 60% of patients with most requiring red blood cell transfusions, a poor prognostic factor associated with shorter overall survival and increased risk of leukemic evolution (Bennett & Overload, 2008). Additionally, long-term transfusion therapy predisposes to iron overload with its attendant complications enhancing the difficulties facing patients' long-term quality of life prospects. The limited number of effective therapeutic options to treat anemia in MDS reflects the limited understanding of the underlying molecular mechanisms contributing to the impairment in erythropoiesis. This can be attributed to the complexity of this disease from its development to its evolution as these spectrum of disorders exhibits clinical heterogeneity reflective of the diversity of underlying molecular genetic drivers. While the cause of MDS is largely unknown, primary MDS is likely the result of somatic genetic alterations accumulated with aging. Seminal work has described the accumulation of genomic damage with age that leads to the development of clonal hematopoiesis of indeterminate potential (CHIP), a precursor of the bone marrow failure in MDS (Jaiswal et al., 2014). Yet since those changes are not specific, and arise from common hematologic precursor disorders, MDS often phenotypically resembles other hematologic disorders such as chronic myelomonocytic leukemia (CMML) (Tanaka & Bejar, 2019) (**Figure 1**). Thus, accurate differentiation of MDS from overlap syndromes is often difficult.

Figure 1: Bone Marrow Failure Overlap Diseases
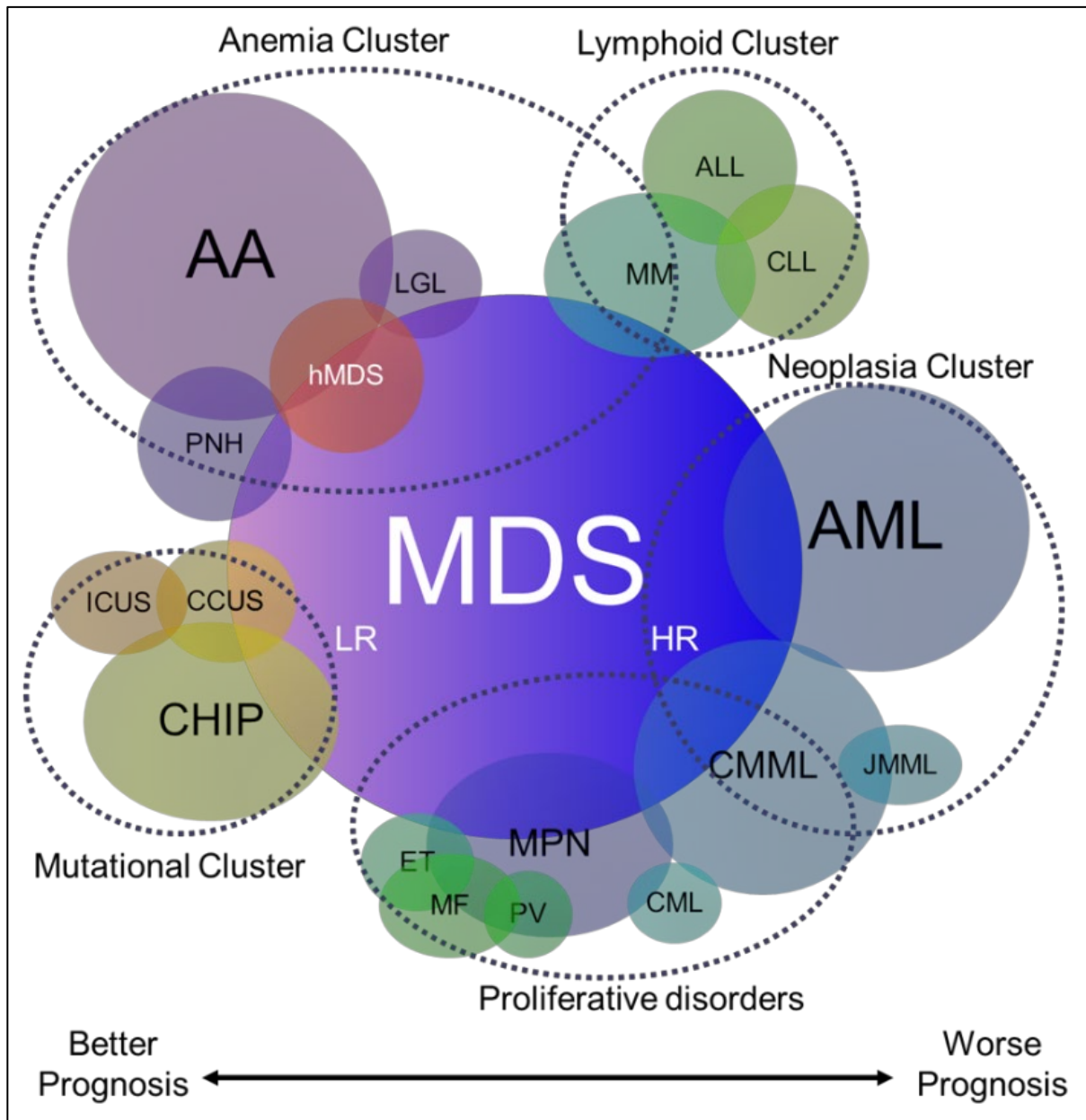
AA, aplastic anemia. **ALL**, acute lymphocytic leukemia. AML, acute myeloid leukemia. **CCUS**, clonal cytopenia of undetermined significance. **CHIP**, clonal hematopoiesis of indeterminate potential. **CLL**, chronic lymphocytic leukemia. **CML**, chronic myelogenous leukemia. **CMML**, chronic myelomonocytic leukemia. **ET**, essential thrombocytosis. **hMDS**, hypocellular/hypoproliferative MDS. **ICUS**, idiopathic cytopenia of undetermined significance. **JMML**, juvenile myelomonocytic leukemia. **LGL**, large granular lymphocytic leukemia. **MDS**, myelodysplastic syndromes. **MM**, multiple myeloma. **MPN**, myeloproliferative neoplasms. **MF**, myelofibrosis. **PNH**, paroxysmal nocturnal hemoglobinuria. **PV**, polycythemia vera

Despite disease heterogeneity in myeloid specific somatic driver gene mutations, in the pathobiology of 90% of MDS patients consistently converge upon certain driver mutations (J. A. Kennedy & Ebert, 2017; Sperling, Gibson, & Ebert, 2017). The major classes of MDS mutations include splicing gene mutations (SF3B1, SRSF2, U2AF1, ZRSR2), transcriptional gene mutations (ETV6, PHF6, RUNX1, SETBP1, TP53, NPM1), signaling mutations (CBL, JAK2, KIT, MPL, NRAS), and methylation gene mutations (ASXL1, TET2, IDH1, DNMT3A, EZH2) (M. Kim et al., 2015). All of these mutations are seem to have important patterns for the induction of genomic instability and aberrant gene expression: *Tet2* loss-of-function mutations occur frequently in MDS patients resulting in genomic hypermethylation and contribute to the MDS phenotype of hyper-mutagenicity, and ultimately leukemia progression (Cimmino et al., 2017; Pan et al., 2017). Mutations in splicing factors, such as $SRSF2^{P95H}$, are associated with aberrant splicing of numerous genes critical for hematopoiesis (Aujla, Linder, Iragavarapu, Karass, & Liu, 2018). While each can replicate a feature of disease pathogenesis, the heterogeneity has also made it challenging to establish mouse models that recapitulate human disease, further perpetuating the difficulty in understanding these disorders.

Myelodysplastic Syndromes are currently classified according to the International Prognostic Scoring System (IPSS) as "Lower risk" (LR) patients (included those with an IPSS score 0-1) and "higher risk" (HR) patients (an IPSS of 1.5+). These scores are based upon the severity of cytopenia, percent blast cells in the bone marrow, and cytogenetics (**Table 1**). Additionally, MDS can be broken down into 7 subtypes as classified by the World Health Organization (Arber et al., 2016; Vardiman et al., 2009). MDS patients have variable survival ranging from a median survival of 0.7 years in high-

risk cases to 6 years in lower risk disease (Estey, 2007; Look, 2005; Nimer, 2008). For MDS patients who fail bone marrow transplant, there is a 6-year survival rate in low-risk patients and a 5-month survival rate in high-risk patients. A 2013 survey revealed that the majority of pathologists and hematologists are currently uncomfortable with diagnosing MDS (Glauser et al.).

Table 1 WHO subtypes

Table 1. MDS subtypes based on blast percentage, cytopenias, and transformation risk.							
WHO Subtype	2008	2016	Cytopenia	Dysplasia	Percent Blasts	Transformation Risk	Other
Single Lineage Dysplasia	RA	SLD	One Cell Type	≥ 10% of the affected cell type	<5%	Low	refractory anemia (RA), neutropenia (RN) thrombocytopenia (RT)
Multilineage Dysplasia	RCMD	MLD	1-3	2-3	<5%	Moderate	
RA with isolated 5q deletion	Del 5q	Del 5q	1-2	1-3	<5%	Low	Loss of the long arm of chromosome 5
RA with ring sideroblasts	RARS	RS	1-3	1-2	<5%	Low	15% of RBCs have Ring Sideroblasts , 5% if SF3B1 mutation is present
RA with excess blasts I	RAEB I	EBI	1-3	0-3	5-10%	High	
RA with excess blasts II	RAEB II	EBII	1-3	0-3	11-20%	High	
Unclassified	MDS-U	MDS-U	Yes		<5%		

Current therapy and major clinical challenges in MDS

More than 50,000 cases of MDS are diagnosed annually in the US with the overall disease burden increasing as a result of our aging population (Luskin & Abel, 2017). Ineffective erythropoiesis and significant morbidity remain the major clinical challenges Patients have largely relied on frequent red blood cell transfusions, which lead to iron accumulation and ultimately organ damage. Other available treatment options have limited effect and can be associated with severe side-effects and high

economical costs. This lack of effective therapeutic options for MDS patients is derived primarily from the empiricisms of therapeutic development that has put a heavy focus on the already genetically altered MDS HSPC clones, rather than a better understanding of molecular mechanisms of the microenvironment forcing current therapeutic strategies to remain non-specific.

Current therapeutic options include erythroid stimulating agents, immunosuppressive therapies, azanucleosides, immunomodulatory drugs, and allogeneic stem cell transplant (Epling-Burnette, McDaniel, Wei, & List, 2012; Komrokji, Lancet, & List, 2010; A. List et al., 2005). Most of these are non-specific with reduced response rates and limited efficacy, underscoring the importance of developing biologically rational therapies aimed at targets relevant to disease pathobiology. This leaves their end goal to treat the anemia, especially in lower risk MDS were 80-90% will require frequent blood transfusions, rather than eradication of the disease (Komrokji et al., 2010; Shenoy, Vallumsetla, Rachmilewitz, Verma, & Ginzburg, 2014). These transfusions carry themselves negative implications of long-term transfusion dependence are two-fold: first, transfusion dependence is associated with poor overall survival and an increased tendency for progression to AML; second, it increases the risk of iron overload, which can lead to significant morbidity and mortality (Bennett & Overload, 2008; Shenoy et al., 2014). Recent studies indicate that iron overload inhibits erythroid colony formation *in vitro*, suggesting that long-term transfusion treatment further exacerbates ineffective erythropoiesis (Taoka et al., 2012).

Chapter 2: Introduction to the Pathobiology of MDS

The innate immune bone marrow microenvironment in MDS

While the exact etiology of MDS remains unknown and multiple abnormal events are implicated in the development of MDS (reviewed in (Chung & Park, 2017; Yang, Qian, Eksioglu, Epling-Burnette, & Wei, 2015)), recent work has highlighted the role of the microenvironment in the initiation and progression of bone marrow failure (Cull & Rauh, 2017; Fozza, Crobu, Isoni, & Dore, 2016). This has been highlighted more recently through key studies demonstrating a prominent role for the aberrant activation of the innate immune microenvironment in the bone marrow of MDS (Basiorka et al., 2016; X. Chen et al., 2013b; Schneider et al., 2016; Starczynowski & Karsan, 2010; Starczynowski et al., 2010; Zambetti et al., 2016). Symptomatic anemia represents a nearly universal hematological deficit, affecting the vast majority of patients with lower risk disease and corresponds to the presence of an intrinsic increase in cell death and inflammation (Chung & Park, 2017; Epling-Burnette & List, 2009). One prominent feature, discovered by our group, is the development of inflammation-associated cell death, or pyroptosis, in the bone marrow that contributes to the initial cytopenia in early stage MDS (Basiorka et al., 2016). Evidence indicates that pyroptosis is intrinsically increased in HSPCs and this process is linked to the presence of increased inflammatory mediators in the bone marrow microenvironment and can even be used as a diagnostic biomarker (A. A. Basiorka et al., 2018; Basiorka et al., 2016). Hence, malignant HSPC selection and expansion occurs through a natural selection process

that leads to survival and autonomous growth advantage of the myeloid clone. Promoted by the acquisition of genetic abnormalities, the clonal HSPC expansion eventually overtakes the space available to healthy HSPCs and prevents the production of healthy hematopoietic lineages. Indeed, for those patients with lower risk MDS, ineffective erythropoiesis predominates, and clinical management goals emphasize ways to improve hematopoiesis and correct hematological deficits (Chung & Park, 2017; Hellstrom-Lindberg, 1995; Hellstrom-Lindberg et al., 1998; A. F. List, Vardiman, Issa, & DeWitte, 2004).

Immune suppressive signaling, pyroptosis, inflammatory environment in MDS.

Mounting evidence implicates activation of innate immune signaling in both hematopoietic senescence and the pathobiology of MDS (Cull & Rauh, 2017; Fozza et al., 2016). Innate immune signaling promotes excess generation of inflammatory molecules (danger-associated molecular pattern (DAMP)), expansion of regulatory T cells, as well as the up-regulation and activation of Toll-like receptors (TLR).

We have demonstrated that myeloid-derived suppressor cells (MDSC) are a group of pathologically activated immature myeloid cells, known to accumulate in tumor bearing mice and cancer patients, and contribute to T cell immunosuppression and cancer progression (X. Chen et al., 2013b). These immature myeloid cells, defined in humans by the presence of the inhibitory receptor CD33, represent a mixed group of immature myeloid cells and myeloid progenitors increased in proportion in the MDS bone marrow microenvironment (X. Chen et al., 2013b). The principal factors implicated in MDSC-mediated immune suppression include arginase (ARG1), TGFβ, IL-10, and ROS (Veglia, Perego, & Gabrilovich, 2018).

Our previous studies have demonstrated that MDSC serve as a primary source of inflammatory molecules, and their suppressive activity is in part driven by secreted inflammation-associated signaling molecules, specifically S100A9 (Basiorka et al., 2016; X. Chen et al., 2013b). S100A9 heterodimerizes with S100A8 and interacts with innate immune receptors involved in immunosuppressive activation and while both S100A8/A9 are implicated in the induction of ineffective hematopoiesis (X. Chen et al., 2013b; Schneider et al., 2016), we demonstrated that S100A9 alone was the key driver of MDSC activation in MDS (X. Chen et al., 2013b). Moreover, we have shown that S100A9 can induce genomic instability, secretion of genotoxic mediators such as ROS and initiates death of HSPC in the bone marrow indirectly, through cellular killing (Cheng et al., 2019), and directly in a feed forward mechanism through the induction of pyroptosis, an inflammatory form of cell death (Basiorka et al., 2016; X. Chen et al., 2013b; Schneider et al., 2016).

This implicates that activation of pathways downstream of S100A9 as critical for the induction of ineffective hematopoiesis in MDS and development of pan-cytopenias, which has been further validated in bone marrow mesenchymal stromal cells, showing that S100A9 contributes to DNA damage in the stem cells in a ROS-dependent manner (Zambetti et al., 2016). Importantly, our group recent report on blocking the S100A9 receptor and resultant signaling as a novel therapeutic strategy for MDS (Eksioglu et al., 2017b). Therefore, a better understanding of the mediators downstream of S100A9/pyroptosis activation in MDS could help us understand the importance of these mechanisms and provide avenues for the development of therapeutic strategies that can reduce or block this feed-forward signaling and restore healthy hematopoiesis.

The pyroptosis activation that induces ineffective hematopoiesis in MDS is mediated by the NLRP3 inflammasome preventing HPSCs from maturing to terminally differentiated blood cells, causing the characteristic pancytopenia observed in patients (Basiorka et al., 2016). This has also been demonstrated to contribute to the selective pressures upon which malignant clones arise giving way to future transformation (Bowman, Busque, & Levine, 2018). Upon inflammasome activation, caspase-1 is recruited to NLRP3, through the caspase activation and recruitment domains (CARDs) adapter molecule ASC (apoptosis-associated speck-like protein containing a CARD), to undergo autocatalytic activation (Sallman, Cluzeau, Basiorka, & List, 2016). Active caspase-1 subunits then cleave pro-IL1β, pro-IL-18 and the pore forming protein, gasdermin D, leading to pyroptotic lytic cell death.

Cells then release their intracellular contents including DAMPs, cytokines, and lactate dehydrogenase (LDH), into the extracellular space triggering a feed-forward process that propagates inflammasome and innate immune activation in neighboring cells (Jorgensen, Zhang, Krantz, & Miao, 2016). One such DAMP, ASC specks are large (1 to 2µM), durable, protease resistant, filamentous clusters, (Stutz, Horvath, Monks, & Latz, 2013), these characteristics have allowed us to establish their potential as diagnostic biomarkers, not only to define the extent of pyroptosis but as a way to detect MDS peripheral blood specimens (A. A. Basiorka et al., 2018). This discovery highlights the importance of better understanding the DAMPs produced subsequent to pyroptotic activation, both for improved diagnosis of MDS as well as a better understanding of the feed-forward activation of this inflammatory process.

Mitochondrial DAMPs as potential markers and mediators of MDS pathogenesis

Pyroptosis, is an explosive form of cell death, where the cell swells and expels all of its contents including. In MDS the activation of the innate immune system happens in the absence of infection, often referred to as sterile inflammation (G. Y. Chen & Nunez, 2010). Mitochondrial membrane depolarization leads to the release of ATP, Cytochrome C, Mitochondrial inflammatory proteins (MADS), Calcium (Dela Cruz & Kang, 2018; Gurung, Lukens, & Kanneganti, 2015). Among the leaked DAMPs, upon mitochondrial membrane depolarization from pyroptotic HSPC, is oxidized mitochondrial DNA (ox-mtDNA) (Shimada et al., 2012; Vollmer et al., 2004).

The mitochondria is ancestrally linked with bacteria and its DNA is small, circular, unmethylated, and prone to oxidation due to reactive oxygen species (ROS) generated by the mitochondria (Collins, Hajizadeh, Holme, Jonsson, & Tarkowski, 2004; Sandhir, Halder, & Sunkaria, 2017) making its depolarization an important source of ox-mtDNA. Potential receptors for ox-mtDNA as a DAMP include NLRP3, Toll-like receptor (TLR)-9 and cGAS–STING (Grishman, White, & Savani, 2012; Shimada et al., 2012; Xiao & Fitzgerald, 2013; J. Z. Zhang, Liu, Liu, Ren, & Sun, 2014). Furthermore, MDS patients exhibit increased levels of cellular and mitochondrial ROS which not only contributes to inflammasome activation but may also increase vulnerability of the mitochondrial DNA to oxidation (Basiorka et al., 2016; X. Chen et al., 2013a; Zambetti et al., 2016).

Prior studies have suggested a correlation between ox-mtDNA and inflammation: autoimmune diseases (Becker et al., 2019; Franceschi & Campisi, 2014; Giles & Boackle, 2013; Hajizadeh, DeGroot, TeKoppele, Tarkowski, & Collins, 2003),

and other inflammatory conditions (Garcia-Martinez et al., 2016; Gu et al., 2013; Harrington, Choi, & Nakahira, 2017; Lindqvist et al., 2016; Scozzi et al., 2021).

However, neither the role of ox-mtDNA nor TLR9 in MDS have been well characterized and can provide a novel targetable therapeutic/diagnostic axis to reduce the feedforward innate immune activation that gives rise to the pathogenesis of this disease. This dissertation work is focused on TLR9 and ox-mtDNA as a ligand/receptor pair; demonstrating that ox-mtDNA is an efficient diagnostic marker for MDS and that targeting the ox-mtDNA/TLR9/myD88/NLRP3 axis has strong therapeutic potential through the restoration of hematopoiesis in ex vivo treated specimens. We propose several targets along the ox-mtDNA/TLR9/myD88/NLRP3 and show that hitting these targets significantly improved hematopoietic potential in colony formation assays, suggesting that these targets are ready to move into *in vivo* studies.

Chapter 3: Oxidized Mitochondrial DNA a Disease Biomarker for Myelodysplastic

Syndromes

Abstract

Myelodysplastic syndromes (MDS) are heterogeneous hematopoietic stem cell malignancies that can phenotypically resemble other hematologic disorders. Thus, tools that may add to current diagnostic practices could aid in disease discrimination. Constitutive innate immune activation is a pathogenetic driver of ineffective hematopoiesis in MDS through Nod-like receptor protein 3 (NLRP3)–inflammasome-induced pyroptotic cell death. Oxidized mitochondrial DNA (ox-mtDNA) is released upon cytolysis, acts as a danger signal, and triggers inflammasome oligomerization via DNA sensors. By using immortalized bone marrow cells from murine models of common MDS somatic gene mutations and MDS primary samples, we demonstrate that ox-mtDNA is released upon pyroptosis. ox-mtDNA was significantly increased in MDS peripheral blood (PB) plasma compared with the plasma of healthy donors, and it was significantly higher in lower-risk MDS vs higher-risk MDS, consistent with the greater pyroptotic cell fraction in lower-risk patients. Furthermore, ox-mtDNA was significantly higher in MDS PB plasma compared with all other hematologic malignancies studied, except for chronic lymphocytic leukemia (CLL). Receiver operating characteristic/area under the curve (ROC/AUC) analysis demonstrated that ox-mtDNA is a sensitive and specific biomarker for patients with MDS compared with healthy donors (AUC, 0.964),

other hematologic malignancies excluding CLL (AUC, 0.893), and reactive conditions (AUC, 0.940). ox-mtDNA positively and significantly correlated with levels of known alarmins S100A9, S100A8, and apoptosis-associated speck-like protein containing caspase recruitment domain (CARD) specks, which provide an index of medullary pyroptosis. Collectively, these data indicate that quantifiable ox-mtDNA released into the extracellular space upon inflammasome activation serves as a biomarker for MDS and the magnitude of pyroptotic cell death.

Figure 2: ox-mtDNA Biomarker Visual Abstract
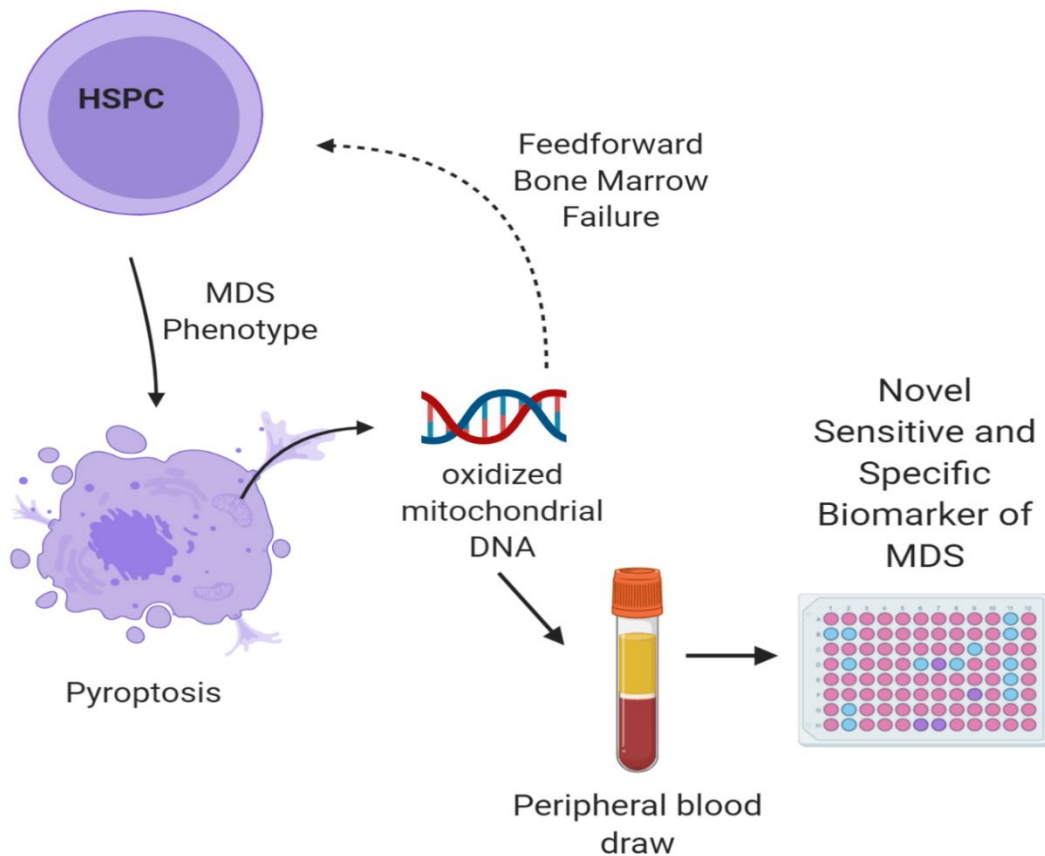
Introduction

MDS phenotypically resembles overlap syndromes such as chronic myelomonocytic leukemia (CMML) that can affect diagnosis and potentially lessen timely and effective treatment (Albitar et al., 2002; Cogle, 2015; Tanaka & Bejar, 2019; Valent, 2019). Current MDS diagnosis is based on peripheral blood cytopenias and bone marrow dysplasia while risk stratification is determined by severity of cytopenias, cytogenetics, and blast count (Montalban-Bravo & Garcia-Manero, 2018). Correct diagnosis is crucial to allow for the provider and patient to make important quality of life decisions such as how aggressively to pursue bone marrow transplant, which treatment will be best and the likelihood of leukemic transformation. Thus, an easily accessible and quantitative companion diagnostic biomarker is necessary for improving patient outcomes.

Mitochondrial DNA that is prone to oxidation by ROS is implicated as a key mediator of systemic sterile inflammatory states (G. Y. Chen & Nunez, 2010; Collins et al., 2004; Fernandes-Alnemri et al., 2007; Lotze et al., 2007; Ojeda et al., 2018; Picou et al., 2019; Yu et al., 2014; Q. Zhang et al., 2010; Zhong et al., 2018). Further, during inflammasome assembly, the mitochondrial membrane depolarizes releasing mitochondrial DNA into the cytosol, and upon pyroptotic cell death, the ox-mtDNA is released with other intracellular DAMPs into the extracellular matrix. DAMP release potentiates innate immune activation in proximate cells either through engagement of DNA sensors or by direct interaction with NLRP3 (L. S. Huang et al., 2020; Shi et al., 2015; Vollmer et al., 2004; Yu et al., 2014; Zhong et al., 2018). Importantly, elevated levels of cell-free DNA have been reported in several chronic systemic inflammatory

disorders (Giles & Boackle, 2013; Hajizadeh et al., 2003). Here, we investigated whether ox-mtDNA serves as a candidate disease biomarker of medullary pyroptosis in MDS.

Methods

Primary Samples

Peripheral blood and bone marrow plasma from cases (**Table 1**) and controls were acquired between Jan 1, 2005, and Jan 12, 2017, through protocols approved by the Institutional Review Board or equivalent regulatory committees for each institution that provided specimens from patients with myelodysplastic syndromes, hematological malignancies, reactive conditions, and healthy controls. MDS cases were stratified according to the International Prognostic Scoring System (IPSS) with lower risk (LR) cases having an IPSS ≤ 1 and higher risk (HR) cases having an IPSS ≥ 1.5.

CRISPR

CRISPR gene knockout THP1 cells were created by CRIPSR/Cas9 gene editing using guide RNA to ASC (F-GCTAACGTGCTGCGCGACAT, R-GCTAACGTGCTGCGCGACAT), Caspase-1 (F-GCTTTAAACCACACCACACCA, R-TGGTGTGGTGTGGTTTAAAGC), NLRP3 (F-GACAATTCTCTGGGGGACCCA, R-TGGGTCCCCCAGAGAATTGTC), or Scrambled control (F-GACGGAGGCTAAGCGTCGCA, R- TGCGACGCTTAGCCTCCGTC) into a green (Caspase-1, NLRP3, Scrambled) or red fluorescent protein (ASC) (GFP/RFP)-expressing pL-CRISPR.SFFV plasmid (pL-CRISPR.SFFV.GFP, pL-CRIPSR.SFFV.tRFP) that was a gift from Benjamin Ebert (Addgene plasmid # 57827, ;

http://n2t.net/addgene:57827 ; RRID:Addgene_57827; Addgene plasmid # 57826 ;

http://n2t.net/addgene:57826 ; RRID:Addgene_57826).(Heckl et al., 2014) Forward and

reverse guide oligonucleotides were purchased from Integrated DNA Technologies

(Coralville, IA). CACC on forward and AAAC on reverse oligonucleotides were added 5'

for plasmid ligation. Guide containing plasmids were transformed into Stbl3 competent

cells. CRISPR plasmids were packaged into lentivirus as and transduced as previously

described.(Basiorka et al., 2016) After 3 days GFP/RFP+ cells were sorted and

expanded.

Inflammasome Stimulation

To stimulate inflammasome assembly, cells were treated for 24 hours with 5 mM

ATP (Sigma-Aldrich) and 0.1 µg/mL lipopolysaccharide (Sigma-Aldrich), then 5 µM

Nigericin (Sigma-Aldrich) for 1-hour (denoted as LAN), or with 1.5 µg/mL recombinant

human (rh) S100A9 for 24 hours. Inflammasome activity and pyroptosis was assessed

using the Caspase-Glo® 1 Inflammasome Assay and LDH release using the LDH-Glo™

Cytotoxicity Assay, respectively, on a GloMax® Discover Microplate Reader (Promega

Corporation Madison, WI) according to manufacturer's protocols. In addition, cells were

harvested for western blotting and flow cytometry, and supernatants were frozen at -

80°C until use. Rho0 cells were generated according to previously described methods

(King & Attardi, 1989). Briefly, U937 and SKM1 cells were cultured in RPMI with 10%

FBS, 1% penicillin-streptomycin, 100 ng/mL ethidium bromide (EtBr, Sigma-Aldrich),

100 mM sodium pyruvate (Thermo Fisher Scientific), and 50 µg/mL uridine (Sigma-

Aldrich). Absence of mitochondrial DNA was confirmed by PCR using mitochondrial

specific primers (below) and by immunofluorescence (IF) using 10 mM 5-bromo-2'-

deoxyuridine (BrdU) staining (Abcam, Cambridge, England) to assess incorporation after cell treatment with 7 µM aphidicolin (APH) for 2 hours (Sigma-Aldrich). Inflammasome assembly was also triggered by treating cells with 50 ng/mL ox-mtDNA that was generated by PCR amplification of *ND1* from THP1 mtDNA isolations using oxidized guanosine.

Enzyme-Linked Immunosorbent Assay (ELISA)

Oxidized DNA (oxDNA) in peripheral blood plasma, bone marrow plasma, and cell supernatants was quantified using the DNA/RNA Oxidative Damage (High Sensitivity) ELISA Kit (Cayman Chemical Company, Ann Arbor, MI). Plasma glucose concentration was measured by the Glucose Colorimetric Assay Kit (Cayman Chemical Company). S100A8 and S100A9 levels were measured using CircuLex S100A8/MRP8 and CircuLex S100A9/MRP14 ELISA kits (MBL International Corporation, Woburn, MA).

Cells

Myeloid leukemia cell lines THP1 (TIB-202) and U937 cells (CRL-1593.2) were obtained from American Type Culture Collection (ATCC) and the MDS transformed SKM1 (ACC 547) from the Leibniz-Institute DSMZ–German Collection of Human & Animal Cell Lines. The human cell lines were cultured in RPMI 1640 (Thermo Fisher Scientific, Waltham, MA) supplemented with 10% FBS (Corning Inc. Corning, NY) and 1% penicillin-streptomycin (Life Technologies, Grand Island, NY). To generate a renewable source of murine SGM models with inflammasome activation, we immortalized bone marrow mononuclear cells (BM-MNC) from $Tet2^{-/-}$, $Srsf2^{P95H}$, and wildtype (WT) control mice with an estrogen-regulated *Hoxb8* transgene.(Wang et al., 2006) Immortalized cells were cultured in RPMI with 10% FBS, 1% penicillin-

streptomycin, 0.5 µM β-estradiol (Sigma-Aldrich, St. Louis, MO) and 50 ng/mL recombinant murine stem cell factor (SCF) (PeproTech Inc. Rocky Hill, NJ).

Rho0 cells were generated according to previously described methods.(King & Attardi, 1989) Briefly, U937 and SKM1 cells were cultured in RPMI with 10% FBS, 1% penicillin-streptomycin, 100 ng/mL ethidium bromide (EtBr, Sigma-Aldrich), 100 mM sodium pyruvate (Thermo Fisher Scientific), and 50 µg/mL uridine (Sigma-Aldrich). Absence of mitochondrial DNA was confirmed by PCR using mitochondrial specific primers (below) and by immunofluorescence (IF) using 10 mM 5-bromo-2'-deoxyuridine (BrdU) staining (Abcam, Cambridge, England) to assess incorporation after cell treatment with 7 µM aphidicolin (APH) for 2 hours (Sigma-Aldrich). THP1 cells demonstrated particularly sensitive to EtBr, resulting in almost complete cell death, and thus were not useful for further experiments.

Immunofluorescence

Immunofluorescent methods were performed at room temperature and antibody dilutions were made in 2% BSA (Thermo Fisher Scientific) in phosphate buffered saline (PBS). BM-MNC isolated by the Ficoll® Paque (Sigma-Aldrich) method, and cell lines, were washed in PBS (Life Technologies Corporation, Carlsbad, CA), cytospun at 1,000 rpm for 2 minutes, and fixed with BD cytofix (Thermo Fisher Scientific) for 10 minutes at 37°C. Slides were washed in PBS and immediately used or frozen at -20°C until use. Cells were permeabilized with 0.5% Triton X-100 (Sigma-Aldrich), blocked with 2% BSA/PBS, and stained with anti-oxDNA/RNA FITC, which targets oxo-8-dG to label oxDNA (Abcam, 1:1000). At least 200 cells per condition were imaged for mean fluorescence intensity (MFI) analysis. Mitochondrial DNA visualization was performed

after cells were incubated for 2 hours with 10 mM BrdU and 7 µM APH. After permeabilization and blocking, cytospins were hydrolyzed with 1 M Hydrochloric Acid (HCL) for 30 minutes and washed three times with PBS then stained with BrdU (Thermo Fisher Scientific, 1:200) and Alexa 488 goat anti-mouse (1:400). Slides were washed and ProLong® Gold anti-fade reagent with DAPI (Thermo Fisher Scientific) was added with a coverslip. Quantification ASC specks by IF was done by staining cytospins with ASC (Santa Cruz Biotechnology Dallas, TX, 1:200) and Alexa 488 goat anti-mouse (1:400) antibodies then counting the number of speck containing cells out of at least 200 cells per slide. Slides were imaged with a Leica SP8 laser scanning confocal microscope (Leica Microsystems GmbH, Wetzlar, Germany) where samples were excited with 405, and 488 diode lasers and emissions were tuned to appropriate settings for each dye. Images were captured through a 63X/1.4NA objective lens using two PMT detectors set for DAPI and FITC/Alexa488 detection. All system settings remained consistent for all samples within each experiment. Images were viewed and exported in 8-bit TIF format with LAS X software version 3.1.5 (Leica Microsystems GmbH). Mean Fluorescence Intensity (MFI) was performed on the TIF images with Definiens Tissue Studio version 4.7 (Definiens AG, Munich, Germany). In the software the nucleus detection and cell growth algorithms were used to segment individual cells within each image. Using this cell segmentation, the MFI (scale: 0-255) was calculated from the cells for each image. All data were exported to Microsoft Excel where fold change between controls and mutant or treated was calculated.

Western Immunoblot

Cells were treated, harvested, washed twice with cold PBS, then lysed in RIPA buffer with added phosphatase and protease inhibitors for 20 minutes. Immunoprecipitations were done using Protein A and G Agarose, Fast Flow beads (Millipore Sigma, Burlington, MA, according to the manufacturer's protocol. Briefly, 100 uL of plasma diluted 1:3 in PBS was added to 4µg of the oxDNA antibody and the mixture was rotated at 4°C overnight. The following morning Agarose G beads were washed thrice with cold RIPA buffer then 50 µL were added to each tube of plasma. This mixture was rotated at 4°C for 2 hours following which it was washed thrice with cold RIPA buffer, then boiled for 5 min in Laemmli sample buffer. Proteins were separated by SDS polyacrylamide gel electrophoresis and transferred to polyvinylidene difluoride (PVDF) membranes. Membranes were blocked in 5% milk in phosphate-buffered saline with Tween® detergent (PBST), incubated in primary antibody (1:1000) overnight at 4°C, washed, then incubated in secondary antibody (1:5000) for 90 minutes at room temperature. The following antibodies were used; caspase-1, NF-κB p65, caspase-3, PARP, Histone H3, TFAM (Cell Signaling Technology, Inc. Danvers, MA), human IL-1 beta / IL-1F2 (R&D Systems, Inc. Minneapolis, MN), ASC antibody (Santa Cruz Biotechnology) Anti-NLRP3 Antibody (Millipore Sigma), β-actin (Sigma-Aldrich), and appropriate HRP conjugated secondary antibodies (GE Healthcare, Chicago, IL).

Dot Blot

Genomic DNA was extracted following the QIAamp DNA Mini Kit manufacturer's protocol with added RNase (Qiagen Hilden, Germany). DNA was denatured by a 5 min 99'C heat shock followed by 10 min on ice; then neutralized with equal parts Ammonium

sulfate (2M, pH 7.0) for 5 min on ice, followed by 30 sec sonication. Four micrograms of DNA was loaded onto Amersham Hybond-N+ membrane, then UV crosslinked to the membrane (1200J/m2, UVP/Analytik Jena). The membrane was blocked with 10% for 15 min, probed with 5hmC antibody for 15 min, washed with PBST, probed with the secondary antibody for 15 min, washed and exposed. The same membrane was later stained with 0.4ug/mL of PI for the loading control. Images captured with the Odyssey Fc Imaging System (LI-COR).

Flow Cytometry

Cells were permeabilized with ice-cold 100% methanol for 10 minutes at -20°C, washed with PBS and incubated with anti-DNA/RNA damage antibody (Abcam, 1:200) for 15 minutes at room temperature. Cells were then washed, re-suspended in PBS, and run on the BD FACSCalibur (Becton, Dickinson and Company, Franklin Lakes, NJ). Primary cells were collected and incubated in 10% autologous plasma 10% FBS IMDM overnight, the next day cells washed and pelleted. Next cells were blocked with Human FcR Blocking Reagent (Miltenyi Biotec, Bergisch Gladbach, Germany) for 20 min in the dark, then stained with anti-DNA/RNA damage antibody (Abcam), Ki-67 (BioLegend, San Diego, CA) washed in 2% FBS in PBS, resuspend in 1µg/mL DAPI solution and run on the BD LSR II Flow Cytometer. FCS files were analyzed using FlowJo v10 (FlowJo LLC. Ashland, Oregon).

DNA Isolation and PCR

Cell-free DNA was isolated using QIAamp DNA Blood Mini Kit with the provided carrier RNA according to the manufacture's protocol (Qiagen, Hilden, Germany). Cellular DNA was isolated using QIAamp DNA Mini Kit according to the manufacturer's

protocol (Qiagen). DNA was eluted in water and quantified on a NanoDrop™ 1000 Spectrophotometer (Thermo Fisher Scientific). Fifty nanograms of DNA was amplified using mitochondrial or nuclear specific primers (mitochondrial forward: 5'-CTATATACAACTACGCAAAGGCC-3', mitochondrial reverse: 5'-AGGTGTTCTTGTGTTGTGATAAG-3'; nuclear forward: 5'-GGAGACCAAGGGTGCAGTTATGCCTCAG-3', nuclear reverse: 5'-CCCAATTGCAGGTAAAACAG-3') and GoTaq® Green Master Mix (Promega) in a BioRad MyCycler Thermal Cycler (94°C for 2 minutes; 40 cycles of 94°C for 30 seconds, 57°C for 30 seconds, 72°C for 45 seconds; followed by 72°C for 5 minutes) (Bio-Rad Laboratories, Inc. Hercules, CA.) PCR products were loaded on a 1% agarose gel containing EtBr. Ox-mtDNA used for cell stimulation was synthesized from mtDNA extracted using the Mitochondrial Extraction Kit according to the manufacture's protocol (Active Motif. Carlsbad, CA) and amplified by *ND1* primers (ND1 Forward: 5'-CCCTAAAACCCGCCACATCT-3'; ND1 Reverse: 5'-GAGCGATGGTGAGAGCTAAGGT-3') with the addition of oxidized guanosine to the nucleotide master mix.

Statistical analysis

Student's *t*-test was used to assess significance in the MDS murine SGM models and inflammasome activated cell lines. Paired patient samples (peripheral blood and bone marrow) were compared using two-tailed paired *t*-test. The two-tailed *t*-test of log10-transformed glucose normalized peripheral blood plasma ox-mtDNA was used to compare cases and controls. Kruskal-Wallis test was used to compare diseases with n<10. Correlations, corrected for glucose, between log10-ox-mtDNA and log10-

percentage of ASC specks, log10-S100A8, and log10-S100A9 protein concentrations were analyzed using Pearson test. Biomarker efficiency was analyzed using receiver operating characteristics (ROC) and areas under the curve (AUC) as effective measures of accuracy for MDS versus controls or by k-fold cross-validation when comparing MDS to non-MDS cases. WHO classification and mutation analyses were performed by the Kruskal-Wallis test. Statistical analysis was performed using R version 3.5.0 or GraphPad Prism version 8.3.1.

Results

Inflammasome activation generates oxidized DNA

TLR-dependent priming signals initiate the synthesis and oxidation of mtDNA that is necessary to stabilize NLRP3 in a primed state (Aarreberg et al., 2019; Zhong et al., 2018). To determine whether somatic gene mutations with inflammasome activity direct the release of ox-DNA, we investigated the common MDS driver epigenetic modifying (*Tet2*$^{-/-}$) and spliceosome (*Srsf2*^{P95H}) gene mutations in *Hoxb8* immortalized murine HSPC derived from mutant and corresponding wildtype (WT) mice (**Figure 4**) (Jeong et al., 2019; E. Kim et al., 2015; Ko et al., 2011; Smeets et al., 2018). Immortalized murine SGM models display 2-to-4.5x greater caspase-1 activity compared to WT cells, indicative of inflammasome activation and consistent with our previous findings in primary MDS specimens (*Tet2*$^{-/-}$ versus WT*, P* = 1.6 x 10^{-5}; *Srsf2*^{P95H} versus WT*, P* = 7.9 x 10^{-3}) (**Figure 3A**) (Basiorka et al., 2016).

Upon inflammasome assembly, cells undergo mitochondrial membrane depolarization and release mitochondrial contents into the cytosol (Shi et al., 2015; Yu

et al., 2014). Using an antibody that recognizes ox-DNA/RNA, we quantified cytosolic ox-DNA by flow cytometry, demonstrating approximately a 2-fold higher level of ox-DNA in *Tet2*^{-/-} and *Srsf2*[P95H] cells compared to WT cells *(P = 5.1 x 10^{-3} and P = 4.8 x 10^{-2},* **Figure 3B**) which was confirmed by immunofluorescence *(P = 5.0 x 10^{-4} and P = 4.6 x 10^{-2}*, **Figure 3C, Figure 5A, B**). We next investigated whether ox-DNA is released into the extracellular space cells upon pyroptotic cell lysis by quantitating levels of ox-DNA in supernatants of *Tet2*^{-/-} and *Srsf2*[P95H] versus WT cells. Ox-DNA concentrations were significantly higher in supernatants from *Tet2*^{-/-} and *Srsf2*[P95H] versus WT cells *(P = 1.9 x 10^{-2} and P = 1.5 x 10^{-3}*, respectively) (**Figure 3D, Figure 5C**).

To determine that these findings were not specific to cultured SGM immortalized murine cell lines, we isolated bone marrow mononuclear cells (BM-MNCs) from MDS patients and age-matched normal controls and assessed ox-DNA levels by immunofluorescence. We found significantly greater cytosolic ox-DNA in MDS cases compared to healthy donors ($P = 3.3 x 10^{-3}$) (**Figure 3E, Figure 5D**).

MDS cells maintain a higher proliferative index compared to normal cells due to inflammasome directed activation of β-catenin. As such, we found significantly elevated levels of Ki-67 staining in MDS bone marrow cells compared to normal donors ($P = 3.5 x 10^{-2}$) that correlated positively with the levels of ox-DNA (r = 0.983, $P = 5.7 x 10^{-3}$) (**Figure 6A, B**). These data indicate that cytosolic ox-DNA accumulates in MDS and immortalized murine HSPC harboring SGM of varied functional classes and is released into the extracellular space where it may serve as an inflammasome catalyst in neighboring cells.

The malignant MDS bone marrow is highly proliferative as demonstrated by the high blast percentage and characteristic clonal cell expansion (Alexandrakis et al., 2004; Ben-Ezra, Trinh, Harris, & Kornstein, 1998; Lin et al., 2002). Therefore, we assessed the correlation of ox-DNA and cellular proliferation as readout by Ki-67 expression. MDS patient BM samples have significantly higher ox-DNA compared to Normal Donors evaluated by flow cytometry (P = 8.5 x 10^{-3}) **(Figure 3F)**. These results were further evaluated with respect to Ki-67 expression. MDS BM cells have significantly higher levels of ox-DNA than the Normal Donors in the high Ki-67 cells (P = 3.9 x 10^{-2}) but not significantly so in the low Ki-67 cells (P = 5.5 x 10^{-2}). Accordingly, Ki-67 and ox-DNA are positively correlated (r = 0.9631, P = 2.0 x 10^{-3}) **(Figure 3G)**.

Figure 3: Inflammasome activation generates oxidized DNA
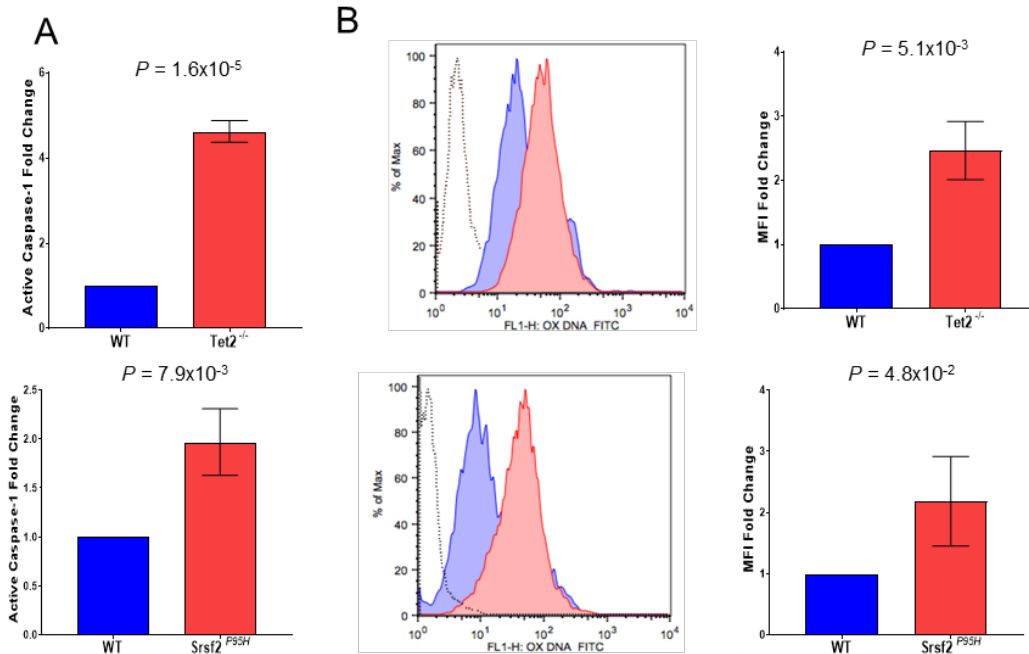
(**A**) Immortalized murine SGM model cell lines [*Srsf2* P95H and *Tet2* -/-, (red)] display increased activity of caspase-1 assessed by Caspase-1 Glo® assay in mutant compared to WT (blue) cells (mean ± SD of three independent experiments). (**B**) Increased intracellular ox-DNA assessed by flow cytometry (mean MFI ± SD of three independent experiments) in immortalized murine SGM model cell lines [*Srsf2* P95H and *Tet2* -/-, (red)] compared to WT controls (blue)

Figure 3 Cont: Inflammasome activation generates oxidized DNA
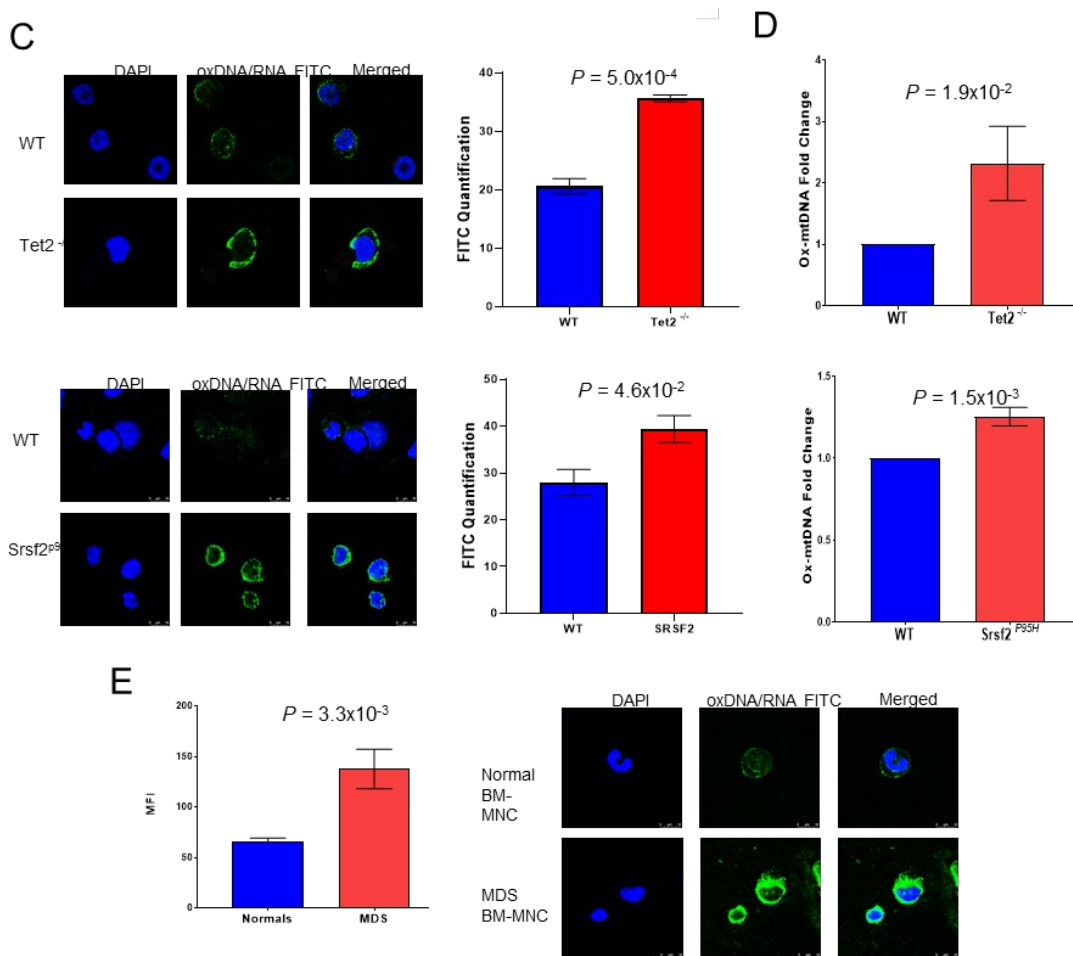
(**C**) Confocal IF of immortalized murine SGM models stained for oxDNA [x2520, DAPI (blue), oxDNA/RNA (green)]. Micrographs are representative figures. MFI of cells was quantified (minimum 200 cells per sample, three samples per groups, mean MFI ± SD). (**D**) Cell free oxDNA was assessed by ELISA in media supernatants of immortalized SGM cell lines (mean ± SD of three independent experiments). (**E**) Confocal IF of cytosolic ox-mtDNA in MDS BM-MNC samples compared normal BM-MNC samples (x2520, DAPI, ox-mtDNA FITC). Representative Micrographs. MFI of cells was quantified (minimum 200 cells per sample, three samples per groups, mean MFI ± SD).

Figure 4: Workflow for Somatic Gene Mutation Model immortalization

A
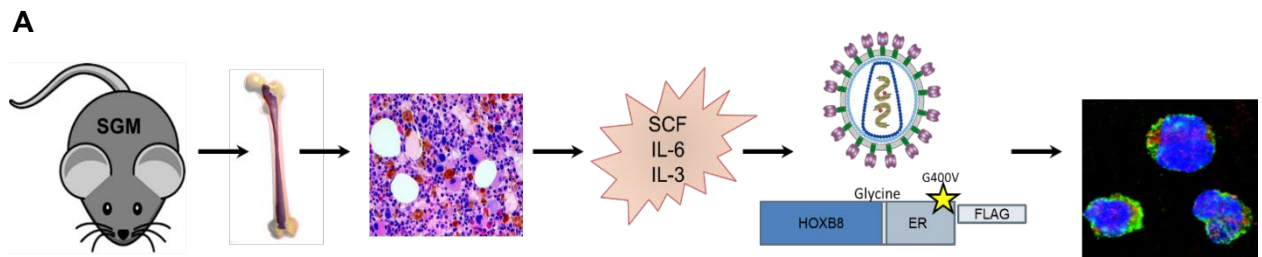
A. The SGM models were developed following the protocol outlined in Wang *et. al.*

2006. In brief, BM-MNC were isolated from appropriate MDS driver mutation murine

models. BM-MNC were incubated mSCF, IL6, and IL3 to active induced to cycling. Next

the Hoxb8-ER vector was introduced to the cells, and the cells retain hematopoietic

stem-progenitor cell properties by being cultured in murine stem cell factor and estrogen

they can be differentiated with the removal of estrogen and the addition of various

cytokines.

B
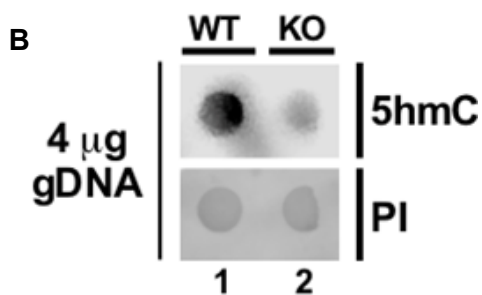
B. Dot blot demonstrating decreased 5-hmC in Tet2 $^{-/-}$ immortalized cells compared to WT, demonstration of loss of active Ten-eleven translocation methylcytosine dioxygenase 2 (Tet2) by dotblot for 5hmC (Cell Signaling Technologies)

and total DNA by propidium Iodide (PI, Sigma Aldrich). Loss of Tet2 and the SRSF2^{P95H}

mutation was further confirmed by sanger sequencing

Figure 5 SGM & BM-MNC Phenotyping:

A.
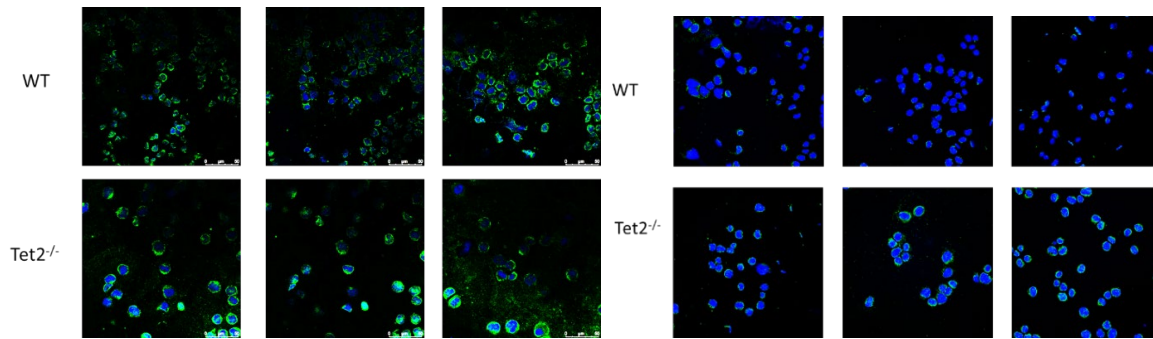
B.
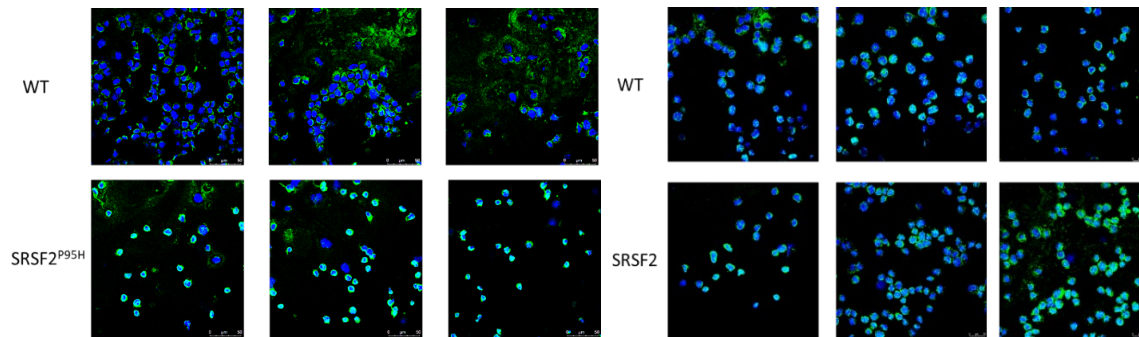
Additional micrographs of (A) Tet2-/- vs WT and (B) SRSF2P95H vs WT cells. 630X

DAPI (blue), oxDNA (green).

$P = 6.5 \times 10^{-3}$ $P = 2.0 \times 10^{-2}$

C.
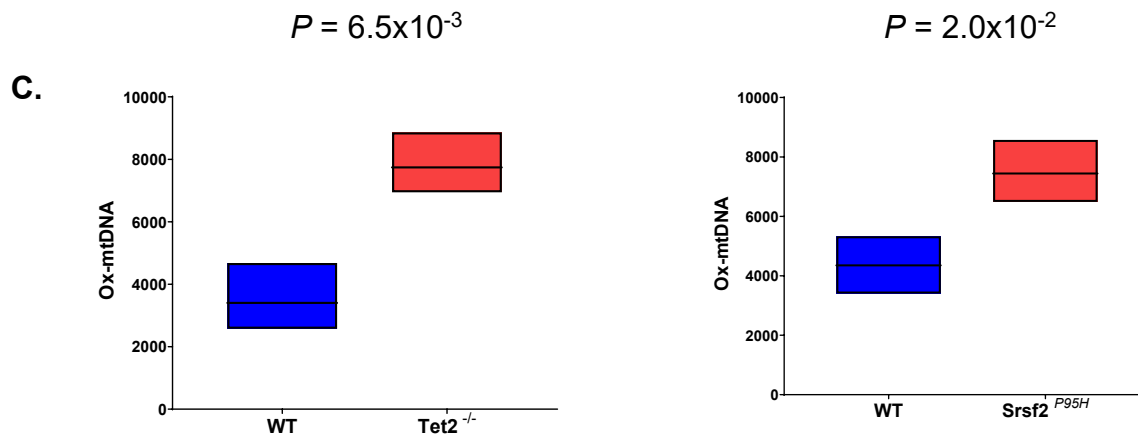
(C) Raw oxDNA ELISA values of media / cell-free oxDNA Tet2 P = 0.0065, n = 3.

SRSF2p95h P = 0.0200, n = 3.

Figure 5 Cont: SGM & BM-MNC Phenotyping

D.
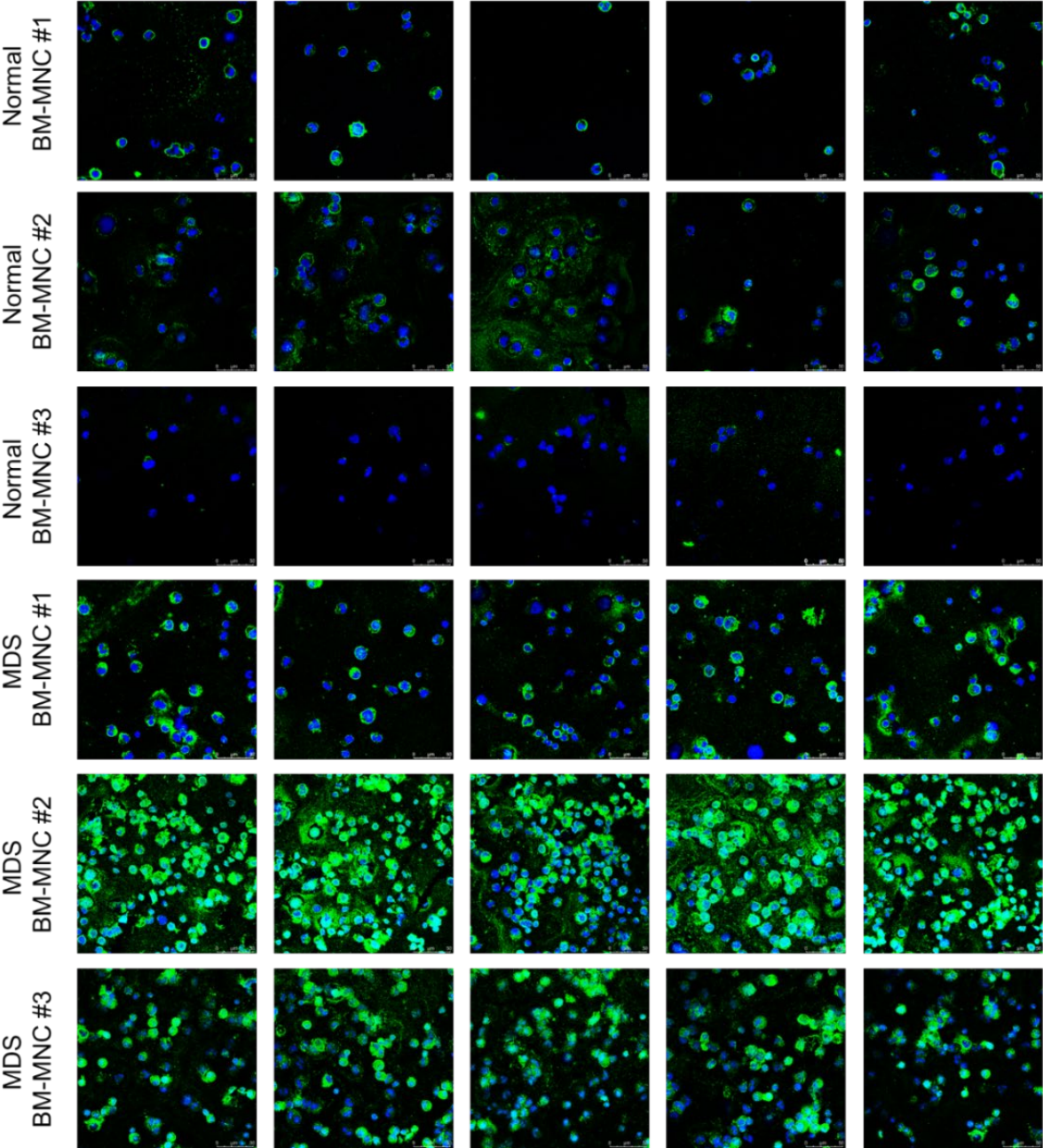
(D) Additional micrographs of normal and MDS BM-MNC stained with DAPI (blue) and oxDNA (green); 630X

Figure 6: ox-DNA vs. Ki-67

A.
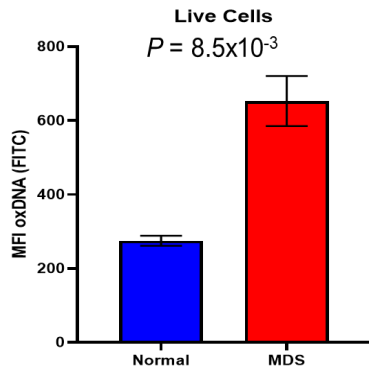
A) Ox-DNA (FITC) assessed by flow cytometry (MDS vs Normal three samples per groups, mean MFI ± SD).

B.
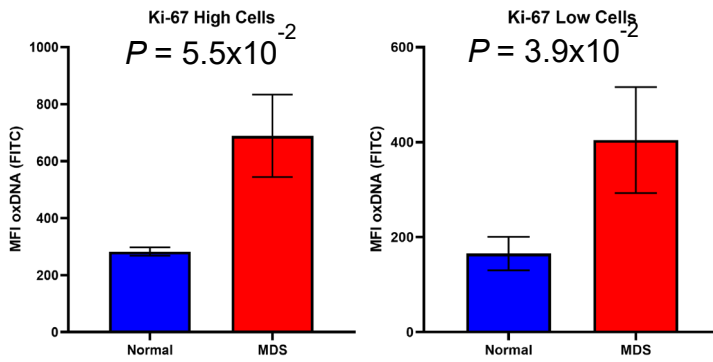
(B) Ox-DNA (FITC) assessed by flow; differentiated by Ki-67 (PE) level.

C.
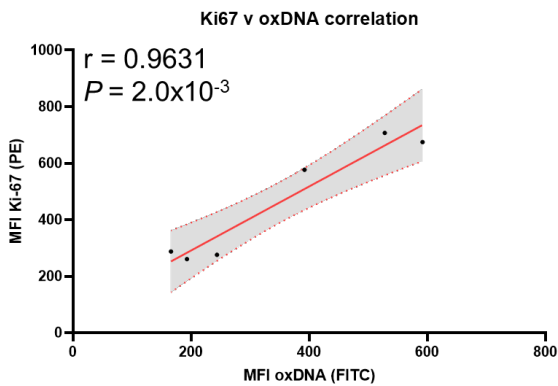
(C) Correlation of Ki-67 MFI vs ox-DNA MFI.

We next interrogated ox-DNA release following external inflammasome activation and execution of pyroptosis. The canonical pyroptotic TLR4 signaling pathway was activated in THP1, SKM1 and U937 cells by incubation with LPS, ATP, and nigericin (LAN) (Perregaux & Gabel, 1994). Following inflammasome activation, we observed a significant increase in extracellular ox-DNA by ELISA ($P = 1.0 \times 10^{-2}$, 9.0×10^{-7}, and 4.0×10^{-4}, respectively; **Figure 7A**) that was accompanied by an elevation in intracellular cytosolic ox-DNA as evidenced by confocal immunofluorescence ($P = 3.2 \times 10^{-2}$, 1.3×10^{-2}, and 2.7×10^{-2}, respectively; **Figure 7B**). To assess whether ox-DNA release was dependent upon a fully functional inflammasome complex, we used CRISPR/Cas 9 genetic editing to selectively knock out ASC, total caspase-1, and NLRP3. Upon LAN treatment, the control cells transfected with the scrambled guides released a 2.5-fold increase in ox-DNA while media from knockout cells had no significant change in ox-DNA (Scram $P = 1.9 \times 10^{-2}$, ASC KO $P = 0.21$, Casp-1 KO $P = 0.84$, NLRP3 (upper band) KO $P = 0.89$ (**Figure 7C, Figure 8**).

Oxidized Mitochondrial DNA is released following inflammasome activation

Next, we investigated whether cytosolic ox-DNA released upon inflammasome activation is of mitochondrial or nuclear origin. To this end, we depleted mitochondrial (mt) DNA to generate Rho0 cells. This was accomplished by culturing cell lines in the presence of low levels of ethidium bromide to block mtDNA replication via DNA polymerase ɣ inhibition (King & Attardi, 1989; Tarrago-Litvak et al., 1978). Absence of BrdU incorporation following treatment with aphidicolin (APH), which inhibits nuclear DNA replication, assessed by immunofluorescence confirmed mtDNA depletion in the Rho0 cells (**Figure 7D**). Loss of mtDNA was further confirmed by PCR using

mitochondrial or nuclear gene specific primers on DNA isolated from Rho0 cells (**Figure 7E**). To demonstrate that the extracellular ox-DNA is of mitochondrial origin, we treated Rho0 and parental cells with either LAN or rhS100A9, a DAMP and TLR4 ligand, to stimulate inflammasome assembly. We found that ox-DNA was not released by Rho0 cells upon inflammasome activation whereas ox-DNA was released by parental cells (SKM1 parental: vehicle versus *LAN, P* = 9.0 x 10^{-7}; versus *S100A9, P* = 2.9 x 10^{-3}; SKM1 rho0: vehicle versus LAN*, P* = 0.49; versus S100A9, *P*=0.52; U937 parental: vehicle versus LAN*, P* = 1.2 x 10^{-2}; versus S100A9*, P* = 5.0 x 10^{-4}; U937 rho0: vehicle versus LAN*, P* = 0.78, versus S100A9*, P* = 0.22) (**Figure 7F, Figure 9**). These data confirm that the ox-DNA released upon inflammasome activation is mitochondrial DNA. Interestingly, while found that ox-mtDNA is part of the NLRP3 inflammasome complex, we did not find that ox-mtDNA is necessary for inflammasome assembly or pyroptosis (**Figure 9**).

Figure 7: Oxidized Mitochondrial DNA is released following inflammasome activation
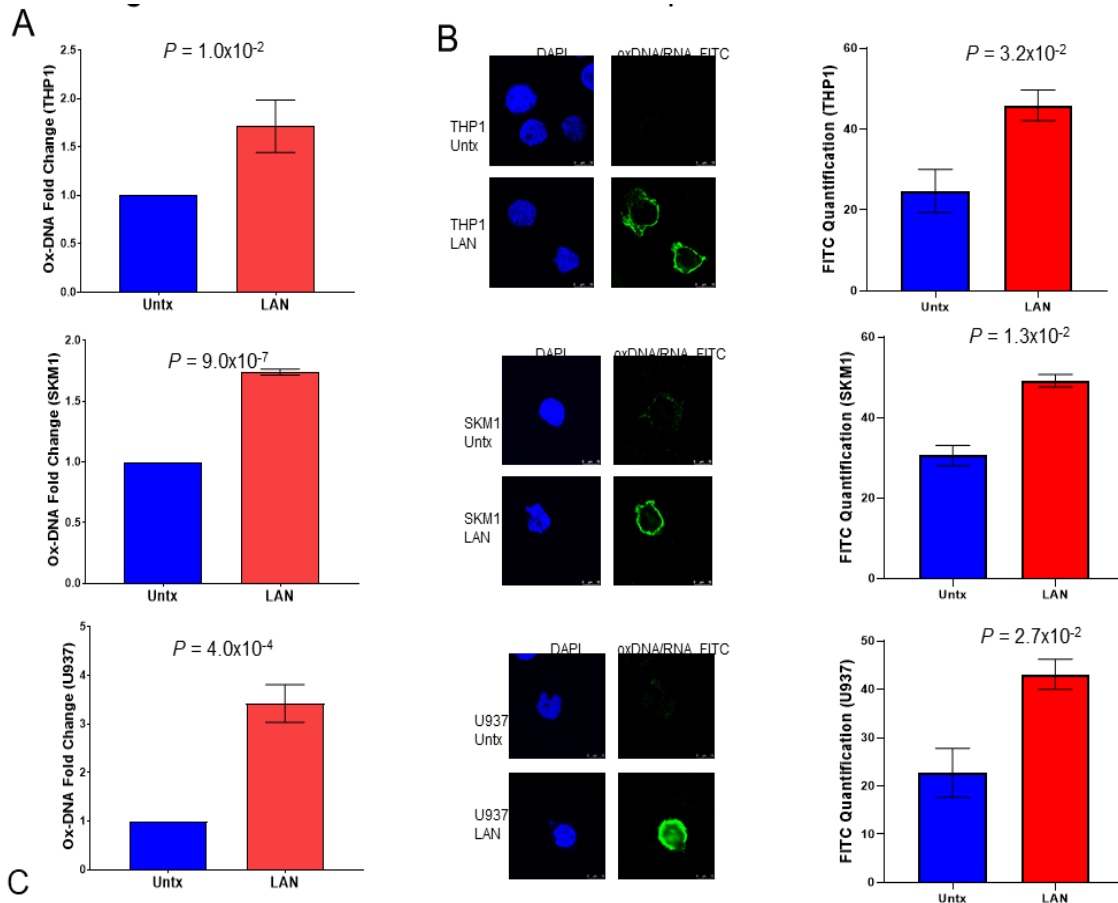
(**A**) Cell free oxDNA levels were analyzed by ELISA in THP1, SKM1, and U937 treated with LPS, ATP, and Nigericin (LAN) demonstrating increased oxDNA in stimulated versus untreated controls, (mean ± SD of three independent experiments). (**B**) Confocal IF showing increased cytosolic oxDNA in LAN stimulated cells compared to untreated controls [DAPI (blue), oxDNA/RNA (green) (x2520)], images are representative micrographs.

Figure 7 Cont.: Oxidized Mitochondrial DNA is released following inflammasome activation
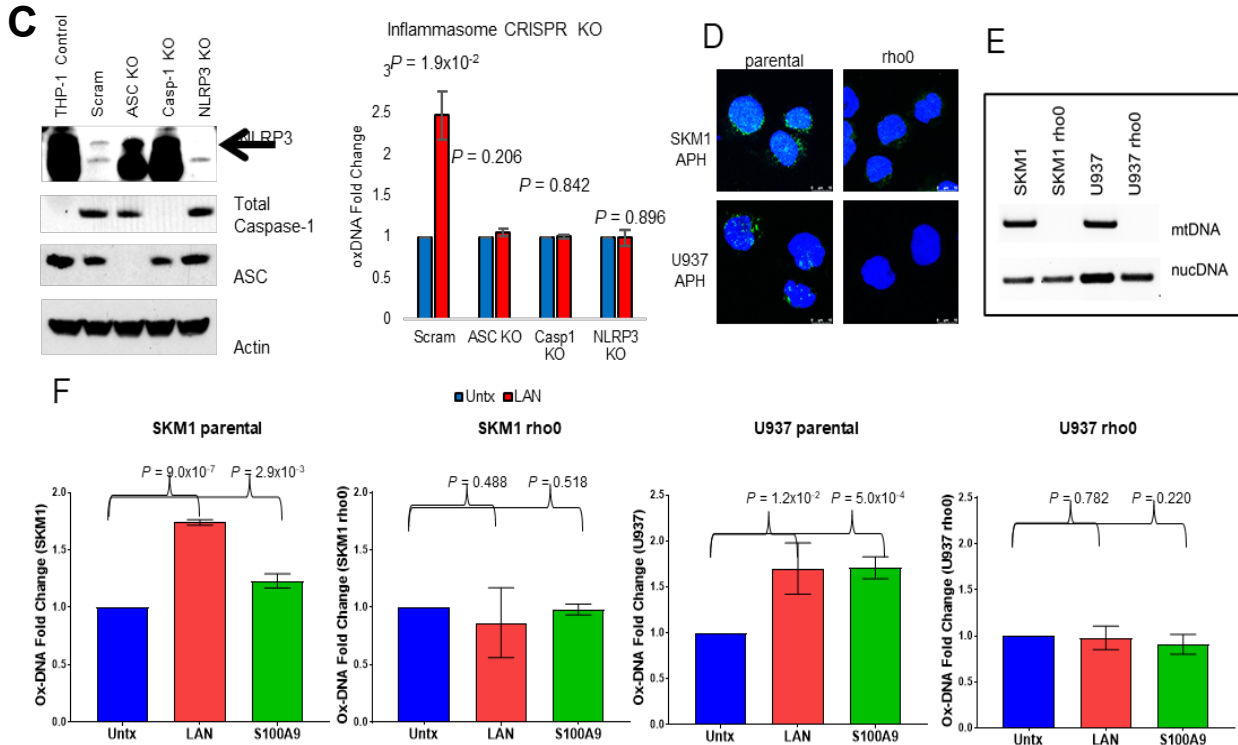
(**C**) Western blot of CRISPR KO cells of NLRP3 (top band, Arrow), full length Caspase-1, and ASC and lack of cell free oxDNA released analyzed by ELISA after treatment with LPS, ATP, and Nigericin (LAN) (mean ± SD of three independent experiments). (**D**) Decreased BrdU (green) incorporation in Rho0 cells by IF (DAPI blue). APH: aphidicolin. (**E**) PCR amplification of nuclear or mitochondrial genes of DNA isolated from rho0 and parental cell lines (**F**) Ox-mtDNA levels assessed by ELISA in parental and Rho0 cells after treatment with LAN or rhS100A9, (mean ± SD, three independent biological replicate experiments).

Figure 8: IFM KO cells

A.
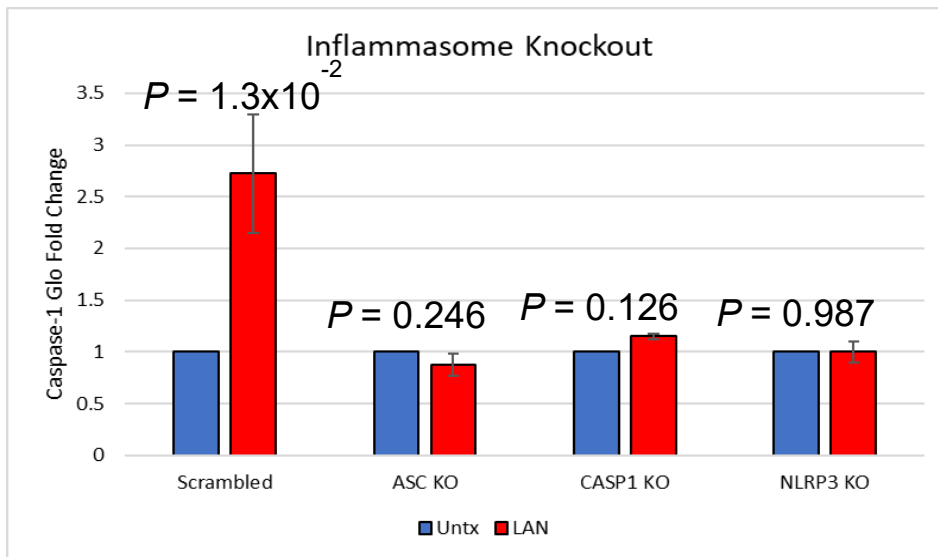
(A) CRISPR knockout of inflammasome proteins ASC, NLRP3, or Caspase-1 causes loss of extracellular Caspase-1 whereas the scrambled CRIPSR control has significant release of caspase-1 in response to canonical TLR4 inflammasome stimulation by Caspase-1 ® Glo assay, n=3.

B.
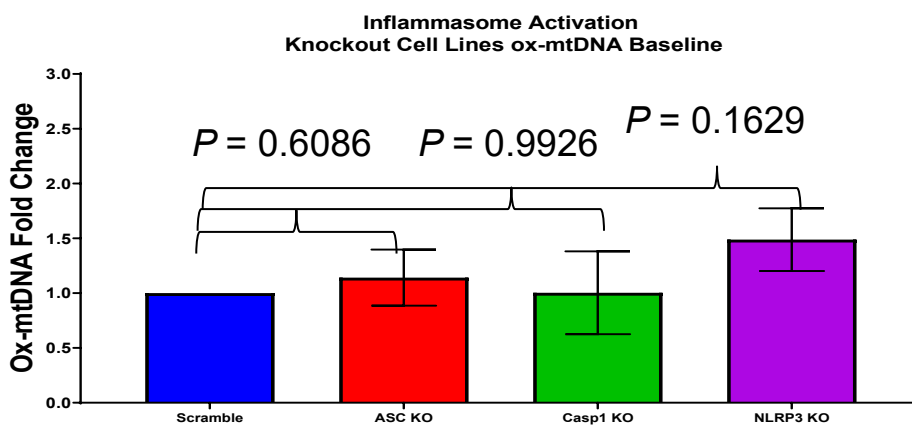
(B) There was no significant change in baseline media ox-mtDNA with various inflammasome knockouts, Caspase-1 ® Glo assay, n=3

Figure 9: Ox-mtDNA and the NLRP3 Complex
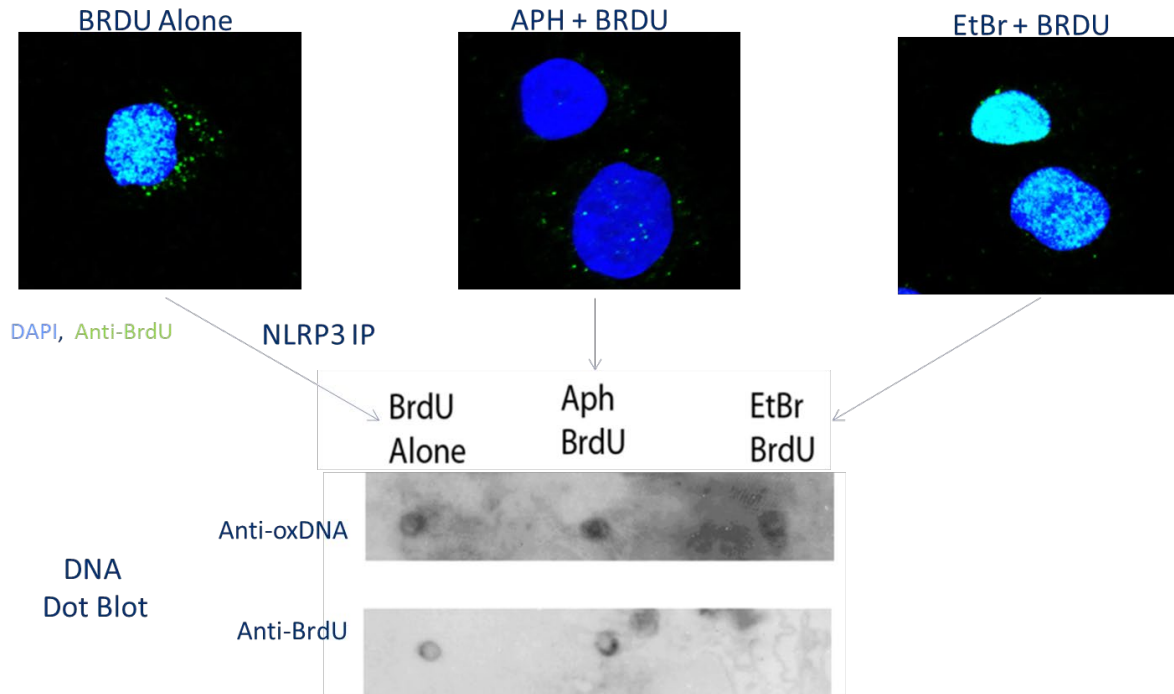
A THP-1 cells were incubated with BrdU, aphidicolin (APH, Nuclear DNA Pol α inhibitor), and Ethidium bromide (EtBr, Mitochondrial DNA Pol γ inhibitor) to selectively label Mitochondrial and Nuclear DNA, specificity is demonstrated by IF (upper) NLRP3 was then immunoprecipitated and bound DNA was probed for by DNA dot blot (lower) which showed that NLRP3 is associated with oxidized mitochondrial DNA

Figure 9 cont.: B
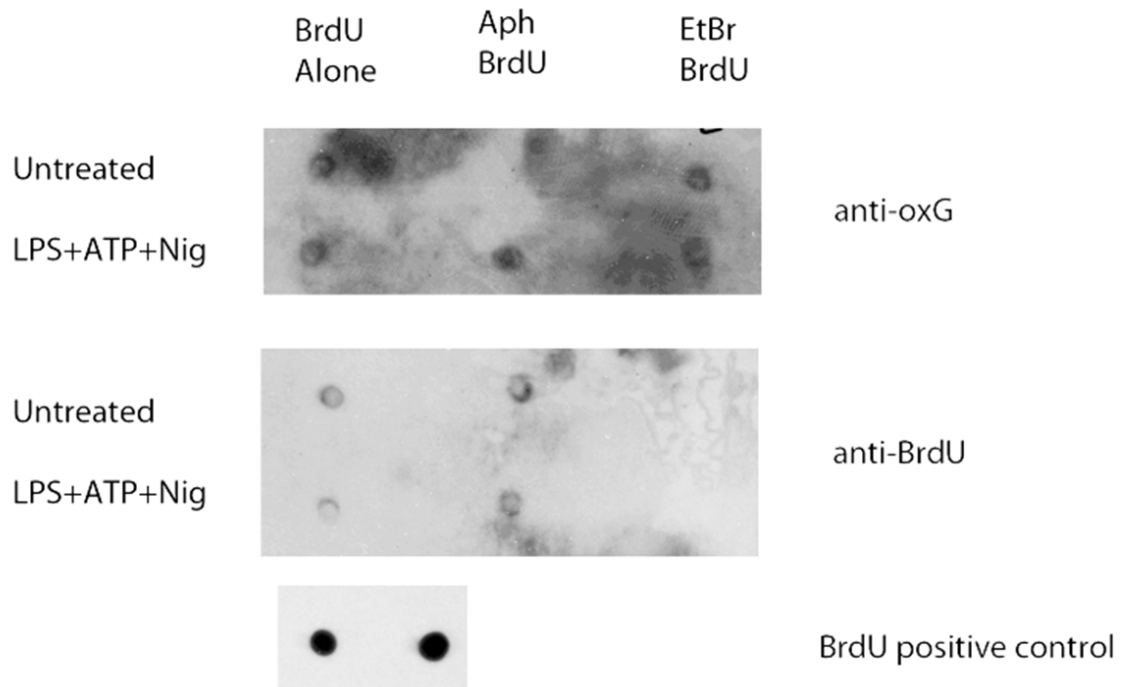
NLRP3 was then immunoprecipitated and bound DNA was probed for by DNA dot blot which showed that NLRP3 is associated with oxidized mitochondrial DNA regardless of IFM activation.

Figure 9 cont.: C mtDNA depleted Rho0 cells undergo inflammasome activation in response to canonical DAMPs as readout by Caspase-1 ® Glo.

SKM1

SKM1 rho

U937

U937 rho0
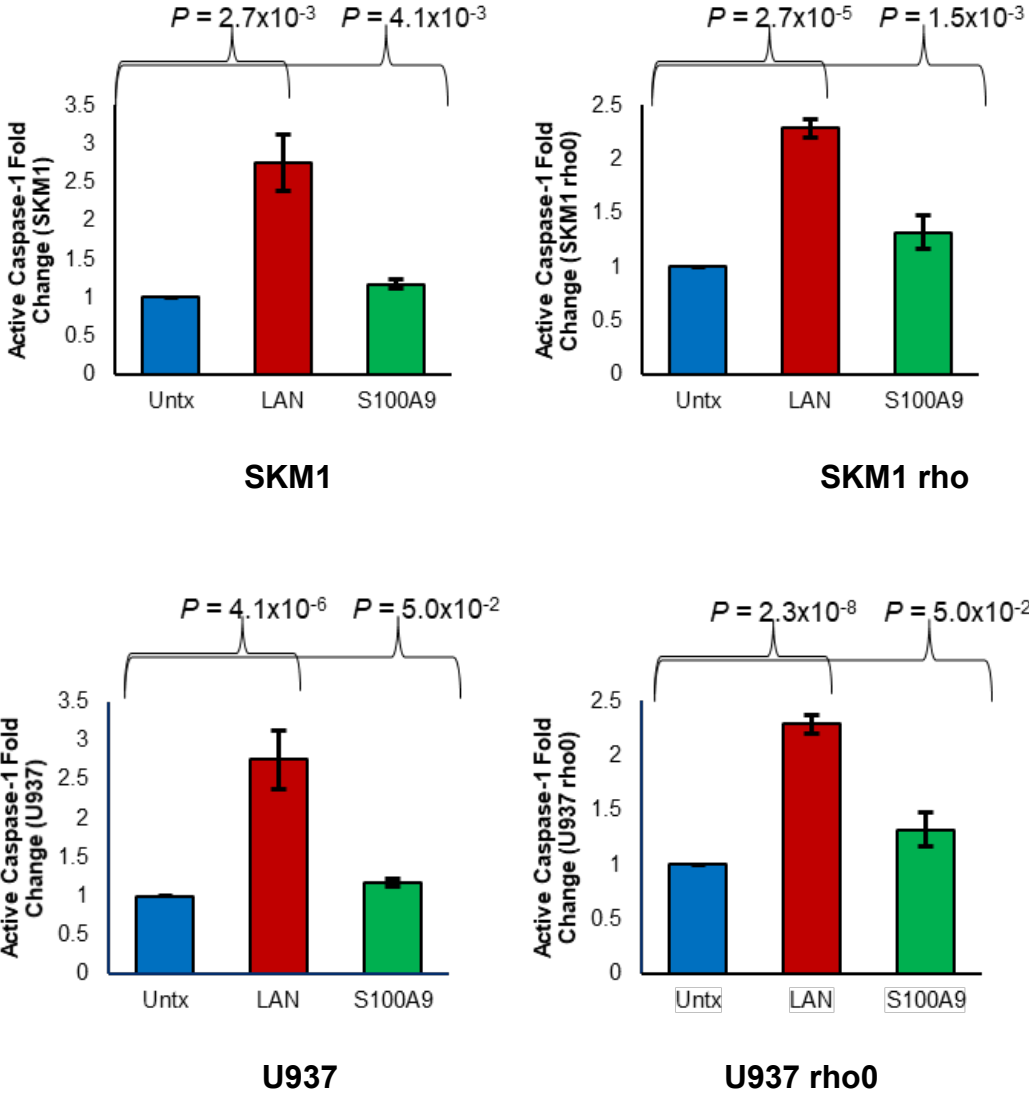
Levels of ox-mtDNA are elevated in MDS patient peripheral blood plasma

NLRP3-inflammasome-directed pyroptosis is responsible for the extensive medullary cell death and the cytopenias characteristic of lower risk MDS (Basiorka et al., 2016). To determine if ox-mtDNA liberated from pyroptotic HSPC is demonstrable in MDS patient plasma, we first performed PCR using mitochondrial and nuclear DNA specific primers on cell-free DNA isolated from MDS patient plasma. We found substantial amplification of mitochondrial genes in PB plasma; however, there was little or no amplification of nuclear genes, indicating that the cell free DNA was of mitochondrial origin (**Figure 10A, Figure 11**). This was further confirmed by immunoprecipitation of oxidized DNA in MDS patient and normal bone marrow plasma and the detection by immunoblot of only mitochondrial associated protein (TFAM), but not the nuclear protein histone H3 (**Figure 12**). Collectively, these data demonstrate that the ox-DNA was of mitochondrial origin.

We then used an ELISA to quantitate ox-mtDNA in patient plasma and compared levels in paired patient bone marrow (BM) and PB plasma. Log_{10}-transformed, glucose-adjusted (to account for possible changes arising from hyperglycemia-induced inflammasome activation (Grishman et al., 2012; Lee et al., 2013)) was detected in both PB and BM plasma with significantly higher levels found in BM plasma *(P = 1.0 x 10^{-3})*, with a positive correlation amongst paired samples (r = 0.339, *P* = 4.0x10^{-3}, n = 71) (**Figure 10B, C**). We next quantified ox-mtDNA in PB plasma from MDS patients compared to age-matched healthy donors (**Table 1**) (Pinti et al., 2014). We found no robust differences in log_{10}-transformed, glucose-adjusted ox-mtDNA levels based on gender, race, co-existing autoimmune diseases, alcohol consumption, or tobacco usage

(**Figure 13**). Log_{10}-transformed, glucose-adjusted ox-mtDNA levels were significantly higher in MDS cases (n=177) compared to healthy donors (n=29, P = 1.0 x 10^{-42}), findings that were validated in an independent cohort of 139 MDS cases and 28 healthy donors *(P* = 1.0 x 10^{-26}) (**Figure 10D, Table 2**). Moreover, log_{10}-transformed, glucose-adjusted levels of ox-mtDNA were highest in lower risk (LR, n = 162) compared to higher risk MDS (HR, n = 14, P = 2.0 x 10^{-4}) patients, consistent with greater medullary pyroptosis (Basiorka et al., 2016). These findings were validated in a separate independent cohort (LR, n = 66; HR, n = 47, P = 3.0 x 10^{-3}) (**Figure 10E, Table 2**). To determine the sensitivity and specificity of ox-mtDNA as a disease specific biomarker for MDS, we performed a receiver operating characteristic/area under the curve (ROC/AUC) analysis and found that log_{10}-transformed, glucose-adjusted ox-mtDNA concentration is a sensitive and specific biomarker when compared to healthy donors (All MDS AUC = 0.964, threshold = 0.541, sensitivity = 0.899, specificity = 0.928, HR AUC = 0.974, LR AUC = 0.959) (**Figure 10F**).

Table 2: Patient demographics of Discovery and Validation MDS and Controls

| | Discovery | | Validation | |
	Myelodysplastic Syndromes (n=176)	Controls (n=29)	Myelodysplastic Syndromes (n=113)	Controls (n=30)
Mean age (Median, SD) years	72.4 (73, 8.45)	65.0 (64, 4.9)	71.8 (73, 7.2)	75 (73, 5.56)
Gender				
Men	99 (56.6%)	0	61 (54%)	3 (10%)
Women	43 (24.6%)	29 (100%)	23 (20.3%)	27 (90%)
Unknown	33 (18.9%)	0	29 (25.7%)	0
Risk category				
Higher-risk	14 (8%)	NA	47 (41.6%)	NA
Lower-risk	162 (92%)	NA	66 (58.4%)	NA
WHO				
SLD	9 (5.1%)	NA	4 (3.5%)	NA
SLD-RS	30 (17.1%)	NA	36 (31.9%)	NA
MLD	36 (20.4%)	NA	12 (10.6%)	NA
MLD-RS	14 (8%)	NA	10 (8.8%)	NA
EB	23 (13.1%)	NA	19 (16.8%)	NA
NOS	58 (33%)	NA	30 (26.6%)	NA
U	6 (3.4%)	NA	2 (1.8%)	NA

SLD: Single lineage dysplasia

RS: ringed sideroblasts

MLD: Multilineage dysplasia

EB: excess blasts

NOS: Not otherwise specified

U: Unclassified

Correlation of ox-mtDNA and clinical features

In addition, $\log_{10}$-transformed, glucose-adjusted ox-mtDNA is negatively correlated with the number of cytopenias (White Blood Cells (WBC), Absolute Neutrophil Count (ANC), Hemoglobin (HgB), platelets, n=0-4) (r = -0.3243, P = 4.12×10^{-2}, n = 40) (**Figure 10G, Figure 14**). Further, $\log_{10}$-transformed, glucose-adjusted ox-mtDNA is correlated with white blood cell (WBC) counts (r = 0.3575, P = 4.46×10^{-2}, n = 32), platelet count (r = 0.5388, P = 1.20×10^{-3}, n = 33), absolute monocyte counts (AMC) (r = 0.3801, P = 0.0349, n = 31) and with absolute lymphocyte counts (ALC) (r = 0.3367, P = 4.80×10^{-2}, n = 35). Of the MDS cases with absolute neutrophil count (ANC) data there is a significant difference in $\log_{10}$-transformed, glucose-adjusted ox-mtDNA between the normal and thrombocytopenic (<100 $\times10^{9}$/L) cases (P = 4.0×10^{-4}, n = 33); as well as between normal and neutropenic cases (<0.80 $\times10^{9}$/L) (P = 4.59×10^{-2}, n = 35) (**Figure 14**). Additionally, $\log_{10}$-transformed, glucose-adjusted ox-mtDNA increased directly with BM fibrosis severity (normal P = 1.41×10^{-4}, mild P = 7.31×10^{-5}, moderate P = 8.55×10^{-4}) (**Figure 10H).**

No robust differences in ox-mtDNA levels were demonstrable based on World Health Organization (WHO) subtype or cytogenetic risk group (**Figure 15, Table 3**). However, within the excess blast (EB) subtypes, EB1 was significantly elevated compared to EB2 (EB1, n = 17; EB2, n = 6, p = 3.0×10^{-2}), in agreement with the more progressive disease state. We found that cases that contain transcriptional gene mutations carried significantly lower PB $\log_{10}$-transformed, glucose-adjusted ox-mtDNA compared to cases without transcriptional gene mutations (p=0.04, **Table 4**), and, cases that harbor *U2AF1* mutations vs WT, had significantly higher ox-mtDNA levels

(p=0.05, **Table 5**), although the number of positive cases was low (n=3), no other correlations with mutational status and ox-mtDNA were observed (**Figure 16, Tables 4, 5**). These data indicate that concentrations of PB plasma ox-mtDNA distinguish MDS from normal control donors, as well as lower risk from higher risk-MDS.

Figure 10: Levels of ox-mtDNA are elevated in MDS patient peripheral blood plasma
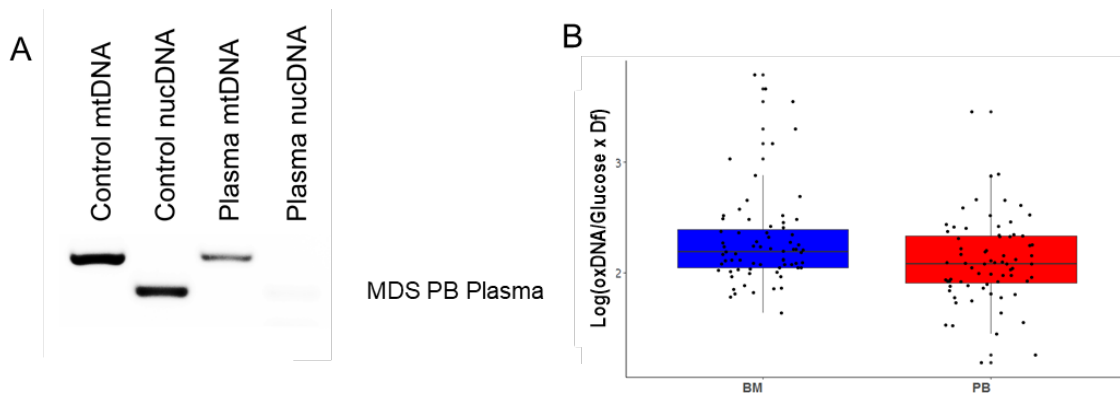
(**A**) DNA isolated from peripheral blood plasma of MDS patients was amplified with nuclear or mitochondrial primers demonstrating that cell free DNA is of mitochondrial origin. Representative image of 8 independent MDS samples. (**B**) Log10-transformed, glucose-adjusted levels ox-mtDNA levels from MDS peripheral blood (PB) and bone marrow (BM) plasma.

Figure 10 Cont.: Levels of ox-mtDNA are elevated in MDS patient peripheral blood plasma
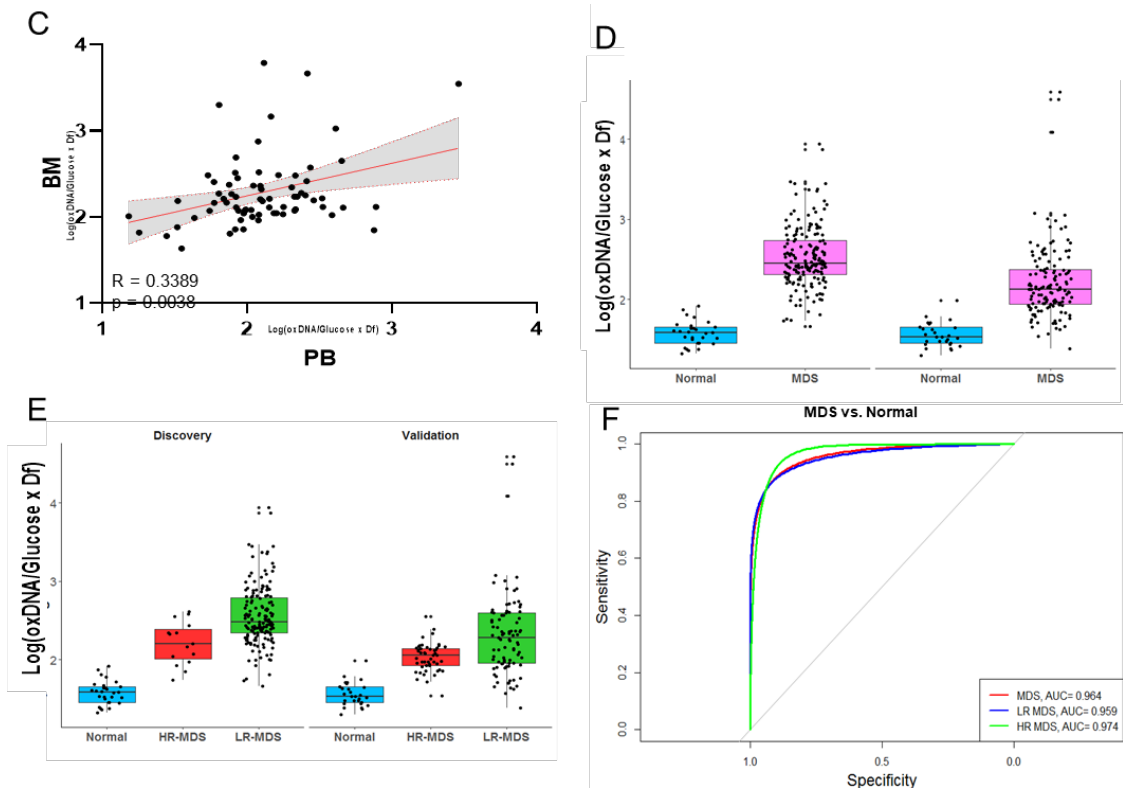
(**C**) Correlation of Peripheral Blood and Bone Marrow log10-transformed, glucose-adjusted levels of ox-mtDNA within a given MDS sample. (**D, E**) Log10-transformed, glucose-adjusted levels of ox-mtDNA in cases compared to controls in both a discovery and validation set. (**D, E**) Log10-transformed, glucose-adjusted levels of ox-mtDNA in cases compared to controls in both a discovery and validation set.

Figure 10 Cont.: Levels of ox-mtDNA are elevated in MDS patient peripheral blood plasma
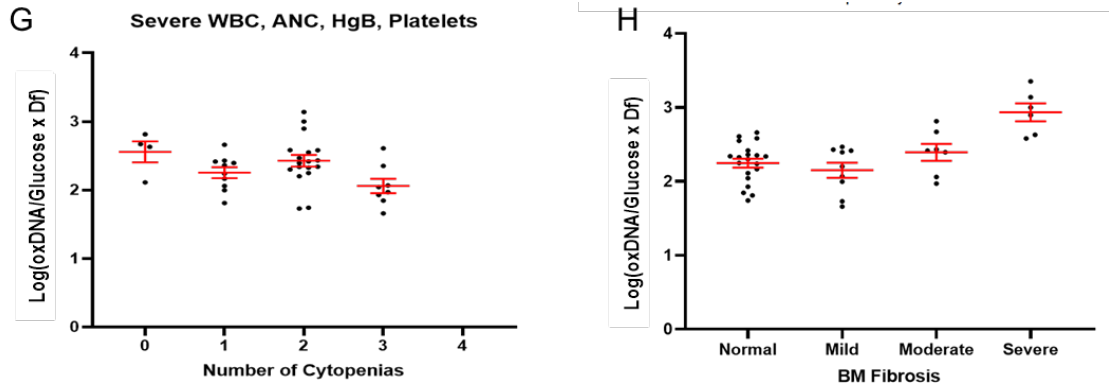
(**G**) Log10-transformed, glucose-adjusted levels of ox-mtDNA stratified by number of severe cytopenias (WBC [<5x10^4], ANC [<0.80 x10^9/L], HgB [<10 g/dL], Platelets [<100 x10^9/L]) (0-4). (**H**) Log10-transformed, glucose-adjusted levels of ox-mtDNA stratified by severity of BM fibrosis.

Figure 11: MDS Plasma DNA

DNA isolated from MDS 8 independent patient peripheral blood plasma samples was amplified with nuclear (nuc) and mitochondrial (mt) primers demonstrating that patient plasma DNA is mitochondrial.
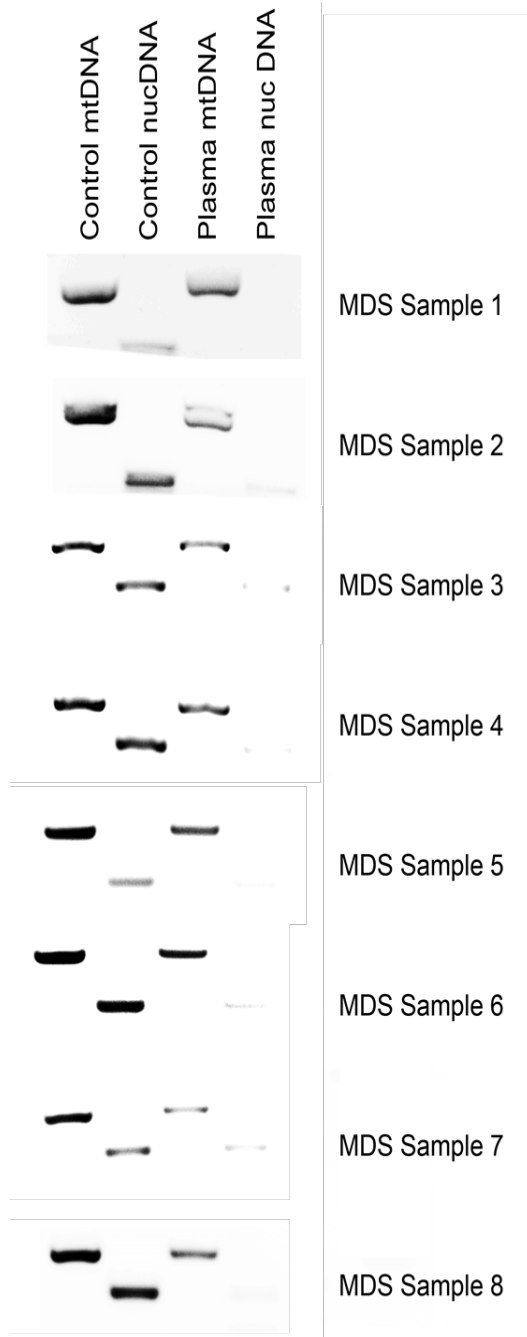
Figure 12: DNA associated Plasma Proteins

Immunoprecipitation of oxidized DNA in MDS patient and normal bone marrow plasma and immunoblotting for the mitochondrial DNA associated protein TFAM (Transcription Factor A, Mitochondrial) the nuclear DNA associated protein Histone H3. Nuclear fractionation used as positive control (SKM1 Abcam Nuclear Extraction Kit, according to manufacturer's protocol).
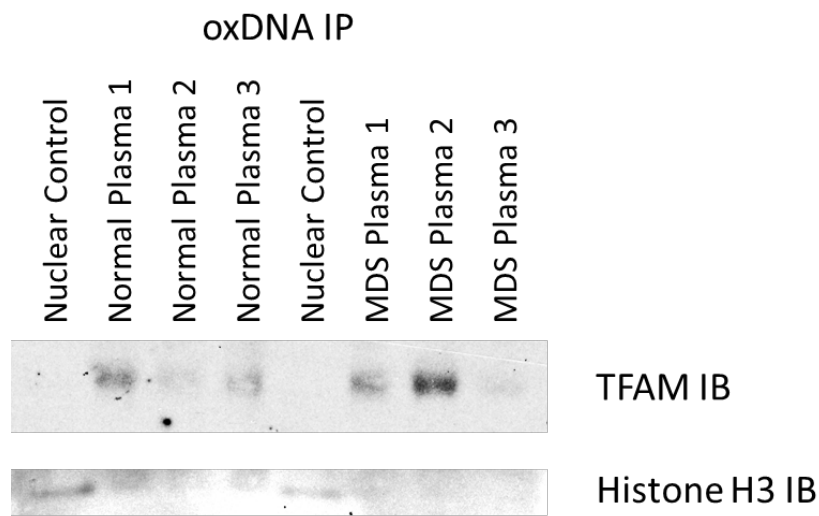
Figure 13: Other identifying variables

Evaluation of log10, glucose adjusted oxDNA with (**A**) Gender (B) Race (**C**) Co-existing autoimmune disease (**D**) Alcohol Usage (**E**) Tobacco Usage. Ox-DNA levels are not significantly related to any of these factors.
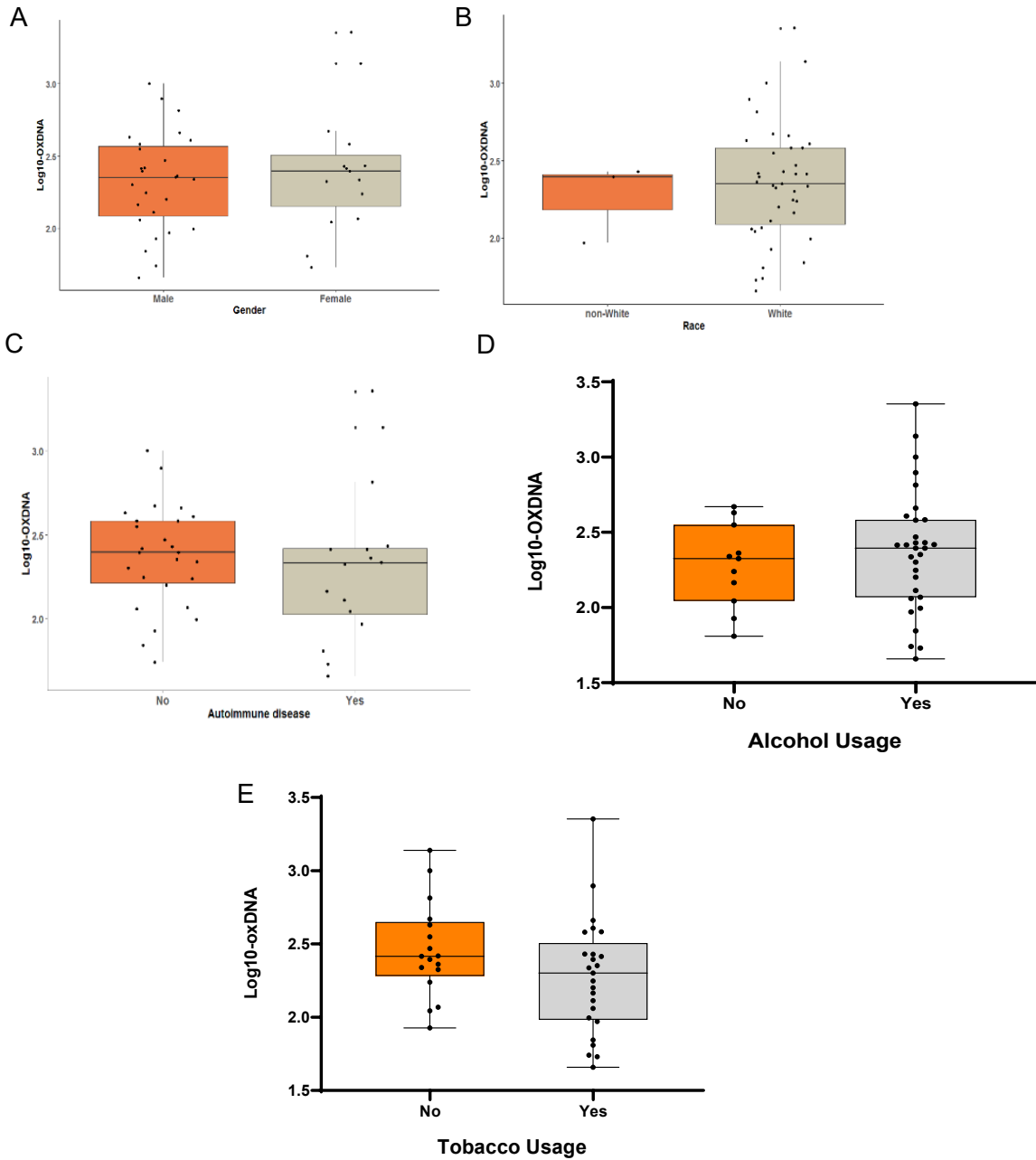
Figure 14: ox-mtDNA and cytopenias

A).
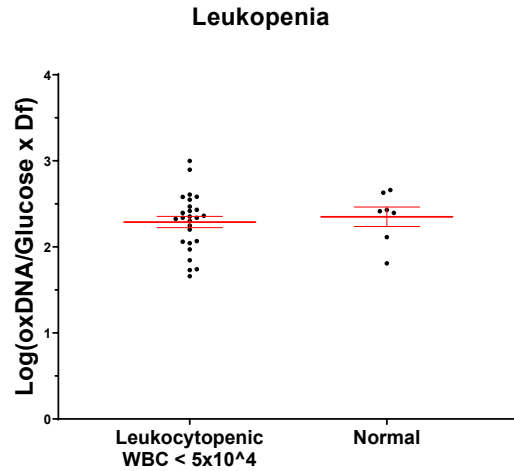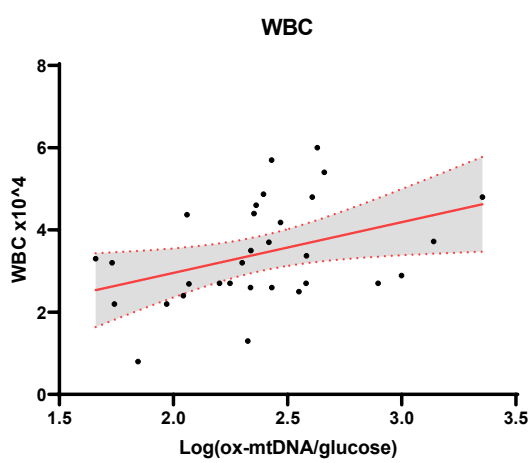
B).
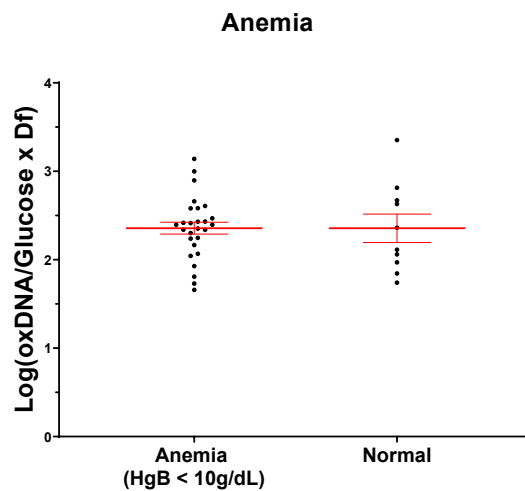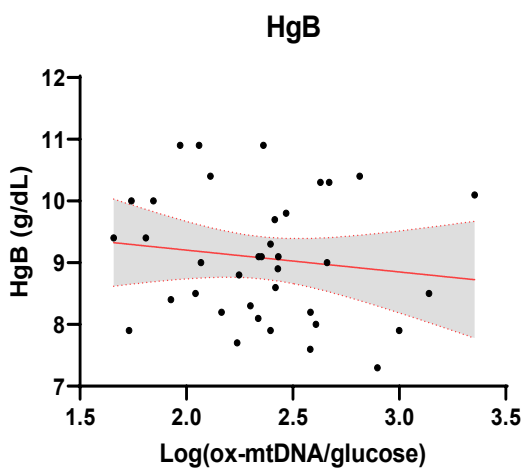
Correlation and levels of log10, glucose adjusted oxDNA with (**A**) white blood cell count
and leukopenia (WBC <5x10⁴) (**B**) hemoglobin levels and anemia (HgB <10 g/dL),

Figure 14 Cont.

(**C**).
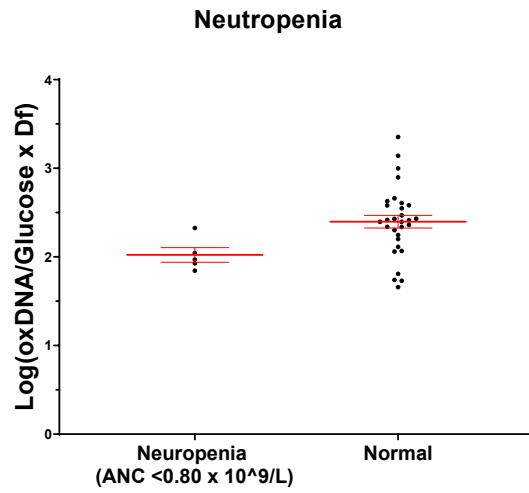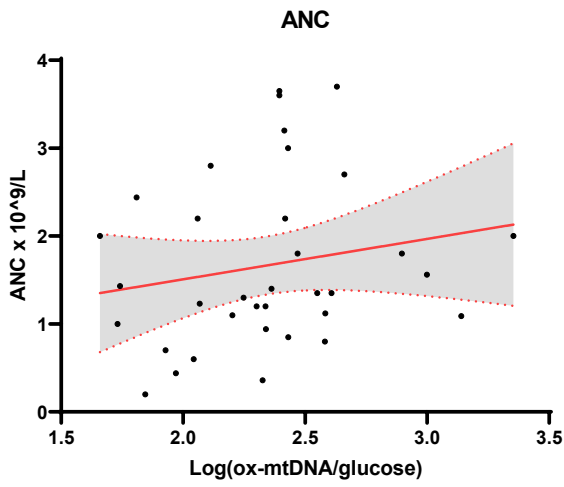
D).
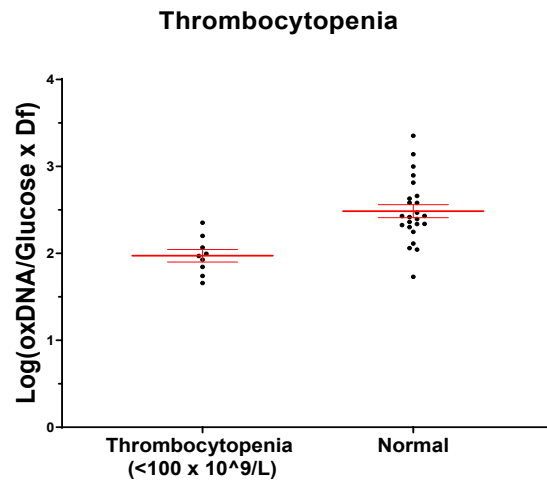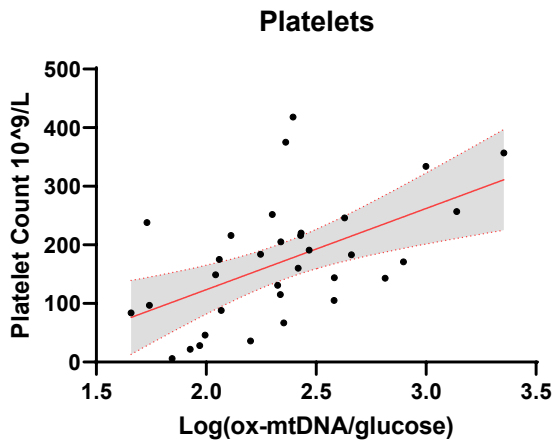
C) absolute neutrophil count and neutropenia (ANC <0.80 x10^9/L) (**D**) platelet count and

thrombocytopenia (platelets <100 x10^9/L)

Figure 14 Cont.

E).
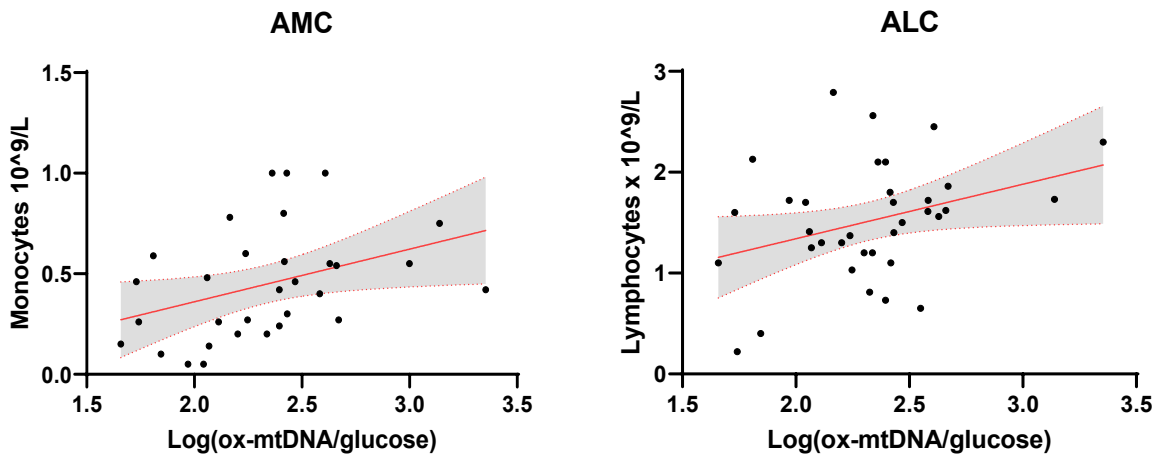
F).
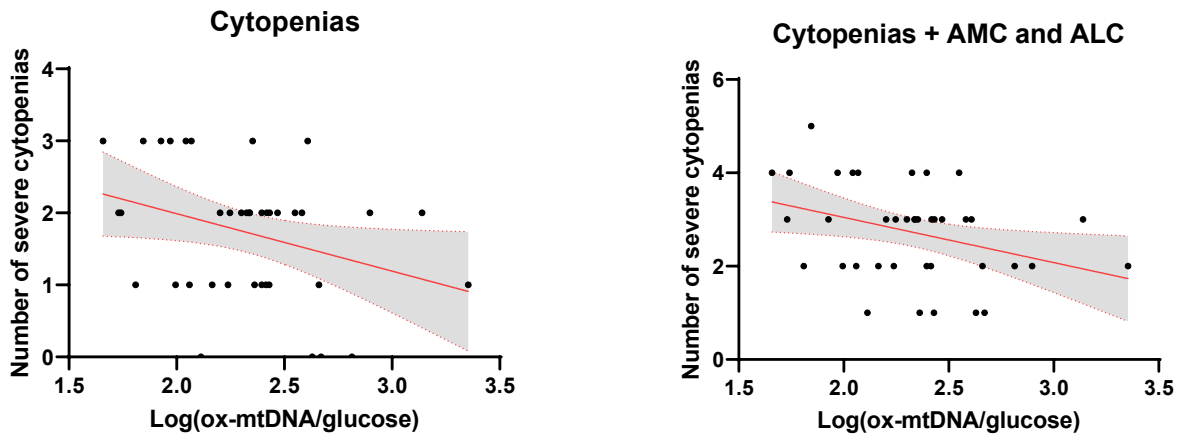
(**E**) absolute monocyte (AMC) and lymphocyte counts (ALC), (**F**) number of cytopenias

(HgB, ANC, WBC, platelets, and cytopenias with AMC and ALC added.

Table 3*: MDS PB ox-mtDNA stratified by WHO subtype.*

	n	Mean	Median	sd	p-value*
MDS-5q	22	2.45	2.78	0.29	
MDS-EB1	17	2.46	2.43	0.35	
MDS-EB2	6	2.13	2.12	0.18	
MDS-MLD	36	2.44	2.43	0.38	
MDS-MLD-RS	14	2.39	2.43	0.38	2.96×10^{-2}
MDS-NOS	58	2.63	2.49	0.42	
MDS-SLD	9	2.61	2.58	0.33	
MDS-SLD-RS	30	2.59	2.53	0.356	
MDS-U	6	2.56	2.43	0.39	

Summary statistics of ox-mtDNA in PB plasma of MDS samples stratified by WHO subtype.

Figure 15: ox-mtDNA by WHO and Karyotype
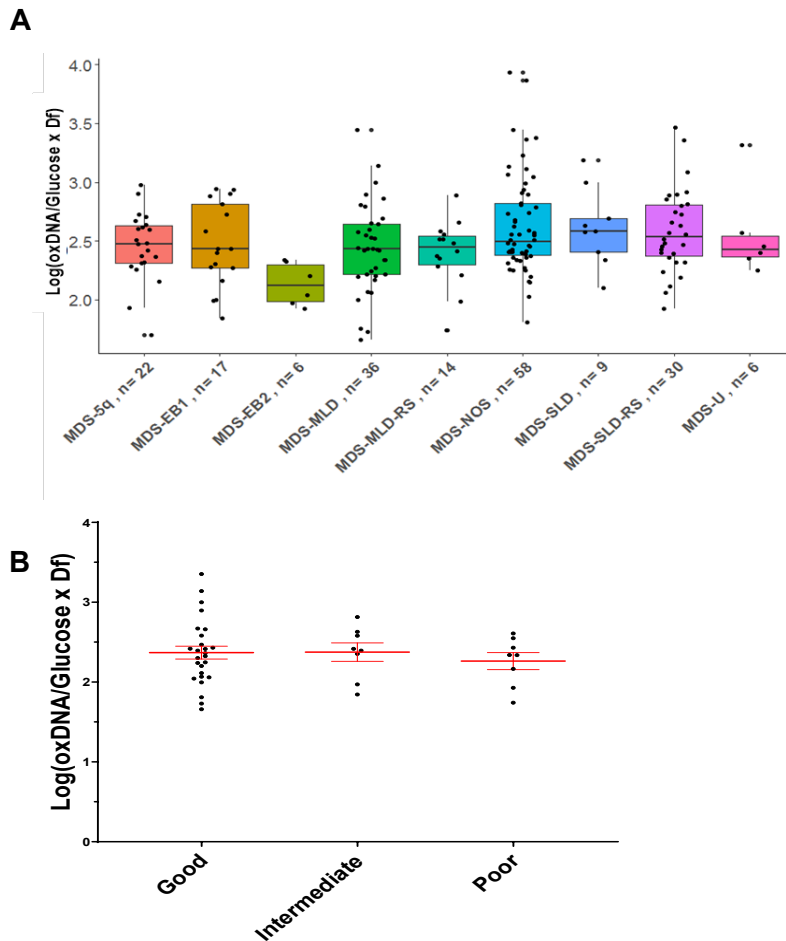
Levels of oxDNA normalized to glucose by (**A**) WHO subtype (**B**) IPSS defined cytogenetic risk group Karyotype defined as: Good: normal karyotype, del(11q) or -Ydel(20q), del(5q), del(12p), or double including del(5q). Intermediate: +8, del(7q), i(17q), +19, or any other single or double independent clone. Poor: -7, inv(3)/t(3q)/del(3q), double including -7/del(7q), or complex (3 or more abnormalities). There is no significant difference between categories, ordinary one-way ANOVA P = 0.7720, n = 42; Good mean = 2.369, Intermediate mean = 2.375, Poor mean = 2.262.

Table 4 Ox-mtDNA stratified by Somatic Mutations

Summary Statistics of Sommatic Mutational Class or Number and Level of Log10-Transformed, glucose-adjused levels of ox-mtDNA levels in PB plasma of MDS samples

	n	Mean	Median	SD	P-value
Splicing gene mutations[a]					4.99×10^{-1}
Yes	86	2.45	2.40	0.55	
No	55	2.45	2.43	0.37	
Methylation gene mutations[b]					9.57×10^{-1}
Yes	62	2.47	2.41	0.61	
No	79	2.43	2.41	0.37	
Transcriptional gene mutations[c]					4.0×10^{-2}
Yes	35	2.36	2.24	0.57	
No	106	2.48	2.42	0.46	
Signaling gene mutations[d]					4.61×10^{-1}
Yes	14	2.50	2.43	0.40	
No	127	2.44	2.40	0.50	
≥1 Mutations					2.44×10^{-1}
Yes	110	2.43	2.41	0.52	
No	31	2.51	2.45	0.37	
Total # of mutations*					
0	31	2.51	2.45	0.37	
1	41	2.42	2.40	0.37	
2	43	2.42	2.42	0.56	9.59×10^{-1}
3	15	2.43	2.31	0.40	
4	10	2.52	2.07	0.97	
5	1	2.41	2.41	NA	

a: SF3B1, SRSF2, U2AF1, ZRSF2

b: TET2, IDH1, DNMT3A, EZH2

c: ASXL1, ETV6, PHF6, RUNX1, SETBP1, TP53, NPM1

d: CBL, JAK2, KIT, MPL, NRAS

*ANOVA

Figure 16: MDS ox-mtDNA stratified by Mutational burden
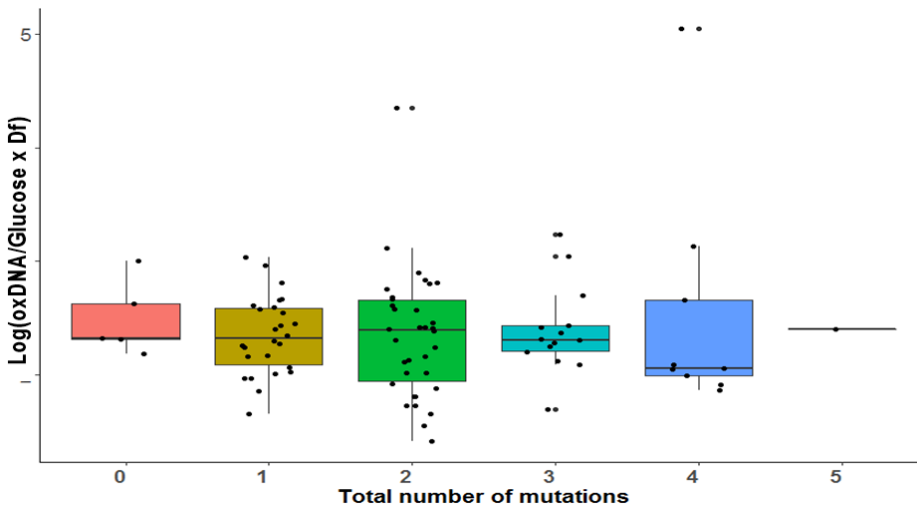
Log10-transformed, glucose-adjusted levels ox-mtDNA levels from MDS peripheral blood stratified by number of mutations present: No significant difference as assessed by ANOVA

Table 5: MDS ox-mtDNA and Mutations

Statistics of somatic mutations and levels of log10-transformed, glucose-adjusted levels ox-mtDNA in PB plasma of MDS samples.

		n	Mean	Median	sd	p-value
SF3B1						2.57×10^{-1}
	yes	71	2.43	2.39	0.59	
	no	70	2.47	2.43	0.37	
SRSF2						8.02×10^{-1}
	yes	8	2.42	2.33	0.34	
	no	133	2.45	2.41	0.50	
U2AF1						5.00×10^{-2}
	yes	3	2.92	2.90	0.38	
	no	138	2.44	2.41	0.49	
ZRSR2						4.81×10^{-1}
	yes	6	2.27	2.40	0.33	
	no	135	2.46	2.41	0.49	
TET2						9.59×10^{-1}
	yes	51	2.51	2.41	0.64	
	no	90	2.42	2.41	0.38	
IDH1						7.42×10^{-1}
	yes	3	2.33	2.40	0.39	
	no	138	2.45	2.41	0.49	
DNMT3A						3.93×10^{-1}
	yes	14	2.45	2.34	0.87	
	no	127	2.45	2.42	0.43	
EZH2						3.43×10^{-1}
	yes	5	2.54	2.58	0.20	
	no	136	2.45	2.41	0.50	
ASXL1						6.70×10^{-2}
	yes	20	2.28	2.18	0.40	
	no	121	2.48	2.41	0.50	
ETV6						4.34×10^{-1}
	yes	4	2.29	2.33	0.18	
	no	137	2.45	2.41	0.49	
PHF6						6.17×10^{-1}
	yes	3	2.99	2.06	1.78	
	no	138	2.44	2.41	0.44	
RUNX1						2.19×10^{-1}
	yes	4	2.22	2.15	0.25	
	no	137	2.46	2.41	0.49	
SETBP1						9.17×10^{-1}
	yes	7	2.38	2.43	0.44	
	no	134	2.45	2.41	0.49	
TP53						8.19×10^{-1}
	yes	3	2.35	2.43	0.22	
	no	138	2.45	2.41	0.49	
NPM1						NA
	yes	1	2.20	2.20	NA	
	no	140	2.45	2.41	0.49	
CBL						4.41×10^{-1}
	yes	4	2.49	2.44	0.12	
	no	137	2.45	2.41	0.50	
JAK2						1.06×10^{-1}
	yes	3	2.10	2.06	0.27	
	no	138	2.46	2.41	0.49	
KIT						2.50×10^{-1}
	yes	2	2.82	2.82	0.58	
	no	139	2.44	2.41	0.49	
MPL						6.50×10^{-1}
	yes	2	2.29	2.29	0.41	
	no	139	2.45	2.41	0.49	
NRAS						9.20×10^{-2}
	yes	3	2.83	2.94	0.37	
	no	138	2.44	2.41	0.49	

Plasma ox-mtDNA concentrations correlate with biomarkers of inflammasome activation

To further investigate the relationship ox-mtDNA and inflammasome activation, we evaluated whether there was a correlation in ox-mtDNA levels and known inflammasome markers. S100A9 and S100A8 are key cell-extrinsic inflammasome activating TLR4 engaging DAMPs in MDS, levels of which can serve as an index of pyroptosis (Basiorka et al., 2016; Simard et al., 2013; Vogl et al., 2007). To evaluate the specificity of ox-mtDNA as a measure of inflammasome activation and pyroptosis, we analyzed the relationship between ox-mtDNA and these DAMPs. Patient plasma ox-mtDNA concentration significantly correlated with S100A8 ($\log_{10}$, glucose-adjusted, n = 134; r = 0.62, *P* = 2.0 x 10^{-15}) and S100A9 concentration ($\log_{10}$, glucose-adjusted; n = 134, r = 0.4, *P* = 2.0 x 10^{-6}) (**Figure 17A**). Further, we previously demonstrated that the percentage of $\log_{10}$-transformed, glucose-adjusted ASC specks is a reliable index of medullary pyroptosis execution in MDS and potentially a disease specific biomarker (Ashley A. Basiorka et al., 2018). ASC specks significantly and positively correlated with ox-mtDNA (n = 134; r = 0.59, *P* = 7.0 x 10^{-14}) (**Figure 17B**). We found that the sensitivity and specificity of ox-mtDNA could not be improved by combining ox-mtDNA and ASC speck levels in the ROC analysis of MDS cases compared to normal controls provided; ox-mtDNA alone had the greatest utility as a biomarker (MDS AUC = 0.940, LR-MDS AUC = 0.950, HR-MDS AUC = 0.934) (**Figure 17C**). These findings indicate that plasma ox-mtDNA concentrations demonstrate a direct correlation with validated indices of pyroptosis, such as ASC specks and S100A9/A8, thereby demonstrating the utility of ox-mtDNA as a biologically relevant biomarker of inflammasome activation.

Figure 17: Plasma ox-mtDNA concentrations correlate with biomarkers of inflammasome activation
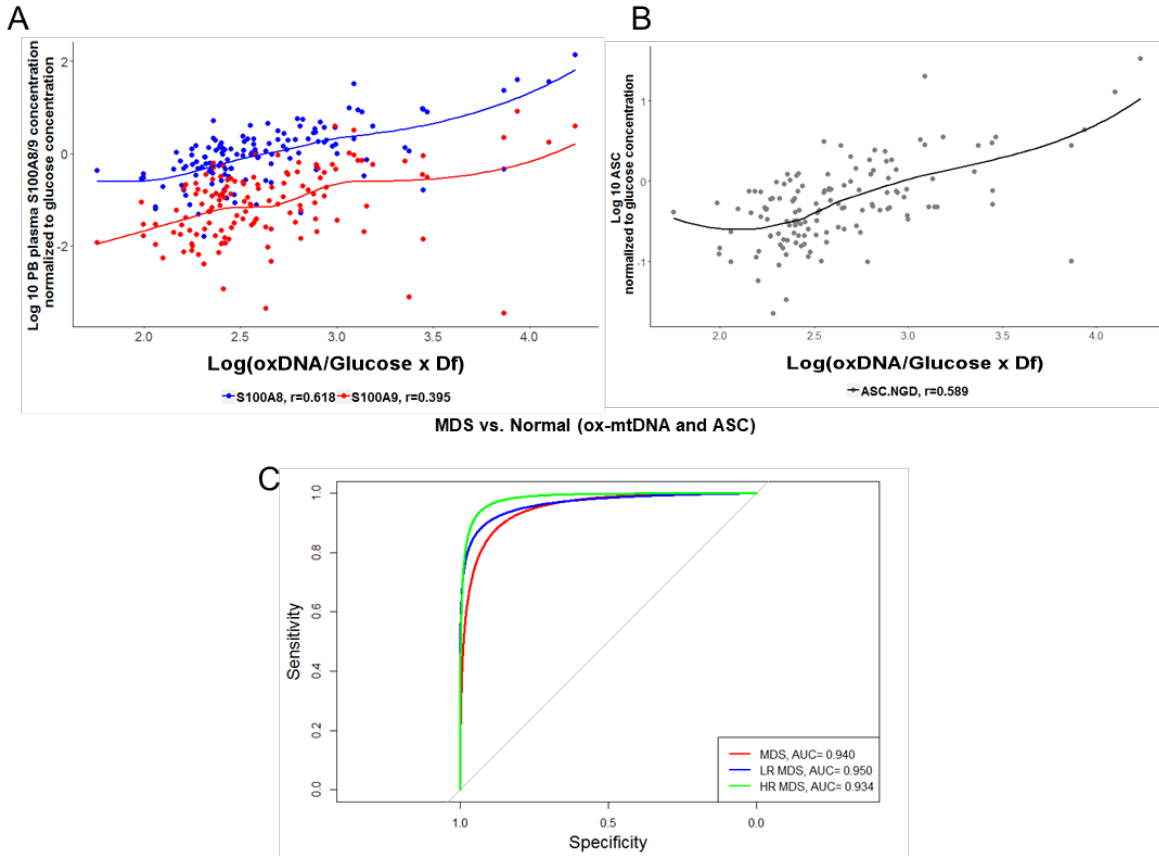
Log10-transformed, glucose-adjusted ox-mtDNA is correlated with known MDS inflammasome activating alarmins in patient PB plasma; (**A**) Log10-transformed, glucose-adjusted S100A8, and S100A9, (**B**) Correlation of Log10-transformed, glucose-adjusted ASC specks and ox-mtDNA. (**C**) ROC/AUC analyses of ox-mtDNA and ASC speck percentage in MDS cases versus controls.

Plasma concentration of ox-mtDNA distinguishes MDS from other hematologic

malignancies

To determine whether elevations in ox-mtDNA plasma levels are specific for MDS, we quantified ox-mtDNA concentration in plasma from patients with non-MDS hematological malignances (**Figure 18A, Table 2**). Further, the inflammasome can be activated due to hyperglycemia which promotes insulin resistance; (Grishman et al., 2012; Lee et al., 2013) therefore, we also analyzed a cohort of 25 type 2 diabetes (T2D) plasma samples with no history of cancer. Log$_{10}$-transformed, glucose-adjusted peripheral blood plasma concentrations of ox-mtDNA were significantly higher in T2D than controls, however, significantly lower than MDS cases (n = 25, *P* = 2.3 x 10^{-21}); Log$_{10}$-transformed, glucose-adjusted peripheral blood plasma ox-DNA levels across disease groups were highest in MDS (n = 177) compared to all other non-MDS hematological malignancies including acute lymphoblastic leukemia (ALL, n = 6, *P* = 2.7 x 10^{-4}), *de novo* (n = 12, *P* = 1.3 x 10^{-6}) and secondary acute myeloid leukemia (AML, n = 26, *P* = 6.5 x 10^{-13}), chronic myeloid leukemia (CML, n = 9, *P* = 1.0 x 10^{-4}), chronic myelomonocytic leukemia (CMML, n = 16, *P* = 1.3 x 10^{-3}), large granular lymphocytic leukemia (LGL, n = 17, *P* = 3.3 x 10^{-5}), myelofibrosis (MF, n = 11, *P* = 2.0 x 10^{-4}), essential thrombocythemia (ET, n = 18, *P* = 2.0 x 10^{-14}), polycythemia vera (PV, n = 18, *P* = 1.2 x 10^{-13}), and multiple myeloma (n = 18, *P* = 1.9 x 10^{-25}) and was shown to be mitochondrial in nature by PCR except for the CLL cohort (**Figure 18A, Table 2**, **Figure 19**).

Of note, ox-mtDNA levels were not significantly higher than levels in chronic lymphocytic leukemia patients (CLL, n = 45, *P* = 0.7) (**Figure 18A, Table 2**). Elevations

in plasma ox-DNA were previously reported in CLL and specifically linked to poor risk chromosomal abnormalities associated with oxidative injury and ROS (Collado et al., 2014; Jitschin et al., 2014; Nelson et al., 2007). When organized into more favorable [normal, del(13q), trisomy 12] and less favorable cytogenetic groups [del(6q), del(11q), and del(17p)], the less favorable cytogenetic CLL patients displayed significantly higher levels of ox-DNA (P = 3.3 x 10^{-2}) (**Figure 20**). Additionally, the less favorable cohort represented a disproportionately high amount of our CLL samples(Nelson et al., 2007). Within our CLL cohort, cell free DNA of nuclear origin was detected in addition to mtDNA. Although oxidized DNA is elevated in CLL, we show that a significant fraction of this DNA is nuclear and readily distinguished from MDS by an accompanying B-lineage lymphocytosis. CLL B-cells also display elevations in cellular ox-mtDNA owing in part to eNOX generation of peroxide in response to B-cell receptor signaling that accumulates as a result of low catalase expression, thereby conferring redox hypersensitivity (Cavallini et al., 2018).

We further investigated key non-malignant reactive conditions including aplastic anemia and pure red cell aplasia (anemia) which exhibit cytopenias without hypercellular and dysplastic bone marrow, as well as in individuals with clonal hematopoiesis of indeterminate potential (CHIP) (Durrani & Maciejewski, 2019; Steensma et al., 2015; Valent et al., 2017). Cases with CHIP or anemia have significantly higher log_{10}-transformed, glucose-adjusted ox-mtDNA PB levels compared to normal donors (P = 2.45 x 10^{-12}, n = 25; P = 7.00 x 10^{-4}, n = 6 respectively) but significantly lower levels than MDS (P = 2.48 x 10^{-16}, P =3.30 x 10^{-4}, respectively **Figure 18A, Table 2**).

We then evaluated whether ox-mtDNA is a specific marker for MDS compared to non-MDS hematological disorders (excluding CLL) using a 5-fold cross-validation (k=5) repeated 30 times. The cross-validation showed that ox-mtDNA was indeed a sensitive and specific biomarker for MDS compared to the other hematological malignancies (MDS AUC = 0.893, LR AUC = 0.909, HR AUC = 0.720) (**Figure 18B**). Similarly, ox-mtDNA is highly specific and sensitive for MDS vs the reactive conditions (T2D, Anemia, CHIP) per cross-validation (MDS AUC = 0.940, LR AUC = 0.960, HR AUC = 0.810) **(Figure 18C).** Importantly, we found that plasma elevation of ox-mtDNA was specific for MDS and not found in other hematologic malignancies with dyshemaopoiesis such as MF, AML, and CMML. These data suggest elevated levels of PB plasma ox-mtDNA are specific to MDS and may be used as a marker for pyroptosis.

Figure 18: Plasma concentration of ox-mtDNA distinguishes MDS from other hematologic malignancies
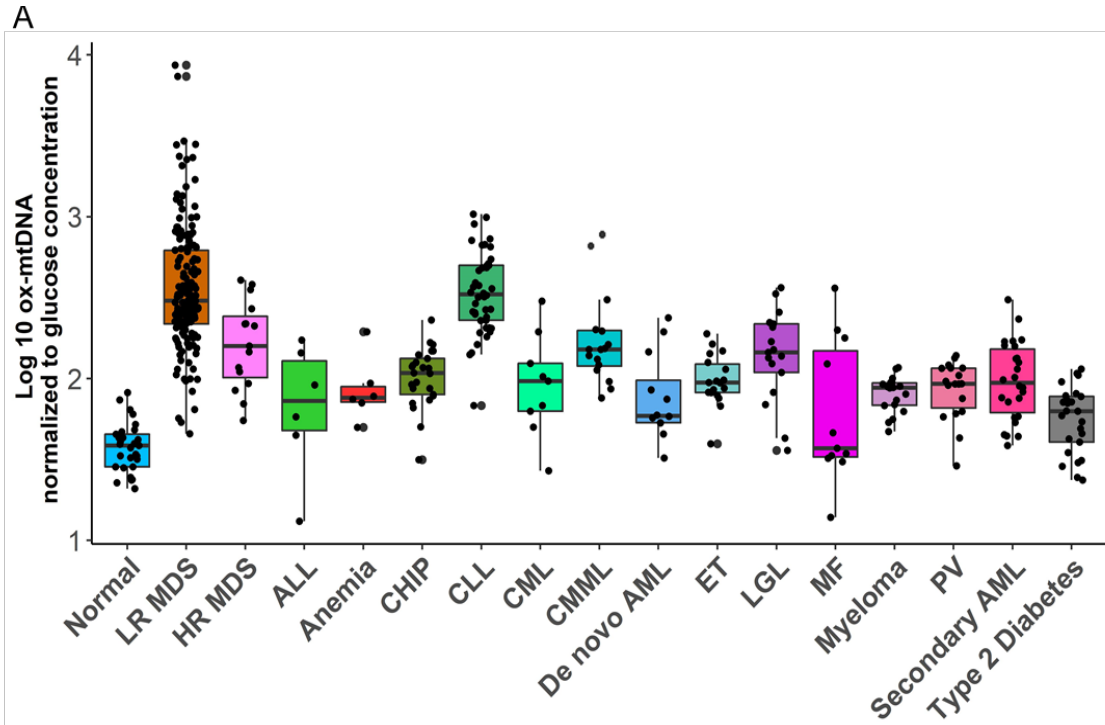
Ox-mtDNA is higher in MDS peripheral blood plasma compared to other hematologic diseases. (**A**) Peripheral blood plasma log 10-transformed, glucose-adjusted ox-mtDNA levels are significantly increased in MDS patients compared to healthy donors, all other hematologic malignancies (except CLL) and in individuals with type II diabetes. ALL, acute lymphocytic leukemia; Anemia (Aplastic & Pure Red Blood Cell); AML, acute myeloid leukemia; CHIP clonal hematopoiesis of indeterminate potential; CLL, chronic lymphocytic leukemia; CML, chronic myelogenous leukemia; CMML, chronic myelomonocytic leukemia; ET, essential thrombocytosis; HR, higher-risk; LR, lower-risk; LGL, large granular lymphocytic leukemia; MDS, myelodysplastic syndromes; MF, myelofibrosis; PV, polycythemia vera; T2D, type II diabetes.

Figure 18 Cont. Plasma concentration of ox-mtDNA distinguishes MDS from other

hematologic malignancies
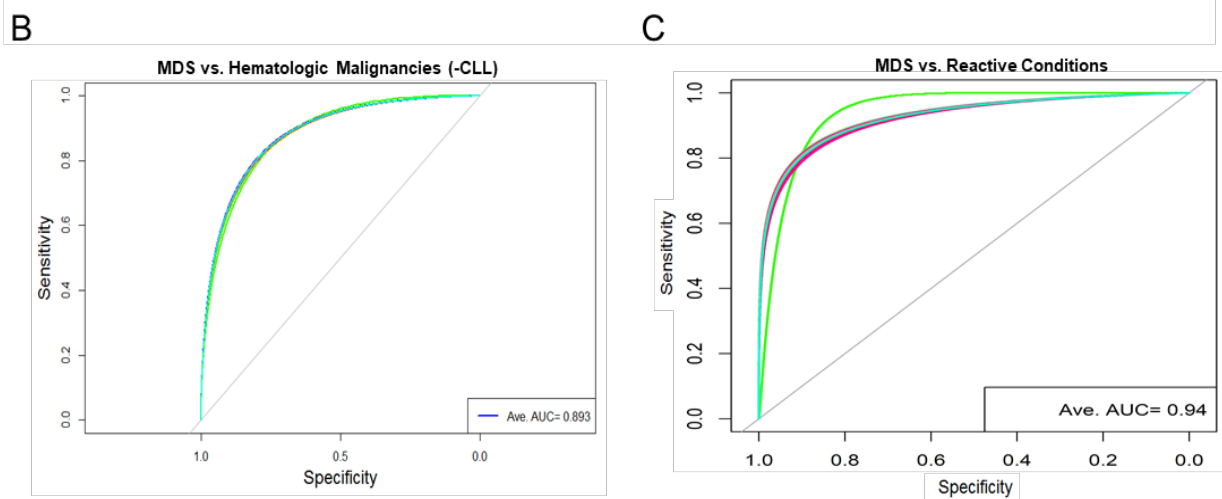
(**B**) Cross-validation analysis of MDS compared to non-MDS hematological controls
(excluding CLL). (**C**) Cross-validation analysis of MDS compared to Reactive Conditions
(T2D, CHIP, Anemia).

Figure 19: DNA isolated from all disease types
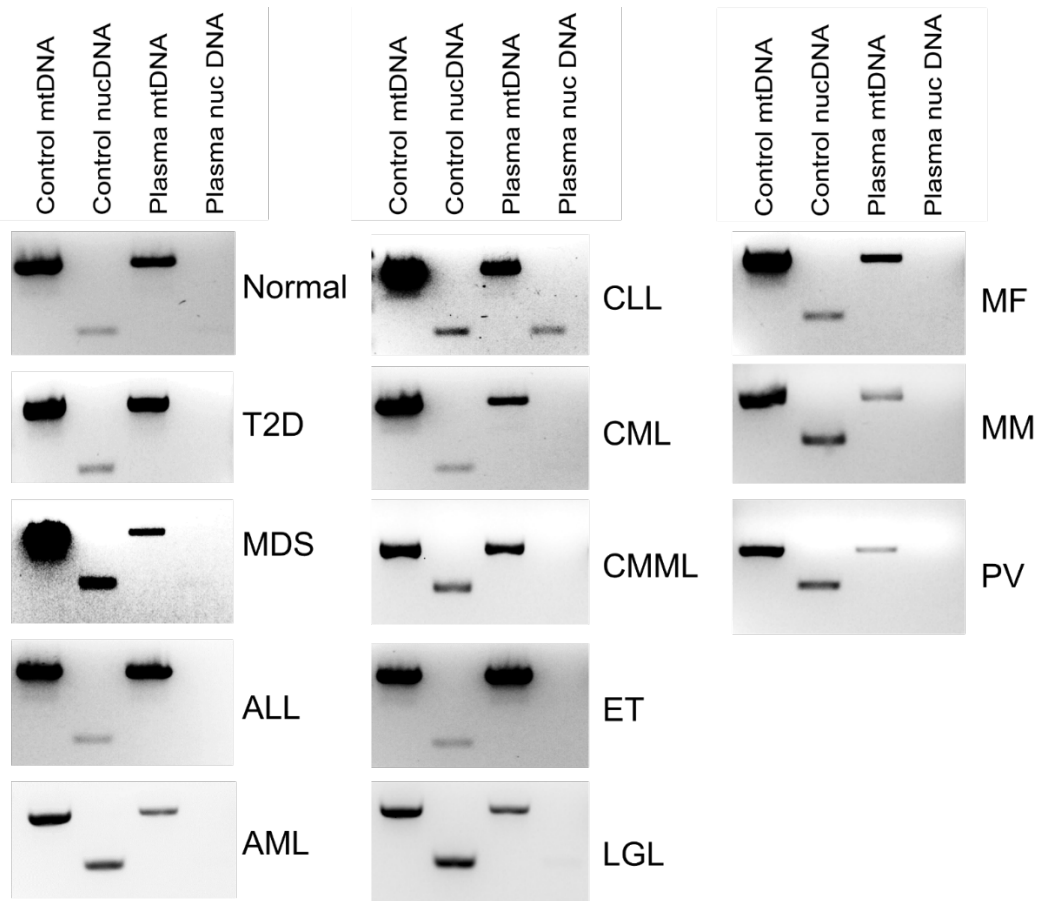
 (3 independent patient samples peripheral blood plasma pooled) amplified with nuclear (nuc) and mitochondrial (mt) primers demonstrating that patient plasma DNA is mitochondrial. ALL, acute lymphocytic leukemia; AML, acute myeloid leukemia; CLL, chronic lymphocytic leukemia; CML, chronic myelogenous leukemia; CMML, chronic myelomonocytic leukemia; ET, essential thrombocytosis; LGL, large granular lymphocytic leukemia; MDS, myelodysplastic syndromes; MF, myelofibrosis; PB, peripheral blood; PV, polycythemia vera; T2D, type 2 diabetes.

Figure 20: CLL Plasma DNA
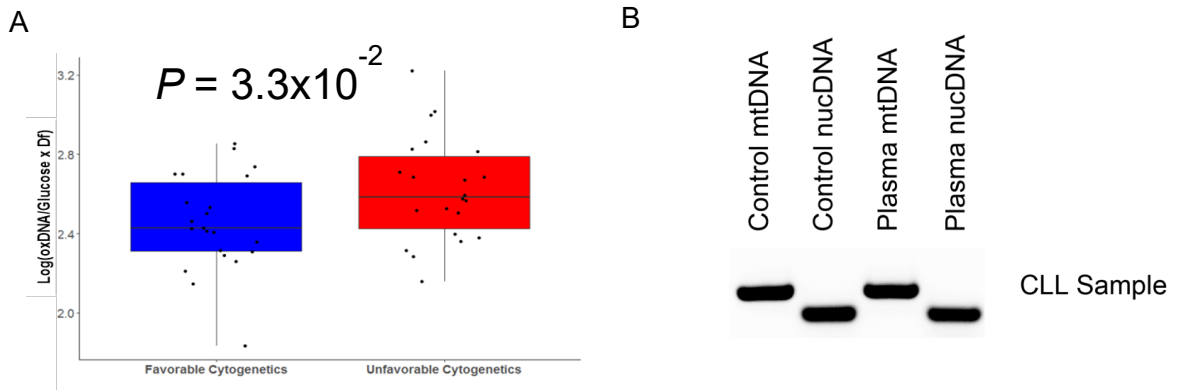
(**A**) DNA isolated from CLL patient peripheral blood plasma was amplified with nuclear (nuc) and mitochondrial (mt) primers demonstrating that DNA is both of nuclear and mitochondrial. Representative image of 4 unique CLL samples. (**B**) Log10-transformed, glucose-adjusted levels ox-DNA levels from CLL peripheral blood (PB) plasma is significantly increased in cases with unfavorable cytogenetics. Favorable: normal cytogenetics, del(13q), trisomy 12: n=22, Unfavorable: del(6q), del(11q), and del(17p): n=22

Table 6: Summary statistics of PB Plasma Log10 Glucose corrected ox-mtDNA in Patients and Healthy participants

	n	Mean	Median	SD	P-value Compared With Normal	P-value Compared With LR MDS	P-value Compared With HR MDS	P-value Compared With MDS
Healthy	29	1.5765	1.585941	0.15	NA	6.9×10^{-44}	1.1×10^{-7}	1.23×10^{-42}
LR-MDS	162	2.557	2.481877	0.38	6.86×10^{-44}	NA	2.1×10^{-4}	NA
HR-MDS	15	2.2089	2.20	0.27	1.1×10^{-7}	2.1×10^{-4}	NA	NA
MDS	177	2.5275	2.452618	0.38	1.2×10^{-42}	NA	NA	NA
ALL*	6	1.8149	1.862336	0.41	4.4×10^{-2}	1.8×10^{-4}	3.6×10^{-2}	2.7×10^{-4}
Anemia*	6	1.9285	1.88186592	0.18	7.0×10^{-4}	2.2×10^{-4}	3.7×10^{-2}	3.3E-04
CHIP	25	2.0085	2.0347573	0.18	2.5E-12	2.4E-17	2.0E-02	2.5E-16
CLL	45	2.5463	2.527587	0.27	1.2×10^{-30}	8.3×10^{-1}	3.6×10^{-4}	7.0×10^{-1}
CML*	9	1.958	1.984861	0.31	9.2×10^{-4}	6.0×10^{-5}	6.0×10^{-2}	1.0×10^{-4}
CMML	16	2.2366	2.179886	0.29	4.9×10^{-8}	5.3×10^{-4}	7.9×10^{-1}	1.3×10^{-3}
De novo AML	12	1.8792	1.770521	0.26	2.3×10^{-3}	6.9×10^{-7}	4.1×10^{-3}	1.3×10^{-6}
ET	18	1.9892	1.975373	0.16	2.1×10^{-10}	2.8×10^{-15}	1.2×10^{-2}	2.0×10^{-14}
LGL	17	2.1418	2.161461	0.28	1.5×10^{-7}	1.3×10^{-5}	5.0×10^{-1}	3.3×10^{-5}
MF	11	1.785	1.570546	0.44	1.5×10^{-1}	1.4×10^{-4}	1.3×10^{-2}	2.0×10^{-4}
Myeloma	18	1.9017	1.943949	0.11	1.1×10^{-10}	1.1×10^{-26}	7.2×10^{-4}	1.9×10^{-25}
PV	18	1.9292	1.967492	0.18	8.9×10^{-8}	2.3×10^{-14}	2.5×10^{-3}	1.2×10^{-13}
Secondary AML	26	1.984	1.973814	0.24	4.1×10^{-9}	1.1×10^{-13}	1.4×10^{-2}	6.5×10^{-13}
T2D	25	1.7453	1.80	0.20	1.4×10^{-3}	2.9×10^{-22}	8.2×10^{-6}	2.3×10^{-21}
Normal discovery	29	1.5765	1.58	0.15	$p=6.1 \times 10^{-1}$ [Ł]			
Normal validation	30	1.5558	1.53	0.15				
MDS discovery	176	2.5275	2.45	0.38	$p=8.4 \times 10^{-10}$ [Ł]			
MDS validation	139	2.2133	2.13	0.47				

*P-values represent Kruskal-Wallis's significance values due to low case numbers.

Ł P-values compare discovery cases to validation cases and discovery normal controls to validation controls

Abbreviations: ALL, acute lymphocytic leukemia; AML, acute myeloid leukemia; CHIP, clonal hematopoiesis of indeterminate potential; CLL, chronic lymphocytic leukemia; CML, chronic myelogenous leukemia; CMML, chronic myelomonocytic leukemia; ET, essential thrombocytosis; HR, higher-risk; LR, lower-risk; LGL, large granular lymphocytic leukemia; MDS, myelodysplastic syndromes; MF, myelofibrosis; PB, peripheral blood; PV, polycythemia vera; T2D, type II diabetes

Discussion

MDS are heterogeneous BM failure disorders with phenotypic similarities to overlap syndromes which requires a high level of experience and expertise in bone marrow disease pathology (Bejar, 2017; Glauser et al., 2013; Tanaka & Bejar, 2019). The addition of diagnostic tools that can discriminate MDS from other hematologic malignancies may have a profound effect on the management of these patients. Our investigations have demonstrated that ox-mtDNA is a sensitive, specific, and objective MDS biomarker that can potentially be utilized as a diagnostic tool. We demonstrated that ox-mtDNA levels are readily, and objectively, quantified by ELISA assay in patient peripheral blood plasma. Diagnostic tools used on peripheral blood are attractive due to the decreased invasiveness of collecting this tissue compared to bone marrow biopsies which is currently standard practice (Fenaux et al., 2020). Additionally, the assay is in an easy-to-use ELISA setup that can be readily scaled for many patients; it works with peripheral blood, which is more accessible and comfortable for patients.

Importantly, we found that elevation in plasma ox-mtDNA was specific for MDS with unique activation of the NLRP3 inflammasome. Our investigations show that plasma ox-mtDNA is a biomarker of medullary pyroptosis in MDS, whose plasma levels directly correlate with other validated indices of pyroptosis, such as concentrations of the S100A8/9 proteins and circulating ASC specks (Ashley A. Basiorka et al., 2018). Of particular interest, inclusion of these additional biomarkers into the ROC analysis did not improve the sensitivity or specificity for MDS over ox-mtDNA alone.

DAMP-induced sterile inflammation in the BM of MDS patients leads to unrestrained inflammasome activation and subsequent pyroptosis, resulting in HPSC

cell death by pyroptosis impeding blood cell maturation and differentiation resulting in patient pancytopenia and malignant clone expansion. Intracellular ox-mtDNA has been shown to associate with NLRP3 stabilizing the protein in an activated state (Zhong et al., 2018). Importantly, although other studies have proposed that ox-mtDNA is an obligate intracellular effector of NLRP3 inflammasome activation, our findings that inflammasome activation by TLR4 ligands is preserved in mtDNA depleted rho0 cells indicates that intracellular mtDNA is dispensable for inflammasome activation (Shimada et al., 2012; Zhong et al., 2018). Future studies should elucidate the role of ox-mtDNA in MDS HSPC inflammasome activation and its potential as a novel therapeutic target. Identification of an important novel local trigger and DAMP, namely ox-mtDNA, may be contributing to this phenotype has clinical implications. By identifying this of inflammasome activation we exposed new understandings of the MDS biologies. Delineating the mechanism of ox-mtDNA-initiated inflammasome activation may allow for the development of novel therapeutic strategies for the treatment of MDS.

Figure 21: MDS Diagnostic Journey
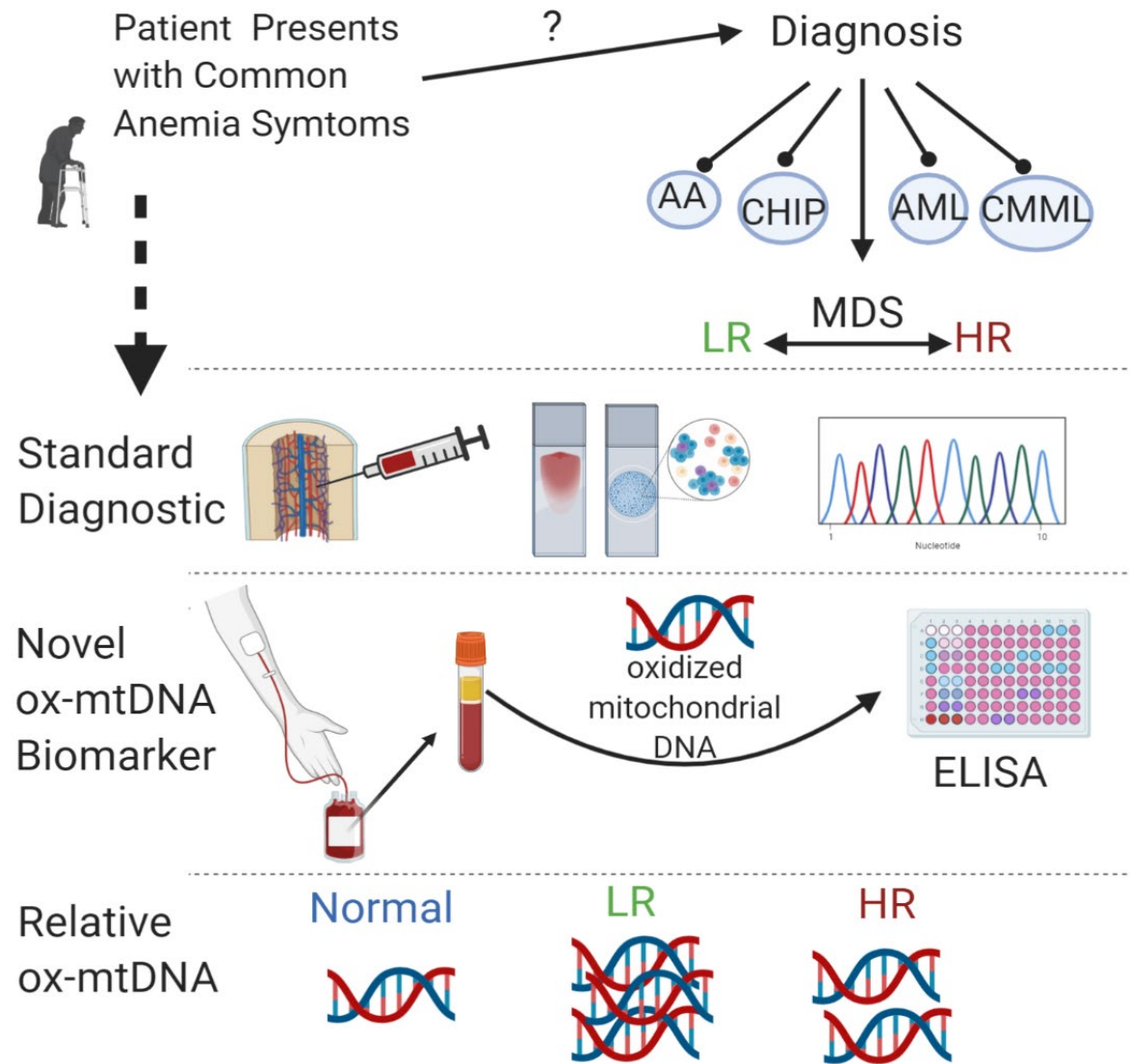
Chapter 4: Oxidized Mitochondrial DNA Engages TLR9 to Activate the NLRP3

Inflammasome in Myelodysplastic Syndromes

Abstract

Myelodysplastic Syndromes (MDS) are bone marrow (BM) failure malignancies characterized by constitutive innate immune activation, including Nlrp3 inflammasome (IFM) driven pyroptotic cell death. We recently reported that the danger-associated molecular pattern (DAMP) oxidized mitochondrial DNA (ox-mtDNA) is diagnostically increased in MDS plasma (Ward et al., 2021) although its role in MDS remains poorly understood. Newly synthesized ox-mtDNA is released into the cytosol upon Nlrp3 IFM pyroptotic lysis where it induces IFM activation and pyroptotic cell death, and upon cytolysis is engaged by TLR9 in neighboring cells increasing inflammation and further release. Ox-mtDNA is recognized as a DAMP by Toll-like receptor 9 (TLR9), an endosomal, DNA sensing pattern recognition receptor that primes and activates the IFM response that is known to be modulated through the oncogenic process. Thus, we hypothesized that ox-mtDNA propagates the IFN-induced inflammatory response in neighboring cells through TLR9 enhancing hematopoietic stem and progenitor cells (HSPC) pyroptotic cell death. We found that extracellular ox-mtDNA triggers the TLR9-myd88-IFM pathway, demonstrated by increased lysosome formation, IRF7 translocation and interferon-stimulated gene (ISG) production. Extracellular ox-mtDNA also induces TLR9 redistribution in MDS HSPC to the cell surface. The effects on Nlrp3

IFM activation were validated by blocking TLR9 activation via chemical inhibition and CRISPR knockout demonstrating that TLR9 was necessary for ox-mtDNA-mediated IFM activation. Inversely, lentiviral overexpression of TLR9-induced sensitization of cells to ox-mtDNA. Lastly, inhibiting TLR9 restored hematopoietic colony formation in MDS BM. We conclude that MDS HSPC are primed for IFM activation via ox-mtDNA released by neighboring pyroptotic cells. Blocking the TLR9/ ox-mtDNA axis may prove to be a novel therapeutic strategy for MDS.

Figure 22: Strategies for Targeting the ox-mtDNA/TLR9 Signaling Axis in MDS
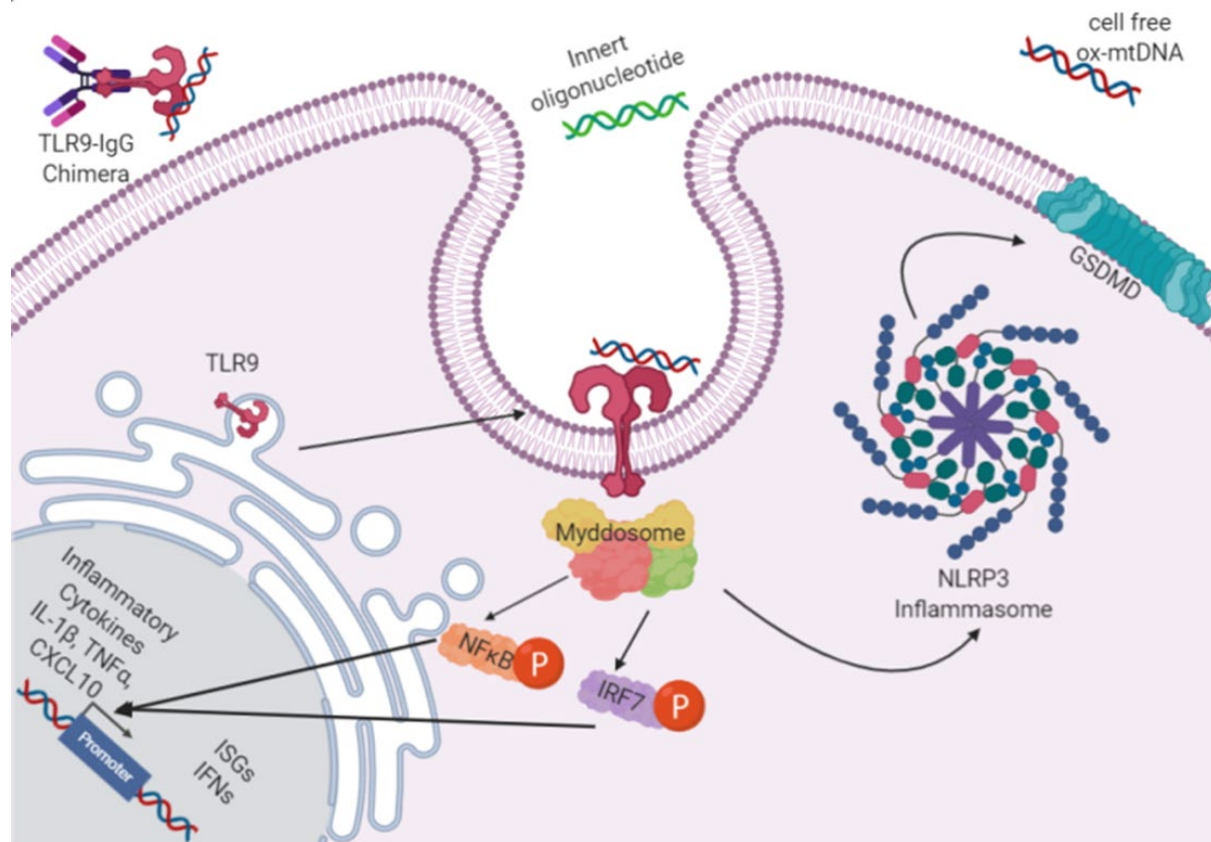
Introduction

Myelodysplastic Syndromes (MDS) are bone marrow failure diseases typified by chronic bone marrow inflammation, ineffective hematopoiesis, and peripheral blood cytopenias (Estey, 2007; Look, 2005; Nimer, 2008). We and others demonstrated that the danger-associated molecular pattern (DAMP) protein S100A9 plays a critical role in the pathogenesis and progression of MDS by creating an inflammatory microenvironment (Basiorka et al., 2016; X. Chen et al., 2013b; Schneider et al., 2016; Zambetti et al., 2016). S100A9 engages TLR4 to initiate an inflammatory form of cell death termed, pyroptosis within, hematopoietic stem and progenitor cells (HSPC) that is mediated through the Nod-like receptor 3 (NLRP3) inflammasome (IFM), leading to the induction of clinically evident ineffective hematopoiesis (Basiorka et al., 2016). Constitutive IFM activation and pyroptosis prevents HPSCs from maturing to terminally differentiated blood cells, causing the pancytopenia and contributing to expansion of the malignant clone clinically manifest in the disease. Upon pyroptotic execution, cells expel their intracellular contents, including DAMPs, into the extracellular space triggering a feed-forward process that propagates IFM and innate immune activation in neighboring cells (Jorgensen et al., 2016). Elucidating those signals contributing to IFM assembly is important for understanding why the IFM is constitutively active in MDS, which may identify novel therapeutic targets or approaches.

Elevated levels of cell-free DNA have been reported in chronic inflammatory disorders (Giles & Boackle, 2013; Hajizadeh et al., 2003). Increased levels of cellular and mitochondrial reactive oxygen species (ROS) are also induced during pyroptotic

events in MDS which not only further contributes to IFM activation but also contributes to the release of cell-free nucleic acid DAMPs into the extracellular space (G. Y. Chen & Nunez, 2010; Collins et al., 2004; Lotze et al., 2007; Q. Zhang et al., 2010; Zhong et al., 2018). Among the DAMPs released by pyroptotic cytolysis of HSPC is ROS-oxidized mitochondrial DNA (ox-mtDNA) which leaks into the cytosol upon mitochondrial membrane depolarization and is recognized by pattern recognition receptors. Ox-mtDNA then aids in the amplification of pyroptotic cell death by direct engagement and activation of NLRP3 IFM, in addition to the DNA-recognition receptors, such as Toll-like receptor (TLR)-9 (Grishman et al., 2012). Recently we demonstrated the diagnostic importance of ox-mtDNA release in MDS by showing a profound elevation of this DAMP in the peripheral blood of MDS patients, compared to healthy donors, which can even be directly increased with the addition of somatic gene mutations to murine models, suggesting that DAMPs like ox-mtDNA aid in the maintenance of the evolutionary pressures that give rise to the malignant clone in MDS (Ward et al., 2021). Therefore, a better mechanistic understanding of the role of ox-mtDNA in MDS pathogenesis warrants further investigation.

In the current study we investigated whether the pyroptotically released DAMP ox-mtDNA mechanistically acts as a catalyst of inflammasome activation to perpetuate bone marrow failure in MDS. We found that ox-mtDNA plays a critical role in the maintenance of the pyroptotic microenvironment via engagement of the TLR9 receptor. Ox-mtDNA affected TLR9 cellular localization, which normally resides in the endoplasmic reticulum (ER), by instead increasing its expression at the surface of MDS cells allowing for the formation of functionally active MyDDosome (MyD88) signaling

complex (Paludan, 2015). Importantly, the use of potential therapeutic strategies that specifically interrupt the TLR9/ox-mtDNA signaling axis decreases inflammatory cell death of HSPC and improves hematopoietic colony forming capacity. Hence our work demonstrates a novel targetable axis in MDS that can have clinical consequences for MDS, a disease with few therapeutic options available.

Methods

Patient Samples

Normal samples were obtained from Stem Express (Folsom California). MDS patient samples were acquired on IRB approved protocols and stratified according to the International Prognostic Scoring System (IPSS). LR is IPSS<1 and HR is IPSS ≥ 1.5.

Cells

THP1 (TIB-202), HEL 92.1.7 (TIB-180) and U937 (CRL-1593.2) cells were obtained from American Type Culture Collection (ATCC) and SKM1 (ACC 547) from the Leibniz-Institute DSMZ–German Collection of Human & Animal Cell Lines. They were maintained in RPMI 1640 (Thermo Fisher Scientific, Waltham, MA.) supplemented with 10% FBS (Corning Incorporated, Corning, NY) and 1% penicillin-streptomycin. THP1 and HEL overexpressing TLR9 were transduced via lentiviral infection, with pcDNA3-TLR9-YFP which was a gift from Doug Golenbock (Addgene plasmid #

13642; http://n2t.net/addgene:13642; RRID:Addgene_13642). Three days post-infection cells were selected with Neomycin and expanded.

Colony forming capacity

MDS patient bone marrow mononuclear cells (BM-MNC), treated as described in the results, were plated in duplicate in 35 mm culture dishes (1×10^5 cells/dish) in complete methylcellulose media (MethoCult™ H4434 Classic, StemCell Technologies), as previously described(Basiorka et al., 2016; Eksioglu et al., 2017a) and following the manufacturer's recommendations. Dishes were incubated at 37°C in 5%CO_2 for 10-14 days, at which point colonies were counted using the StemVision microscope (Catalog # 22006, StemCell Technologies) and used the CFU counting software of the instrument for "14-day human bone marrow" culture to standardize the results. Colony counting of the software was then validated by manual recounting.

CRISPR

U937 and SKM1 TLR9-deficient cells were created using CRISPR CRIPSR/Cas9 gene editing with RNA guides TLR9 (F- CACCGTTGCAGTTCACCAGGCCGTG R- AAACCACGGCCTGGTGAACTGCAAC), or Scrambled control (F- GACGGAGGCTAAGCGTCGCA, R- TGCGACGCTTAGCCTCCGTC) into a puromycin resistance pL-CRISPR.SFFV plasmid (pL-CRISPR.SFFV.PAC) that was a gift from Benjamin Ebert (Addgene plasmid # 57829 ; http://n2t.net/addgene:57829 ; RRID:Addgene_57829).(Heckl et al., 2014) Forward and reverse guide oligonucleotides were purchased from Integrated

DNA Technologies (Coralville, IA). CACC on forward and AAAC on reverse oligonucleotides were added 5' for plasmid ligation. Guides containing plasmids were transformed into Stbl3 competent cells. CRISPR plasmids were packaged into lentivirus and transduced as previously described. After 3 days cells were selected with Puromycin and expanded.

Inflammasome Activation

Ox-mtDNA for treatment was synthesized from mtDNA extracted using the Mitochondrial Extraction Kit according to the manufacture's protocol (Active Motif, Carlsbad CA) and amplified by ND1 primers (ND1 Forward: 5'-CCCTAAAACCCGCCACATCT-3'; ND1 Reverse: 5'-GAGCGATGGTGAGAGCTAAGGT-3') with the addition of oxidized guanosine to the nucleotide master mix. **(Figure 24)** Inflammasome assembly was triggered by treating cells with 50ng/mL of DNA eluted in water. The canonical pyroptotic TLR4 signaling pathway was activated in THP1, SKM1 and U937 cells by incubation with LPS, ATP, and nigericin (LAN) (Perregaux & Gabel, 1994). Cells were harvested and used or immediately frozen at -80°C until use. Promega GloMax® Assays (Promega Corporation Madison, WI) were used to assess Inflammasome activation levels including Caspase-Glo® 1 Inflammasome Assay and LDH-Glo® Cytotoxicity Assay according to manufacturer's protocols. Using our previously published methods from Ward et. Al. oxidized mitochondrial DNA (ox-mtDNA) levels were quantified using the DNA/RNA Oxidative Damage (High Sensitivity) ELISA Kit (Cayman Chemical Company, Ann Arbor, MI) (Ward et al., 2021).

Inhibitors

0.5uM IRAK 1/4 inhibitor (Caymen 17540, CAS 509093-47-4), 1 uM ODN 4048-F, TLR9 Antagonist (5'- cctggatgggaa -3') and ODN 2395 control (5'-tgctgcttttgggggggcccccc -3') (Invivogen), 30uM Hydroxychloroquine (HCQ) (Sigma) to ensure accumulation of autophagosomes for imaging, 10uM HCQ was used in 2 week long CFA, 20ug/mL IRS954 (Barrat, Meeker, Chan, Guiducci, & Coffman, 2007; Pawar et al., 2007) , 1μM RU .521 cGAS inhibitor (Aobious, Gloucester, MA). Cells were treated with inhibitors for 1 hour prior to the addition of ox-mtDNA.

Immunofluorescence

Assays performed at room temperature; dilutions made in 2% BSA (Thermo Fisher Scientific) and phosphate buffered saline (PBS). BM-MNC isolated by the Ficoll® Paque (Sigma-Aldrich) method, and cell lines, were washed in PBS (Life Technologies Corporation, Carlsbad, CA), cytospun at 1,000 rpm for 2 minutes, and fixed with BD cytofix (Thermo Fisher Scientific) for 10 minutes at 37°C. Slides were washed in PBS and immediately used or frozen at -20°C until use. Cells were permeabilized with 0.5% Triton X-100 (Sigma-Aldrich), blocked with 2% BSA/PBS, and stained with conjugated primary antibodies. Slides were washed and ProLong® Gold anti-fade reagent with DAPI (Thermo Fisher Scientific) was added with a coverslip. Primary antibodies used at 1:1000 for IF include anti-oxDNA/RNA FITC, which targets oxo-8-dG to label oxDNA (Abcam), CD289 (TLR9) APC, (Thermo Fisher Scientific), IRF7 Alexa Fluor 647, (Thermo Fisher

Scientific). LysoTracker Deep Red (Invitrogen) following manufacture's protocol, with the addition of 30uM Hydroxychloroquine (HCQ) (Sigma) to ensure accumulation of autophagosomes for imaging. Briefly, Lysotracker was added to the cell culture media for a final concentration of 75nM and incubated for 1 hour at 37°C; following which cells were imaged. Slides were imaged with a Leica SP8 laser scanning confocal microscope (Leica Microsystems GmbH, Wetzlar, Germany) where samples were excited with 405, and 488 diode lasers and emissions were tuned to appropriate settings for each dye. Images were captured through a 63X/1.4NA objective lens using two PMT detectors set for DAPI and FITC/Alexa488 detection. All system settings remained consistent for all samples within each experiment. Images were viewed and exported in 8-bit TIF format with LAS X software version 3.1.5 (Leica Microsystems GmbH).

Quantification ASC specks by IF was done by staining cytospins with ASC (Santa Cruz, 1:200) and Alexa 488 goat anti-mouse (1:400) then counting 1-to-2um speck of least 200 cells per group. At least 200 cells per condition were imaged for mean fluorescence intensity (MFI) analysis. Mean Fluorescence Intensity (MFI) was performed on the TIF images with Definiens Tissue Studio version 4.7 (Definiens AG, Munich, Germany). In the software the nucleus detection and cell growth algorithms were used to segment individual cells within each image. Using this cell segmentation, the MFI (scale: 0-255) was calculated from the cells for each image. All data were exported to Microsoft Excel where fold change between controls and mutant or treated was calculated.

Western Immunoblot

Following treatment, the harvested cells were washed twice with cold PBS, and lysed in a RIPA buffer with phosphatase and protease inhibitors for 20 minutes. Immunoprecipitations were done using Protein A and G Agarose, Fast Flow beads (Millipore Sigma, Burlington, MA, according to the manufacturer's protocol. Briefly, 100 uL of plasma diluted 1:3 in PBS was added to 4µg of the ox-DNA antibody and the mixture was rotated at 4°C overnight. The following morning Agarose G beads were washed thrice with cold RIPA buffer then 50 µL were added to each tube of plasma. This mixture was rotated at 4°C for 2 hours following which it was washed thrice with cold RIPA buffer, then boiled for 5 min in Laemmli sample buffer. Protein was separated via western blot on SDS-PAGE gel and transferred to PVDF membranes. Membranes were blocked in 5% milk in PBS with Tween® detergent for 1 hour at room temperature, then incubated in primary antibody (1:1000) overnight at 4°C, washed, then incubated in secondary antibody (1:5000) for 90 minutes at room temperature. The following antibodies were used; caspase-1, NF-κB p65, LC3, TLR9, Histone H3, caspase-3, PARP, IRF7, phospho-TBK1, phospho-IRF7, phospho-IRF3 (Cell Signaling Technology, Inc. Danvers, MA), human IL-1 beta / IL-1F2 (R&D Systems, Inc. Minneapolis, MN), anti-oxDNA/RNA (Abcam), Anti-NLRP3 Antibody (Millipore Sigma), ASC (Santa Cruz), β-actin (Sigma-Aldrich), and appropriate Amersham ECL HRP Conjugated Antibodies (Thomas Scientific, Swedesboro, NJ). Apoptosis positive control was A431 Whole Cell Lysate EGF Stimulated (Rockland Immunochemicals, Inc. Limerick, PA).

ASC oligomerization was used to assess changes in ASC monomers and ASC higher-order oligomer complexes. Briefly, cell pellets were harvested and lysed on ice for 10 min, the result was pelleted for 10m at 5000rpm at 4°C, this pellet was washed twice more in cold PBS, spin for 10m at 5000 rpm at 4°C each time. The pellet was then resuspended in PBS and fresh 2mM Disuccinimidyl suberate (DSS, Thermo Scientific), and incubated on a rotator for 30 min at room temperature. Following this DSS-crosslinking, the resultant was again pelleted for 10m at 5000 rpm at 4°C. The pellet was run on an SDS-PAGE gel with Laemmli sample buffer. Gels were imaged with ASC (Santa Cruz) antibody.

Flow Cytometry

Cryopreserved Normal and MDS BM-MNC were thawed, washed with 2% BSA-PBS, blocked with Human FcR Blocking reagent (Miltenyi Biotec; Bergisch Gladbach, Germany), and stained for CD14, CD33, CD34, CD38, (Becton, Dickinson and Company, Franklin Lakes, NJ) and TLR9/CD289 and CD71 (Thermo Fisher Scientific; Waltham, MA) and resuspended in 0.1uM DAPI (Thermo Fisher Scientific) and run on the BD LSRII (Becton, Dickinson, and Company). FCS files were analyzed using FlowJo v10 (FlowJo LLC. Ashland, Oregon).

Gene expression analysis

RNA extraction was performed using the Qiagen RNeasy Mini Kit (Hilden, Germany) according to the manufacturer protocol. RNA concentration and integrity were verified using the ND-1000 spectrophotometer (NanoDrop Technologies, Wilmington,

DE). RNA was reverse transcribed using qScript XLT cDNA Supermix (QuantaBio, Beverly, MA) according to the manufacturer protocol. *INFB1/Infb1 and GATA1* expression was quantified using TaqMan Advanced Gene Expression Assays, TaqMan Fast Advanced Mastermix, and 7900HT Fast Real-Time PCR System (Life Technologies, Foster City, CA). The rest were amplified using the primer pairs described in expression were quantified using the primers listed in Supplemental Table S4 and SYBR Green PCR Master Mix (Life Technologies) according to manufacturer protocols. Data was analyzed using the ΔΔCt methodology with *ACTB/Actb* expression for TaqMan assays and *GAPDH/Gapdh* for SYBR assays internal control and the healthy/normal BMMNC as the experimental control to calculate fold-change.

Gene expression profiling data was also obtained from 213 WHO-defined MDS patient specimens at time of diagnosis as well as from 20 healthy donors from the National Taiwan University Hospital using the HumanHT-12 v4 Expression BeadChip (Illumina, San Diego, CA).[25] For each sample, 1.5 µg cDNA was hybridized to Illumina HumanHT-12 v4 Expression BeadChip according to the manufacturer's instructions. Intensities of bead fluorescence were detected by Illumina BeadArray Reader, and the results were transformed to numeric values using GenomeStudio v2010.1 Software (Illumina).

Table 7: qPCR primers

Primer name	Sequence
ISG15 Forward	TCCTGCTGGTGGTGGACAAATG
ISG15 Reverse	CCGCTCACTTGCTGCTTCAGGT
CXCL10 Forward	TTGTCCACGTGTTGAGATCATTGCTAC
CXCL10 Reverse	AGACCTTTCCTTGCTAACTGCTTTCA
IFNα1 Forward	GATCTTCAACCTCTTTACCACAA
IFNα1 Reverse	ACACAGGCTTCCAAGTCATTCA
IFNα10 Forward	AGGGCCTTGATACTCCTGGGACAAAT
IFNα10 Reverse	TGGCTTGAGCCTTCTGGAACTGGT
IFNβ1 Forward	AGAAGGAGGACGCCGCATTGAC
IFNβ1 Reverse	TGATAGACATTAGCCAGGAGGTTC
TLR9 Forward	TGAGCCACAACTGCATCTCGCA
TLR9 Reverse	CAGTCGTGGTAGCTCCGTGAAT
ISG15 Forward	GAGAGGCAGCGAACTCATCT
ISG15 Reverse	CTTCAGCTCTGACACCGACA
CXCL10 Forward	AAGTGGCATTCAAGGAGTACCT
CXCL10 Reverse	AACACGTGGACAAAATTGGCT
SAMD9L Forward	AGGAAAATCCTGCATTTCCAGAG
SAMD9L Reverse	GCAAGGGGCTTACACTTTCC
CCL5 Forward	CCCTCACCATCATCCTCACT
CCL5 Reverse	AGAGGTAGGCAAAGCAGCAG
GAPDH Forward	GAAGGTGAAGGTCGGACT
GAPDH Reverse	GAAGATGGTGATGGGATTTC

Sandwich ELISA

The binding efficacy of the TLR9-IgG chimera was assessed using a Bethyl Labs (Montgomery, TX) Sandwich ELISA kit (ELISA Starter Accessory Kit I), following manufacture's protocol for Indirect ELISA. Briefly, 96 well plate was coated with Coating

Buffer and TLR9-IgG chimera or IgG4 was added in a 2-fold dilution curve and incubated for 1 hour at room temperature and wash three times with the Wash Solution. Then the blocking/postcoat solution was added, incubated at room temperature for 30 min and again wash three times with the Wash Solution. Then the ODN 2006 Biotin (Invivogen), 1 hour at room temperature and wash five times with the Wash Solution. Next Streptavidin-HRP (Cell Signaling Technology) was added and incubated for 1 hour at room temperature and wash five times with the Wash Solution. Following which TMB was added and readout on a plate reader to assess binding of the chimera to the CpG.

Statistical analysis

Statistical analyses were performed using GraphPad Prism Software. Statistical significance to assess two treatment groups only were determined by unpaired Student t tests. Statistical significance to assess fold change was determined by paired Student t tests. A one-way ANOVA was applied to other data with multiple comparison analysis when various treatment groups were analyzed. All analysis and graphics show standard error of the mean bars (SEM) and p values < 0.05 are statistically significant.

Results

Extracellular ox-mtDNA is a DAMP that triggers inflammasome activation

Previous studies have reported that ox-mtDNA triggers both localized and systemic sterile inflammation and has been implicated as an indispensable intracellular effector of NLRP3 inflammasome activation (Collins et al., 2004; Garcia-Martinez et al., 2016; Liu et al., 2019; Q. Zhang et al., 2010). We also recently reported that the pyroptosis-induced extracellular ox-mtDNA can serve as an MDS diagnostic marker

(Ward et al., 2021). We validated the increased levels of ox-mtDNA in lower risk (LR) disease, both in peripheral blood (PB) and bone marrow (BM) plasma compared to healthy bone marrow plasma and found increased levels of ox-mt-DNA in both (**Figure 23A**).

To evaluate its role as a non-canonical extracellular DAMP in pyroptosis induction, we treated SKM1 or U937 cells with increasing doses of synthetic ox-mtDNA (5, 50 and 500ng/mL, **Figure 24**) and observed increased phosphorylation of NFκB and cleavage of caspase-1 at 50 ng/mL, indicating the induction of IFM assembly (**Figure 23B**). The 50 ng/mL dosage is similar to the average LR BM ox-mtDNA observed in figure 1A, demonstrating that this level is physiologically relevant. IFM activation was confirmed through the activation of IL-1β at 50 ng/mL ox-mtDNA (**Figure 23C**) and 2-fold increase in caspase-1 activity through the caspase-1 Glo® assay (**Figure 23D**). Additionally, ox-mtDNA treatment resulted in lactate dehydrogenase (LDH) release indicating lytic cell death (**Figure 23E**). Apoptosis-associated speck-like protein containing a CARD (PYCARD, ASC), which are released by IFM activation and are also diagnostically correlated with MDS (A. A. Basiorka et al., 2018), is the NLRP3 adapter protein that polymerizes to form 1-to-2 μm protease resistant filamentous structures, or 'specks' that serve as a platform for caspase-1 binding and are also released upon lytic death (Ashley A. Basiorka et al., 2018; Basiorka et al., 2016; Fernandes-Alnemri et al., 2007). We assessed whether ox-mtDNA induces generation of ASC after treatment with ox-mtDNA and observed a significant increase in ASC speck formation by immunofluorescence (IF) in both cell lines (**Figure 23F-G**) which was confirmed by western blot of ASC oligomerization (**Figure 23H**). Finally, to demonstrate ox-mtDNA

treatment results specifically in activation of pyroptosis, as opposed to apoptosis, we probed for PARP and caspase-3 activation which was absent upon treatment (**Figure 23I**).

Having confirmed that MDS BM plasma has significantly high levels of ox-mtDNA (Basiorka et al., 2016; Ward et al., 2021) and that this excess is sufficient to induce pyroptosis in leukemic cell lines we next assessed if ox-mtDNA can also induce pyroptosis in healthy BM-MNC and disrupt normal hematopoiesis. As expected, treatment with 50 ug/mL ox-mtDNA induced a significant increase in active caspase-1 and lytic cell death (LDH) in healthy bone marrow (**Figure 23J**). Moreover, incubation with ox-mtDNA significantly decreased hematopoiesis of healthy HSPC, evidenced by decreased colonies (**Figure 23K-L,** n=3). Hence, this confirms that ox-mtDNA is a DAMP capable of triggering the NLRP3 inflammasome, in a time and dose dependent manner, in cell lines and primary cells affecting healthy hematopoietic potential.

Figure 23: Extracellular ox-mtDNA is a DAMP that triggers inflammasome activation
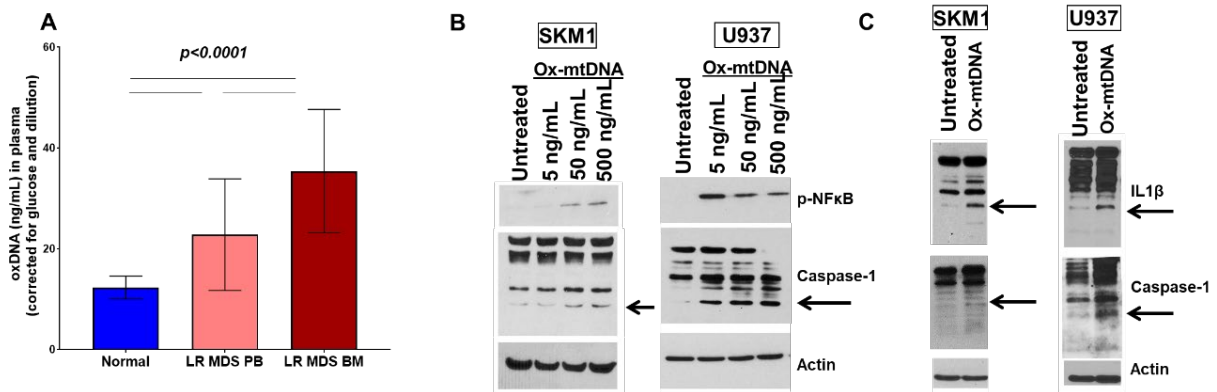
(A) Log10-transformed, glucose-adjusted levels ox-mtDNA levels from Low Risk (LR) MDS peripheral blood (PB) and bone marrow (BM) plasma, and Normal PB. Oxidized-mtDNA induces inflammasome activation in vitro suggesting a feedforward mechanism. U937 and SKM1 cells treated with isolated mtDNA with the ND1 gene region amplified with oxidized guanosine. **(B)** Cells treated with 10-fold increasing ox-mtDNA for 2 hrs to induce Caspase-1 and phosphorylated NFκB to establish dosage. Cleaved Caspase-1 fragment indicated with arrow. <u>Remaining figures, ox-mtDNA treatment is 50ng/mL ox-mtDNA for 2 hours unless otherwise stated.</u> **(C)** Western blot of SKM1 and U937 cells treated with ox-mtDNA showing, cleavage of caspase-1 (arrow depicts cleaved fragment), and IL-1β (arrow depicts cleaved fragment) demonstrating inflammasome activation (representative blot of 3 independent experiments.).

(D) Fold change of caspase-1 activity quantified by Caspase-1 Glo® assay in SKM1 and U937 cells treated with ox-mtDNA, (mean ± SD of three independent experiments). **(E)** Cell death, fold change of LDH media release quantified by LDH-Glo™ Cytotoxicity Assay in SKM1 and U937 cells treated with ox-mtDNA, (mean ± SD of three independent experiments). (F) Representative confocal IF micrographs showing increased ASC specks in ox-mtDNA stimulated cells compared to untreated controls [DAPI (blue), ASC (green) (x2520)]. (G) Quantification of 1-to-2µm ASC speck IF, at least 200 cells counted per group, (mean ± SD of three independent experiments). (H) Immunoblot of ASC following chemical crosslinking, cells treated with ox-mtDNA or positive control LAN (LPS + ATP + Nigericin), arrow indicates oligomers.

Figure 23 Cont.: Extracellular ox-mtDNA is a DAMP that triggers inflammasome activation
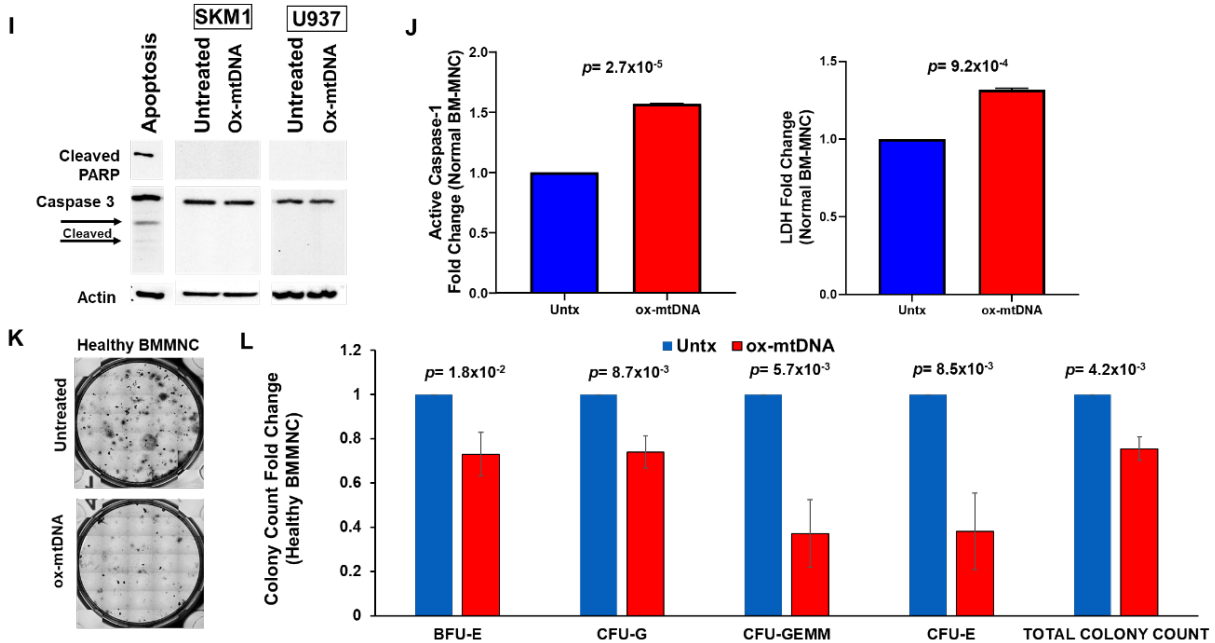
(I) Western Blot for PARP and Caspase-3. Western blot of SKM1 and U937 cells treated with ox-mtDNA, and an apoptosis positive control (A431 EGF Stimulated) showing, induction of PARP1, cleavage of caspase-3 (arrow depicts cleaved fragments), demonstrating that cell death is not driven by apoptosis (representative blots of 3 independent experiments). **(J)** Fold change of caspase-1 activity quantified by Caspase-1 Glo® assay and LDH media release quantified by LDH-Glo™ Cytotoxicity Assay in primary Normal BM-MNC cells treated with ox-mtDNA, (mean ± SD of three independent experiments). **(K)** Colony formation assay for hematopoiesis in Healthy BMMNCs treated with 50ng/mL ox-mtDNA for 14 days. **(L)** Quantification of various erythroid, lymphoid, and myeloid colonies in response to treatment: 50ng/mL ox-mtDNA for 14 days (mean ± SD of three independent experiments).

Figure 24: Oxidized mitochondria DNA Synthesis.
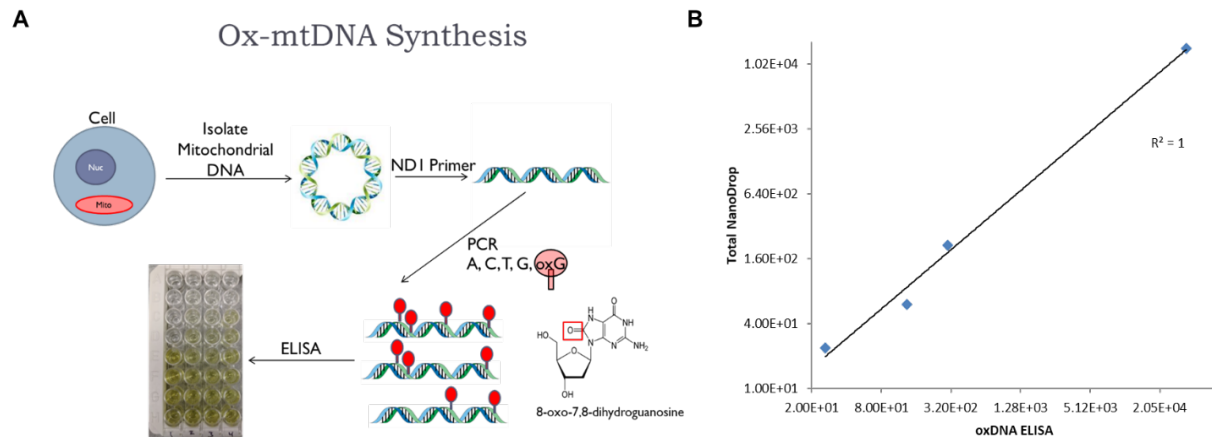
A) Schematic: Mitochondrial DNA was isolated from THP-1 cells via the Mitochondrial Extraction Kit according to the manufacture's protocol (Active Motif, Carlsbad CA) and amplified by the mitochondrial specific ND1 primers (ND1 Forward: 5'-CCCTAAAACCCGCCACATCT-3'; ND1 Reverse: 5'-GAGCGATGGTGAGAGCTAAGGT-3') with the addition of oxidized guanosine to the nucleotide master mix. **B)** Quantification: Synthesized ox-mtDNA was added to the DNA/RNA Oxidative Damage (High Sensitivity) ELISA Kit (Cayman Chemical Company, Ann Arbor, MI) to confirm oxidation.

MDS HSPC and Leukemic Cell Lines have increased expression of TLR9

The observation that ox-mtDNA can induce direct effects on hematopoiesis indicates recognition by the target cells. An inflammatory receptor of cell free DNA is TLR9, which has also been shown to play a role in pyroptosis activation (Kumar, 2020). We observed abundant cytosolic ox-mtDNA in MDS HSPC which colocalized with TLR9 by confocal immunofluorescence, compared to healthy BMMNC that had decreased expression of both and no co-localization of ox-mtDNA and TLR9 (**Figure 25A, Figure 26**). This colocalization was validated by demonstrating that MDS cells had an average of 92% of ox-mtDNA bound to TLR9 compared to 72% in normal donors (**Figure 25B**). We then validated that the cytosolic concentration of ox-mtDNA was significantly increased in the cytoplasm of BM-MNC from MDS specimens, compared to healthy controls (**Figure 25C**), comparable to our observations of increased circulating levels of ox-mtDNA in peripheral blood, and a 2.5-fold increase in TLR9 gene expression in MDS HSPC (**Figure 25D).** confirming previous results showcasing higher TLR9 gene expression in MDS (Kuninaka et al., 2010). Importantly, we found that TLR9 surface expression is increased in MDS, compared to healthy BMMNC (**Figure 25E, Figure 27**) and particularly in the stem (CD34$^+$CD71$^-$CD14$^-$, CD34$^+$CD33$^-$) and progenitor (CD34$^+$CD38$^-$) populations (**Figure 25F, Figure 27**). While the overall CMP (CD34$^+$CD38$^-$) population was not significantly different between MDS and healthy specimens within this small sample size (Normal n=3, MDS n=6), when stratified by risk showed that Lower Risk samples were significantly higher than healthy and Higher Risk samples (**Figure 25G**), similar to our observations that circulating ox-mtDNA is higher in

lower risk specimens (Ward et al., 2021) and that of other showing TLR9 reduction during transformation (Kuninaka et al., 2010).

TLR9 circulates through the cytoplasm and extends to the surface prior to coming to the lysosomes where it meets in proximity with MyD88 and becomes functional (Kumar, 2020). We observed a strong lysosome induction, as read by LC3 and Lysotracker® Deep Red, in MDS samples compared to controls **(Figure 25H-I)**. This increased lysosome activation in the MDS HSPC suggests that the TLR9 pathway is triggered and functional in this disease. We further linked this phenomenon to excess ox-mtDNA in the plasma of MDS patients by demonstrating that treatment of normal BM-MNC with ox-mtDNA results in increased lysosomes with internalized ox-mtDNA and TLR9 phenocopying MDS (**Figure 25I**). This suggests that ox-mtDNA binds to and functionally activates TLR9 in MDS.

Figure 25: MDS HSPC Display Surface TLR9 Induced by Cell Free ox-mtDNA
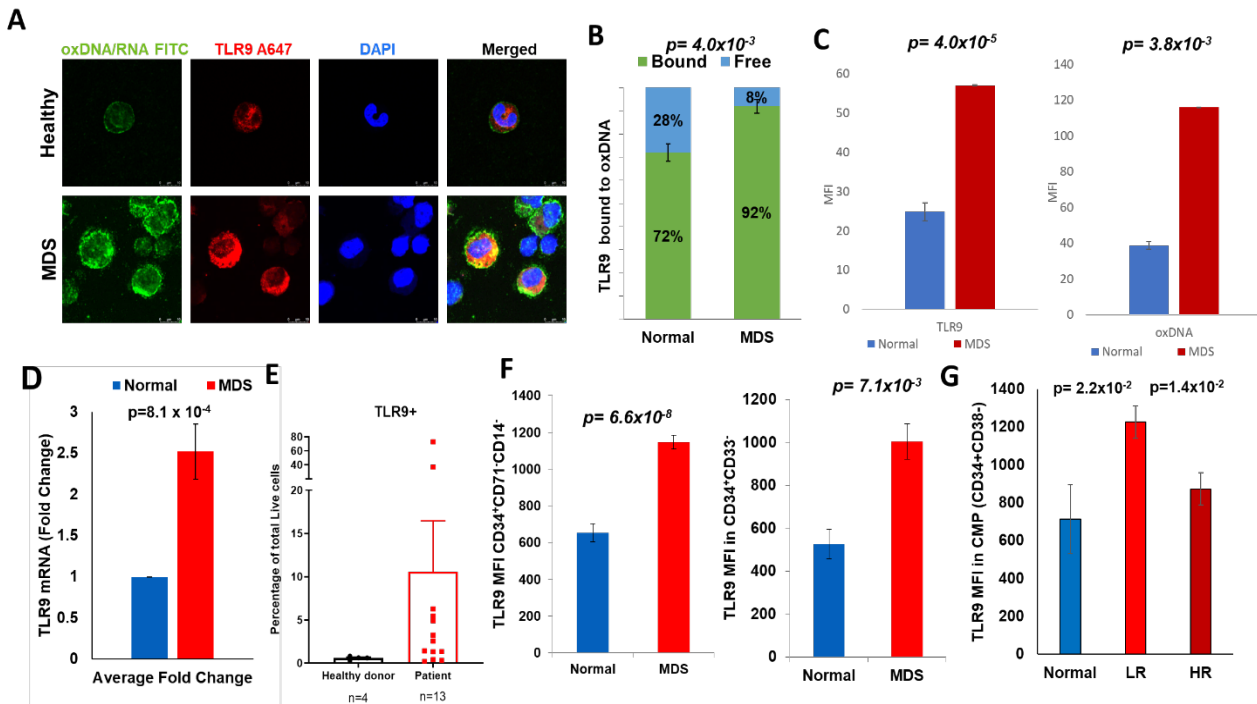
(A) Confocal IF of colocalized TLR9 and ox-mtDNA in MDS BM-MNC samples compared normal BM-MNC samples (x2520, DAPI, ox-mtDNA FITC, TLR9 A647). Representative Micrographs. **(B)** Mander's Coefficient of Colocalization TLR9 bound to ox-mtDNA **(C)** Quantification of fluorescence of TLR9 and oxDNA, comparing Normal and LR MDS BMMNC (minimum 200 cells per sample, three samples per groups, mean MFI ± SD). **(D)** Quantitative PCR to assess the relative expression of TLR9 mRNA, (mean ± SD. 4 normal, 4 LR MDS samples). Flow cytometry analysis of TLR9 surface expression Normal and MDS BMMNC **(E)** all live cells (Normal =4, MDS/MPN = 13), **(F)** $CD34^+$, $CD71^-$, $CD14^-$ cells, and $CD34^+$ $CD33^-$ (Normal =3, MDS = 6), **(G)** Common Myeloid Progenitors, $CD34^+$, $CD38^-$ (Normal =3, LR MDS = 3, HR MDS = 3).

Figure 25 Cont.: MDS HSPC Display Surface TLR9 Induced by Cell Free ox-mtDNA
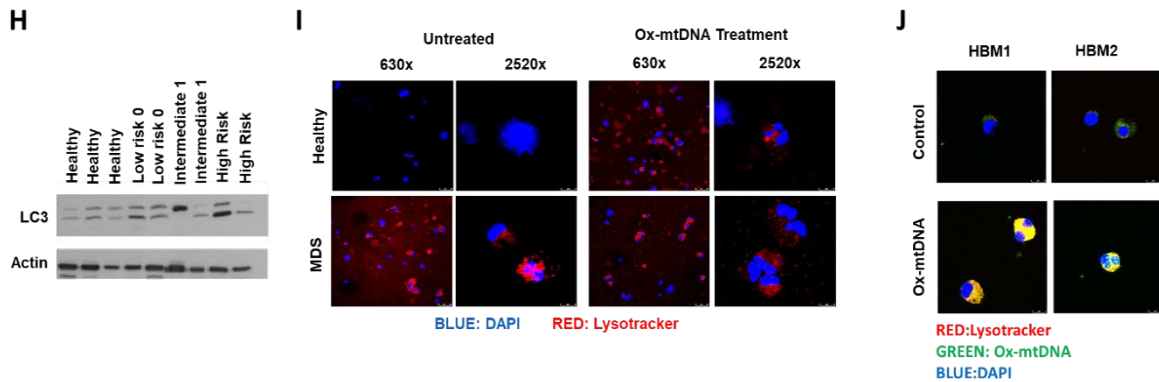
(H) Western blot of healthy and MDS BMMNC lysates probed for the lysosomal marker LC3 and actin. **(I)** Representative confocal IF micrographs showing increased lysotracker in MDS BMMNC compared to Healthy BMMNC, this increase is phenocopied in Normal BMMNC following treatment with 50ng/mL ox-mtDNA for 2 hrs. [DAPI (blue), Lysotracker (Red)]. Three independent experiments. **(J)** Confocal IF of Healthy BMMNC, control and treatment with 50ng/mL ox-mtDNA for 2 hours, co-localization of lysosome and oxDNA demonstrated by yellow pixels. [DAPI (blue), oxDNA (green), Lysotracker (Red)]. Representative of three independent experiments.

Figure 26: Ox-mtDNA and TLR9 co-localization
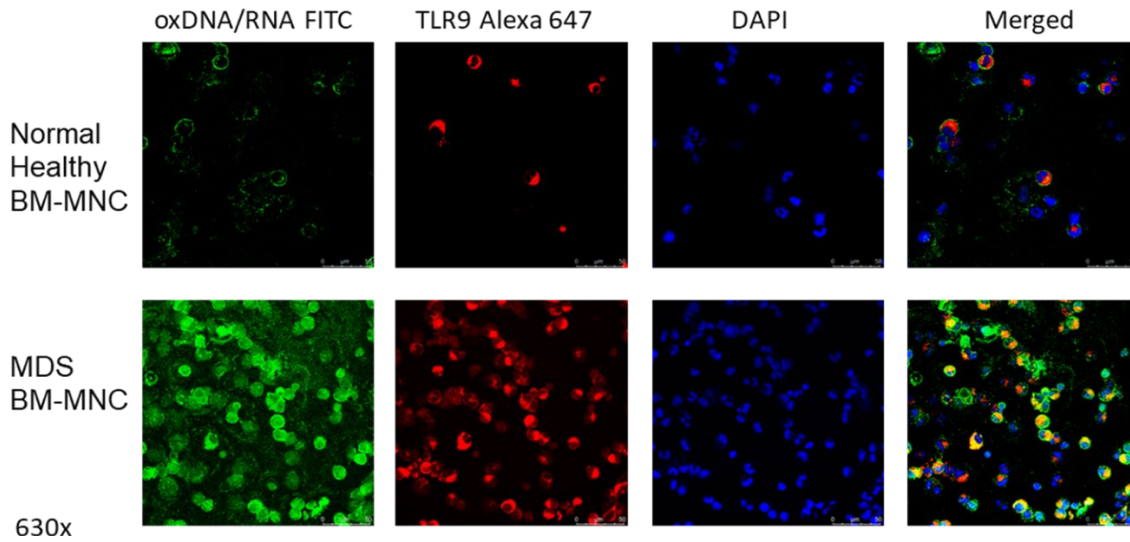
Lower Magnification (630x) of the same data as Figure 25A, showcasing single colors and merged channels.

Figure 27: TLR9 Gating Strategy
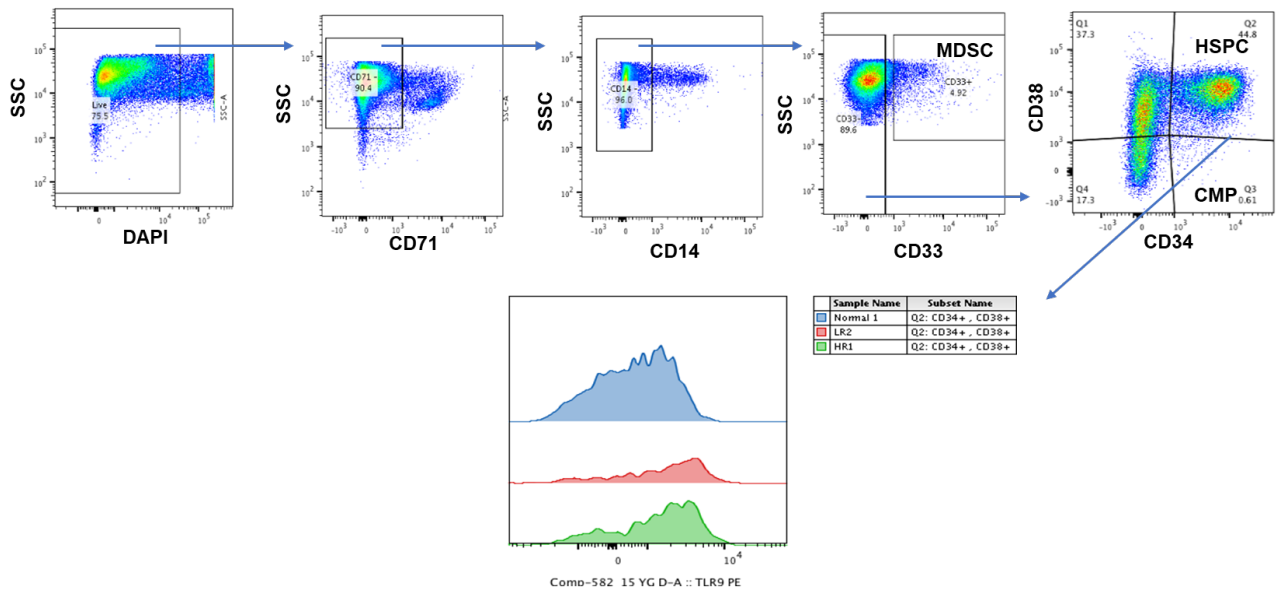
Gating strategy used to quantify the percent of cells with TLR9 surface expression and their subpopulations. HSPC are defined as Lineage-CD34+CD38+ cells.

TLR9 expression in live primary HSPC, defined as Lineage⁻, CD34⁺, CD38⁺

TLR9 is necessary for ox-mtDNA directed pyroptosis

Next, we investigated the impact of TLR9's interaction with ox-mtDNA and the activation of the TLR9/IRF7 signaling axis downstream of their ligation. Upon incubation of SKM1 and U937 cells with ox-mtDNA, we observed a time dependent co-localization of ox-mtDNA with TLR9 as well as internalization of ox-mtDNA (**Figure 28A**). To confirm the binding of ox-mtDNA with TLR9 in these cell lines, following ox-mtDNA treatment we immunoprecipitated TLR9 and confirmed its binding to ox-mtDNA by immunoblotting and conversely the binding of ox-DNA to TLR9 (**Figure 28B**). To further characterize the effect of TLR9 in the ox-mt-DNA mediated activation, we assessed Nlrp3 inflammasome activation by ox-mtDNA, as measured by caspase-1 cleavage, relative to the density of cell lines expressing high TLR9 expression (SKM1), medium expression (U937) and low to absent expression (THP1) (**Figure 28C**). Receptor density is an important determinant of the time interval to caspase-1 cleavage with SKM1 cells, that have the highest TLR9 density, responding within 1 hour of treatment, U937 cells responding within 2 hours and THP1 cells, which have reduced to no TLR9 expression, showing no caspase-1 cleavage in response to ox-mtDNA exposure up to 4 hours after ox-mtDNA incubation (**Figure 28D**). Thus, cellular levels of TLR9 dictate the temporal inflammasome response to ox-mtDNA and therefore the sensitivity of the cells receiving the stimuli of ox-mtDNA.

To determine if TLR9 is solely responsible for Nlrp3 inflammasome activation in response to ox-mtDNA exposure, we created a TLR9 knockout in SKM1 (high TLR9 expression) and U937 (medium TLR9 expression) cells using CRISPR/Cas 9 gene editing and TLR9 specific CRISPR guides **(Figure 29A)**. Ox-mtDNA treatment induces

phosphorylation of NFκB, and the maturation of Caspase-1 and IL-1β in SKM1 cells as expected, but not on those cells were TLR9 expression was silenced by the CRISPR KO (**Figure 28E**). We corroborated these findings by quantifying caspase-1 cleavage using a luciferase reporter assay, and LDH assay, demonstrating no evidence of caspase-1 cleavage in the KO-cells (**Figure 28F-G, Figure 29B-C**). These findings indicate that TLR9 is indispensable for ox-mtDNA dependent inflammasome activation. Lastly, to confirm the necessity of TLR9 to sensitize bystander cells to ox-mtDNA stimuli we used the TLR9 non-expressing THP1 cells and induced overexpression with a lentiviral vector prior to treatment with ox-mtDNA (**Figure 28H-I, Figure 29A**). These data, in combination with our earlier findings in primary cells, led us to suspect that ox-mtDNA is activating the inflammasome via TLR9 as well as directly being internalized by this receptor via its lysosomal trafficking, which we observed in cells treated with ox-mtDNA as read by LC3 and Lysotracker® Deep Red co-localization of lysosome and oxDNA demonstrated by yellow pixels. (**Figure 28J, Supplemental Figure 29D**). These data strengthen the idea that TLR9 is a main receptor for ox-mtDNA with the ability to prime IFM activation and, since we observed significant plasma membrane translocation of TLR9 upon exposure to ox-mtDNA, indicates that ox-mtDNA feeds into a feedforward loop of inflammasome activation via the TLR9 pathway (**Figure 28K, Supplemental Figure 29E**).

Figure 28: Ox-mtDNA triggers internalization via TLR9 activation
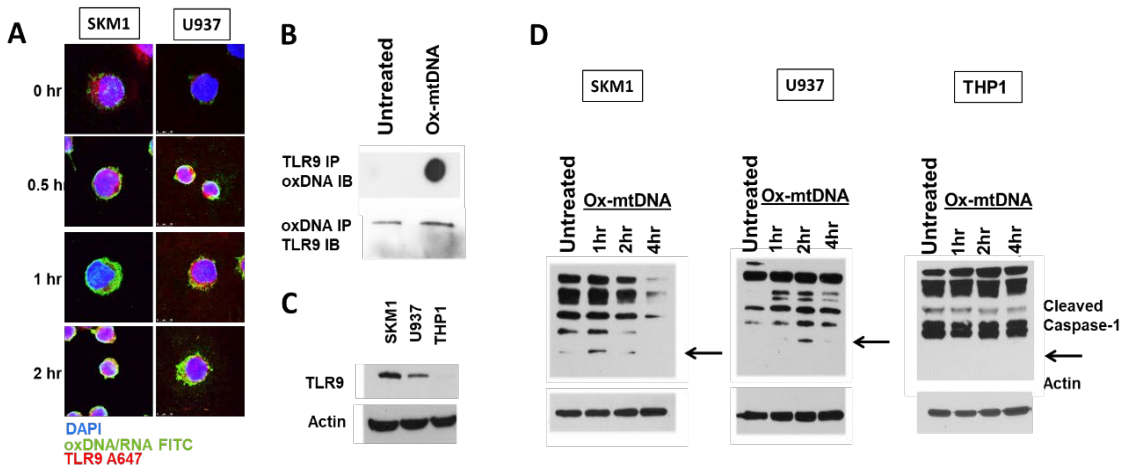
Extracellular ox-mtDNA serves as a DAMP to trigger inflammasome activation through TLR9. **(A)** Time dependent co-localization of ox-mtDNA with TLR9 and receptor:ligand internalization demonstrated by confocal IF, in SKM1 and U937 cells [DAPI (blue), oxDNA (green), TLR9 (Red), representative micrographs of three independent experiments]. **(B)** Following ox-mtDNA treatment TLR9 immunoprecipitated to assess the binding of TLR9 to oxDNA by dot-blot and immunoblot. Three independent experiments. **(C)** SKM1, U937 and THP1 display a range of TLR9 receptor density, Western blot, representative figure of 3 blots. **(D)** SKM1, U937 and THP1cells treated with 50ng/mL ox-mtDNA, SKM1 cells display cleaved caspase-1 as soon as 1 hour, U937 cells responding within 2 hours, and THP1 cells, which have no detectable TLR9, showing no caspase-1 cleavage in response to ox-mtDNA exposure. The latter was confirmed with exposures for 24 and 48 hours.

Figure 28 Cont: Ox-mtDNA triggers internalization via TLR9 activation
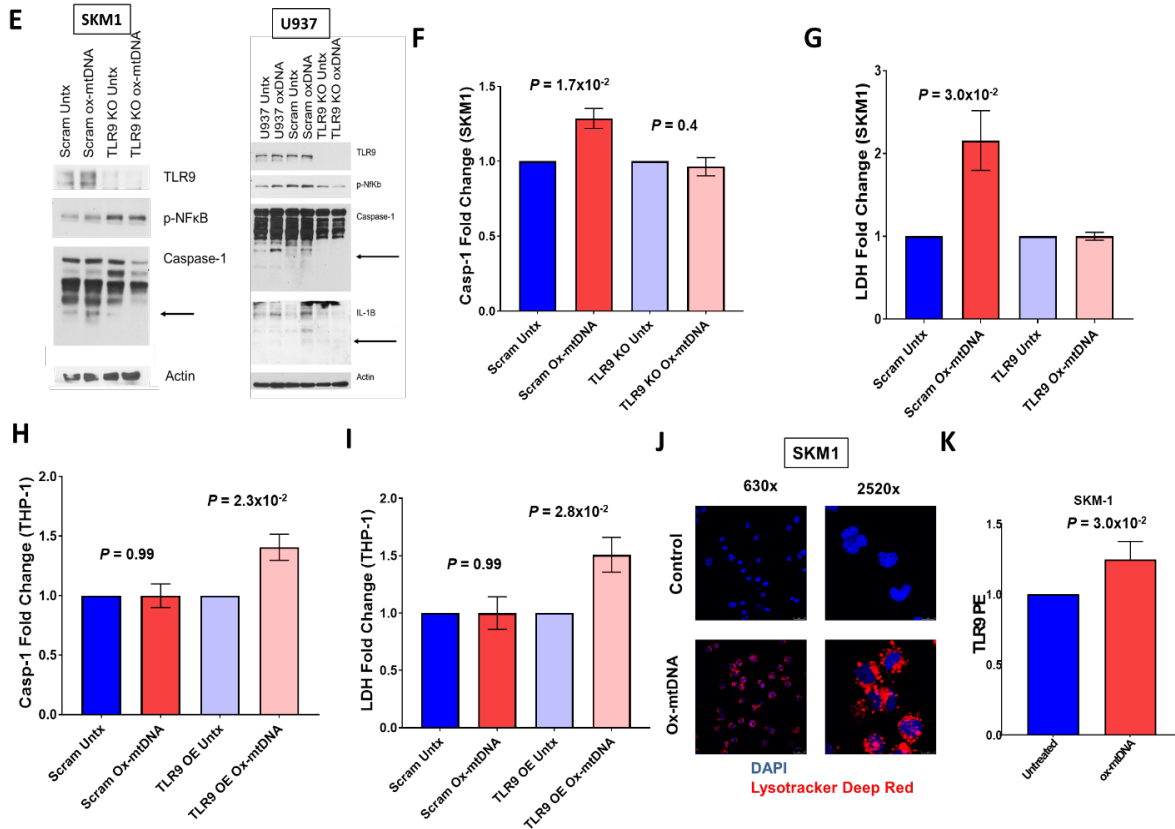
(E) TLR9 knockout in SKM1 and U937 cells using CRISPR/Cas 9 gene editing, ox-mtDNA treatment induces active NFκB, Caspase-1 and IL-1b; these readouts of inflammasome activation were lost upon CRISPR KO of TLR9. **(F)** Fold change of caspase-1 activity and **(G)** LDH media release in TLR9 KO SKM1 and U937 cells treated with ox-mtDNA, (mean ± SD of three independent experiments). **(H)** Fold change of caspase-1 activity and **(I)** LDH media release in TLR9 overexpression THP-1 cells treated with ox-mtDNA, (mean ± SD of three independent experiments). **(J)** Confocal IF of SKM1 cells treatment with 50ng/mL ox-mtDNA for 2 hours to assess induction of lysosomes [DAPI (blue), Lysotracker (Red)]. Representative micrographs, three independent experiments. **(K)** Change in surface expression of TLR9 in response to ox-mtDNA treatment by flow cytometry (MFI ± SD, N=3).

Figure 29: U937 TLR9 KO experiments
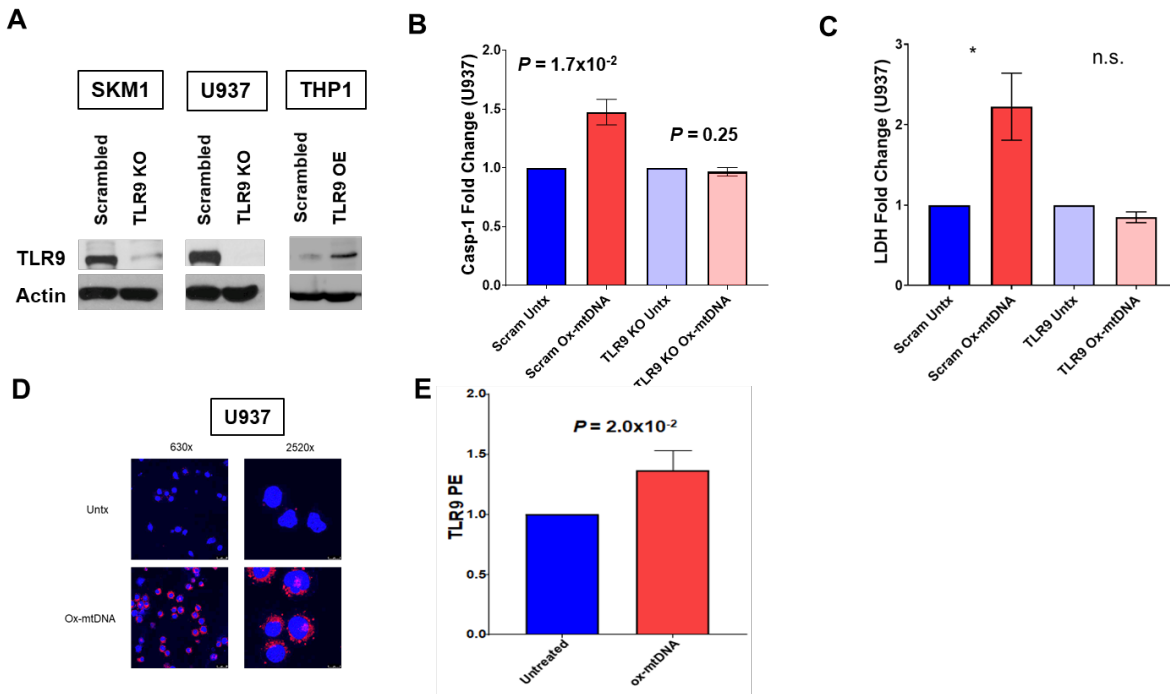
TLR9 expression in lentiviral transduced cell lines, corroboration experiments.

A) Western blot of SKM1 and U937 cells transfected with a lentivirus vector containing TLR9 CRISPR KO guide or western blot of THP-1 cells transfected with a lentiviral vector for TLR9 overexpression. B) Same experiment as Figure 28F measuring caspase-1 activation in U937 cells transfected with scrambled or TLR9KO lentivirus. C) Same experiment as Figure 8G measuring LDH for proliferation of U937 cells transfected with scrambled or TLR9 KO lentivirus. D) Same experiment as Figure 28J in U937 cells following lysosomal activation with Lysotracker red after treatment with ox-mtDNA. E) Same experiment as Figure 28K in U937 cells showing translocation of TLR9 to the surface of cells after treatment with ox-mtDNA.

IRF7 signaling is activated by ox-mtDNA/TLR9 engagement

To confirm that TLR9 signaling is activated after ligation with ox-mtDNA we evaluated the activation of potential mediators downstream of ox-mtDNA/TLR9 activation (TBK1, IRF7, IRF3) and found that only IRF7 was activated by ox-mtDNA treatment of SKM1 cells (**Figure 30A**). Accordingly, IRF7 was translocated to the nucleus upon ox-mtDNA treatment corroborating its activation downstream of ox-mtDNA/TLR9 signaling, demonstrated by western blot and confocal IF (**Figure 30B-C**). This IRF7 nuclear translocation activated by ox-mtDNA also required TLR9 expression as CRISPR KO of this receptor prevented IRF7's nuclear translocation and ASC formation (**Figure 30D, Figure 31A**). This correlated with the level of TLR9 as SKM1 cell had a faster IRF7 translocation (1 hour) compared to U937 (4 hours) that have comparatively less TLR9 than SKM1 cells (**Figure 31B, Figure 30C**). Lastly, we took advantage of our previously published RNA-seq dataset (Cheng et al., 2019) comparing healthy versus LR MDS specimens and found increased activation of genes linked to TLR9 pathway activation, including *CTSB* and *IRF7,* which were accordingly activated by ox-mtDNA (**Figure 31C**).

At baseline, MDS patients have significantly higher levels of type 1 interferons (IFN) (Pellagatti et al., 2006) and, accordingly, gene expression of the ISGs interferon (IFN) α1, IFNα10, IFNβ1, CXCL10, ISG15, SAMD9L and IFI27L2 were elevated in MDS on data obtained from 213 WHO-defined MDS patient specimens at time of diagnosis as well as from 20 healthy donors from the National Taiwan University Hospital (**Figure 30F, Supplemental Figure 32A**). [Additionally, IFNα2, α4, α5, α8, α14, and α21 all significantly elevated, data not shown] This activation correlated with increased

expression of TLR9-mediators, including IRF7 and IRAK in MDS, although there was no difference in these in respect to risk (**Figure 30G, Figure 32B**). To confirm that the ox-mtDNA plays a role in ISG induction through increased activation of the ox-mt-DNA/TLR9/IRF7 axis we analyzed the gene expression of type I IFN genes after treatment with ox-mtDNA and found a time-dependent increase in their activation (**Figure 30H, Figure 33A**). This activation was confirmed to be mediated through TLR9 activation as silencing this receptor abrogated their increase in expression after treatment with ox-mtDNA (**Figure 30I, Figure 33B-D**). These findings show that ox-mtDNA engages and activates the TLR9 pathway through the activation of genes downstream of IRF7 nuclear translocation.

Figure 30: IRF7 signaling is activated by ox-mtDNA/TLR9 engagement
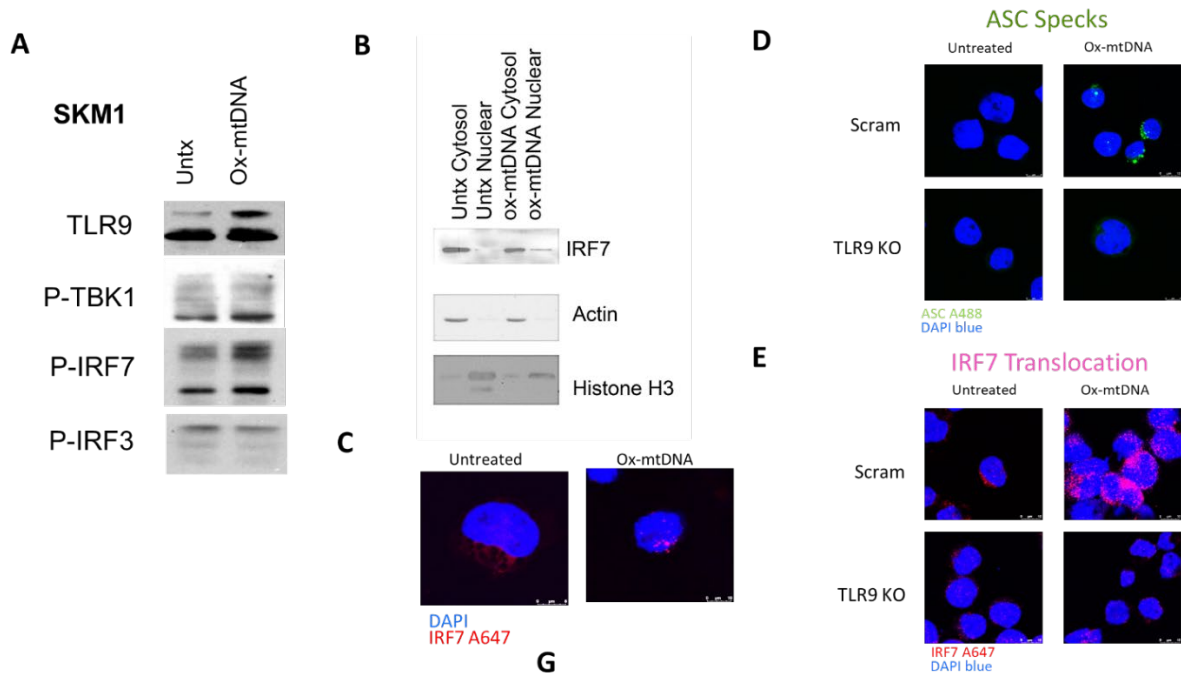
(A) TLR9 pathway activation demonstrated by TLR9 cleavage, and IRF7 phosphorylation. TBK1 and IRF3 unchanged suggesting other DNA sensing pathways are not activated. Representative Western Blot. **(B)** IRF7 translocation to the nucleus (cytosol denoted by presence of actin, nucleus denoted by presence of Histone H3. Representative Fractionation Western Blot. **(C)** Confocal IF to demonstrated IRF7 translocation, [DAPI (blue), IRF7 (Alexa Fluro 647) (x2520)]. **(D)** Confocal IF of TLR9 KO on ASC speck formation and **(E)** IRF7 nuclear translocation [DAPI (blue), ASC (Alexa Fluro 488), IRF7 (Alexa Fluro 647) (x2520)].

Figure 30 Cont.: IRF7 signaling is activated by ox-mtDNA/TLR9 engagement
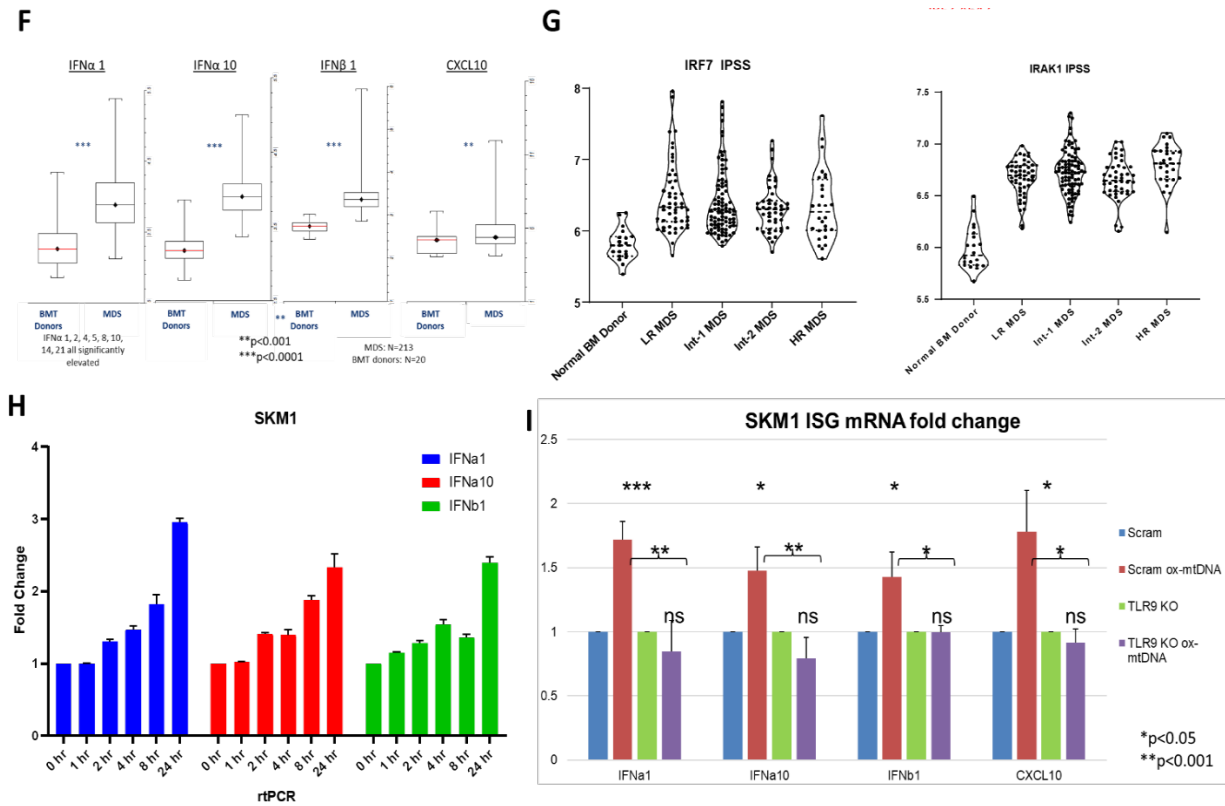
(F) Gene expression array of Type 1 Interferons (IFNα1, α10, β1) and Interferon stimulated genes (CXCL10) **(**MDS N=213, BMT donors N=20) **(G)** IRF7 and Interleukin 1 Receptor Associated Kinase (IRAK)1 (MDS N=213, BMT donors N=20). **(H)** The changes seen in F was phenocopied by 50ng/mL ox-mtDNA treatment 1-24 hours. IFNa1, a10, b1 qPCR (Mean fold change ± SD, N=3). **(I)** Following ox-mtDNA treatment IFNa1, a10, b1, and the ISG CXCL10 are all increased by qPCR, the fold change in mRNA was lost with TLR9 KO.

Figure 31: Nuclear Translocation of IRF7 following TLR9/oxDNA ligation

NAME	SCORE
CTSB	0.11140112
MAP1LC3C	0.041337512
IRF7	0.038532738
MAP1LC3B	0.001482483
IRF3	-0.038418442
MAP1LC3A	-0.094965264
TBK1	-0.13736689
MAP1LC3B2	-0.5967795
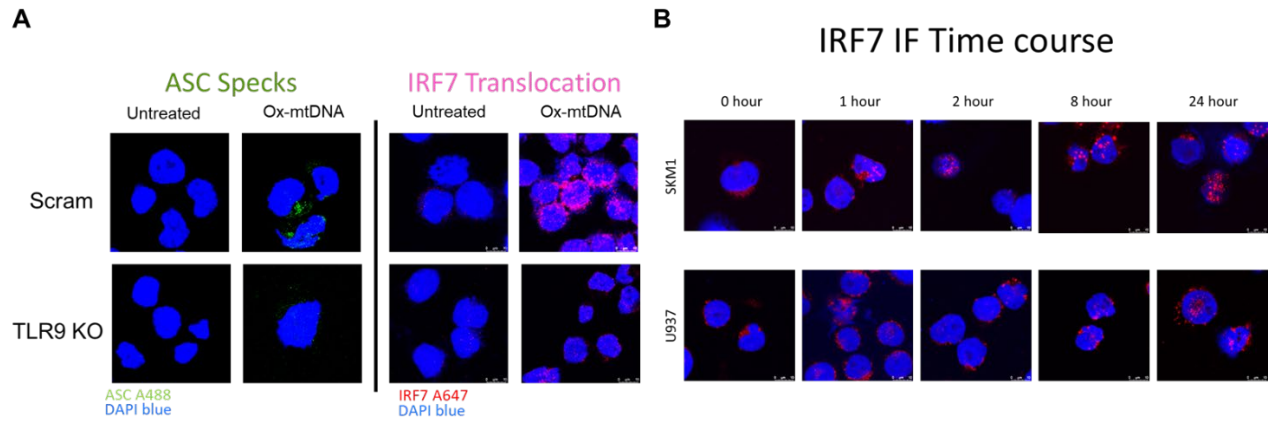
A) Figure 30D and E showing immunofluorescence staining of U937 cells transfected with a lentivirus vector containing TLR9 CRISPR KO guide, or a scrambled control) for the formation of ASC specks (green) or IRF7 (red). **B)** Immunofluorescence time lapse of IRF7 nuclear localization in either SKM1 or U937 cells after treatment with ox-mtDNA. **C)** Analysis of previously published RNA-seq data comparing healthy versus MDS BM-MNC showing genes linked to TLR9 activation including IRF7.

Figure 32: ISG expression is active in MDS
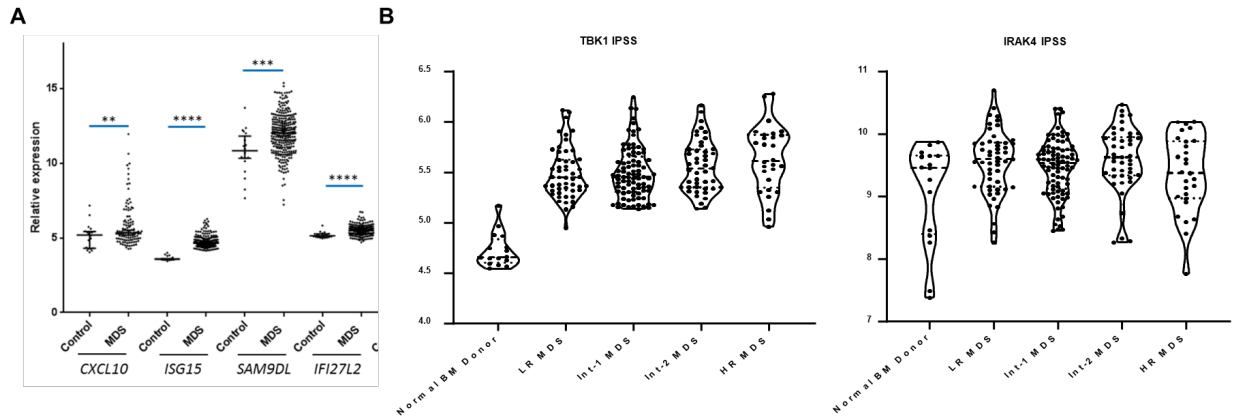
Additional ISG, IFN, and relevant protein assessed by gene expression array (MDS N=213, BMT donors N=20).

A). Gene expression of key ISG were elevated in MDS primary specimens (CXCL10, P = 0.013; ISG15, P < 0.0001; SAMD9L, P = 0.0007; IFI27L2, P < 0.0001).

B). Gene expression of TBK1 and IRAK4 is elevated in MDS primary samples regardless of risk.

Figure 33: U937 ISG activation in response to ox-mtDNA
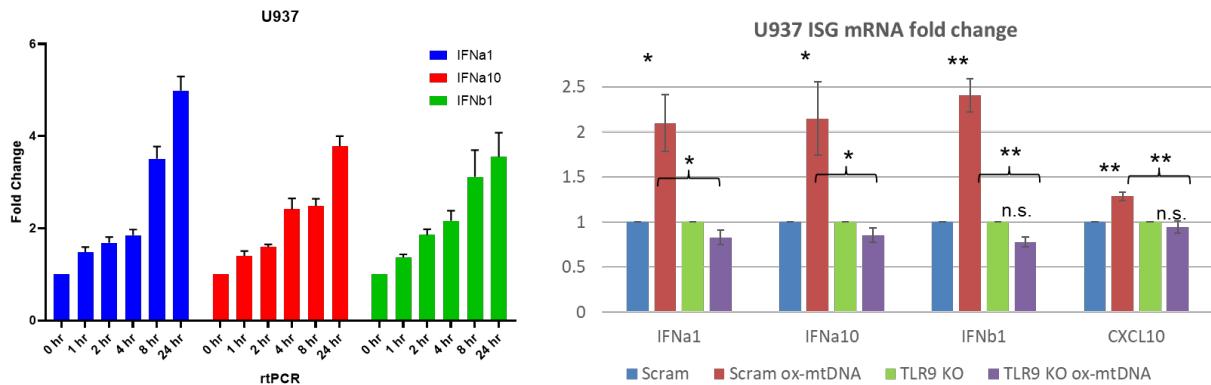
50ng/mL ox-mtDNA treatment 1-24 hours. IFNa1, a10, b1 qPCR (Mean fold change ± SD, N=3). Following ox-mtDNA treatment IFNa1, a10, b1, and the ISG CXCL10 are all increased by qPCR, the fold change in mRNA was lost with TLR9 KO.

Ox-mtDNA/TLR9 signaling can be therapeutically targeted to improve MDS

Recently studies have shown that mtDNA/TLR9 ligation is linked to anemia development during inflammation (Lam et al., 2021). Having established that MDS BM plasma is sufficient to induce pyroptosis in normal BM-MNC and that MDS BM plasma has significantly high levels of ox-mtDNA (Basiorka et al., 2016; Ward et al., 2021), we sought to assess the specific impact of ox-mtDNA and TLR9 in hematopoietic potential. Primary healthy BMMNC un-transfected or transfected with lentivirus vectors to overexpress (OE) TLR9 or knock it down (KO) with a specific CRISPR guide (**Figure 35A**) were treated with synthetic ox-mtDNA prior to assessment of colon forming capacity. As expected, ox-mtDNA treatment of healthy primary BMMNC significantly reduced colony forming capacity in all colony types assessed (**Figure 34A-B**). TLR9 OE in healthy BM-MNC had increased sensitization to ox-mtDNA, particularly in the erythroid compartment (BFU-E, **Figure 34A-B**) while silencing of TLR9 with CRISPR KO disrupted the effect of ox-mtDNA through restoration of hematopoiesis to untreated levels (**Figure 34A-B**). These data indicate that ox-DNA accumulates in the microenvironment in MDS where it binds TLR9 sensitizing cells to IFM activation and can directly affect healthy hematopoietic potential.

Since attempts to develop selective targeted therapeutics on MDS malignant stem cells has been hampered by the lack of therapeutic that specifically target the MDS malignant clone while sparing normal healthy hematopoiesis, our next step was to test the therapeutic potential of targeting the ox-mtDNA/TLR9 axis to restore hematopoietic potential. For this purpose, we evaluated the ability several compounds targeting either TLR9 or ox-mtDNA to block caspase-1 activation in SKM1 or U937 cells

(**Figure 34B and Figure 35B**). Caspase-1 activation was prevented by either blocking

TLR9 signaling with an IRAK inhibitor that prevents downstream activation of Myd88,

oligodeoxynucleotide (ODN)-F (a TLR9 antagonist), blocking ox-DNA with IRS954 (a

non-sense ODN) (Barrat et al., 2007), preventing lysosome internalization with

hydroxychloroquine (HCQ), or depleting excess ox-mtDNA with a soluble TLR9-IgG4

chimeric molecule (the ectodomain of TLR9 fused to the Fc domain of human IgG4)

developed by us to serve as a decoy receptor or ligand trap technology (**Figure 34B**

and Figure 35C). However, using a non-TLR9 targeting cGAS inhibitor (RU.521) did

not prevent the activation of caspase-1, validated by showing that silencing cGAS does

not prevent ox-mtDNA induced caspase-1 activation (**Figure 35D**), further

demonstrating the specificity of ox-mtDNA for TLR9. To fully validate that these

inhibitors would have therapeutic potential in MDS we tested the ability of these

inhibitors to enhance hematopoietic potential in primary MDS BMMNC. Blocking TLR9

signaling with IRAKi, trapping excess ox-mtDNA with TLR9 chimera, blocking binding to

TLR9 with ODN-F or preventing lysosomal internalization significantly improved colony

forming capacity of MDS BMMNC treated ex vivo (**Figure 34C-D**), confirming the

therapeutic potential of targeting the ox-mtDNA/TLR9 axis in MDS. This demonstrates

that targeting the TLR9 pathway can be a novel therapeutic strategy to improve anemia

in Low Risk MDS.

Figure 34: Ox-mtDNA/TLR9 signaling can be therapeutically targeted to improve MDS
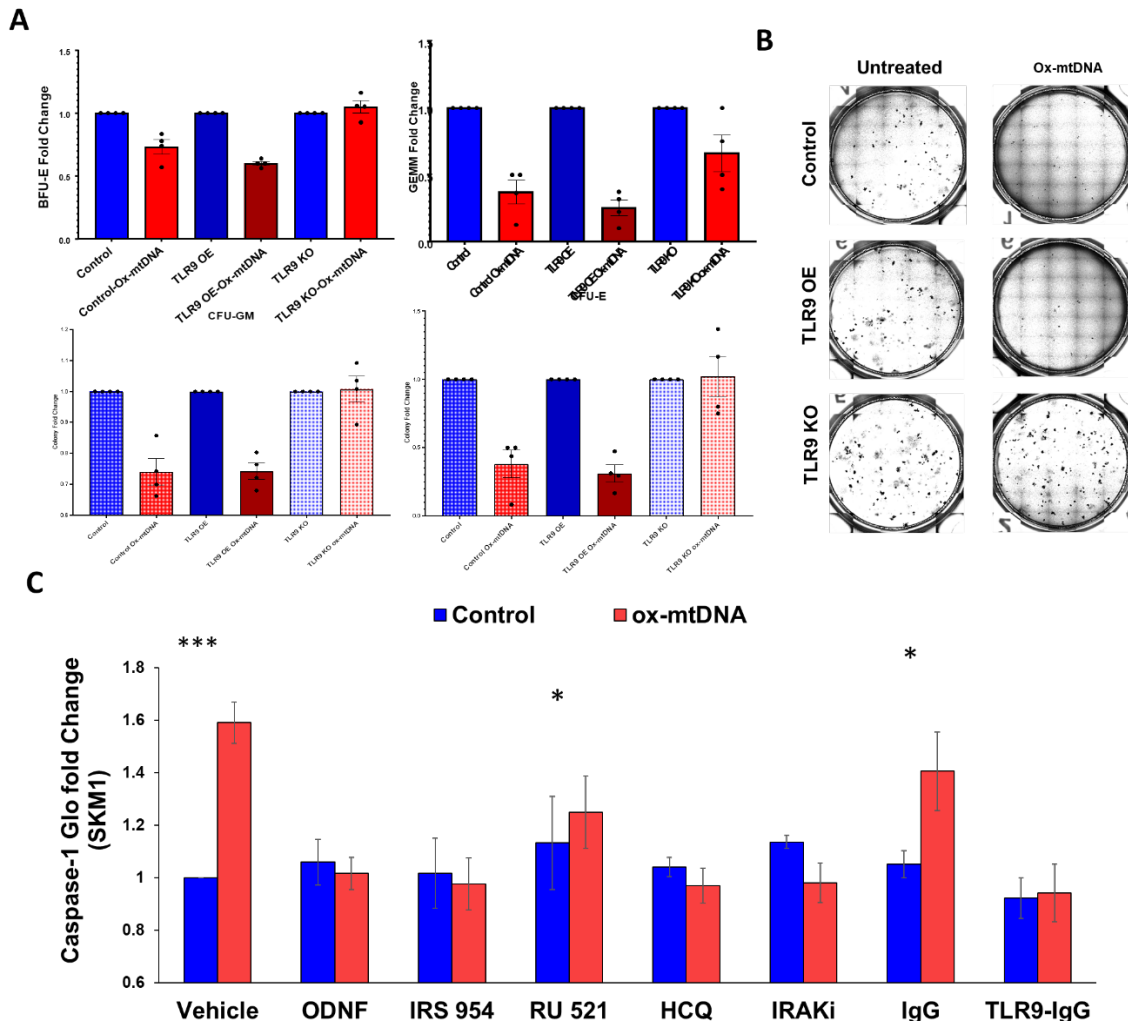
(A-B) Colony formation assay for hematopoiesis in Healthy BMMNCs treated with 50ng/mL ox-mtDNA for 14 days. (mean ± SD of three independent experiments). Cells treated with lentivirus for TLR9 overexpression (OE), and TLR9 knockdown (KD) **(C)** SKM1 cells treated with ox-mtDNA and TLR9 inhibitors (IRS 954, HCQ, ODNF, TLR9-IgG), cGAS inhibitor (RU .521), inflammasome inhibitor (IRAKi), and controls (Vehicle, IgG). Fold change of caspase-1 activity (mean ± SD of three independent experiments).

Figure 34 Cont.: Ox-mtDNA/TLR9 signaling can be therapeutically targeted to improve MDS
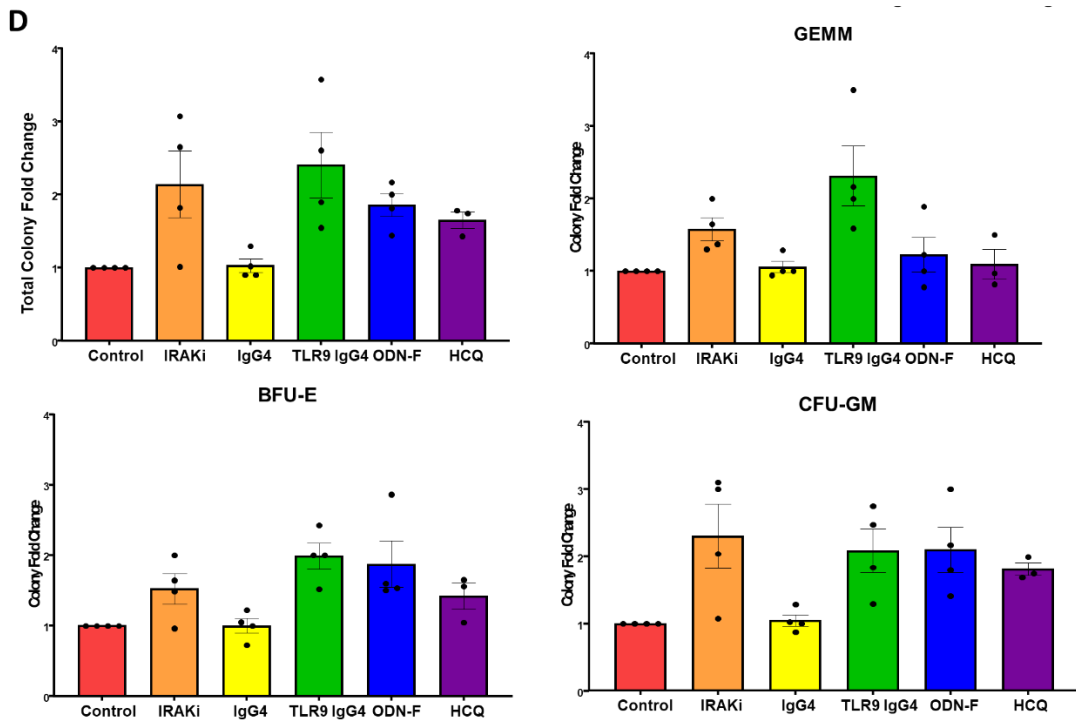
(D) Colony formation assay for hematopoiesis in LR MDS BMMNCs treated with inhibitors 14 days. (mean ± SD of three independent experiments).

Figure 35: ox-mtDNA/TLR9 is a targetable axis in primary MDS, ex-vivo
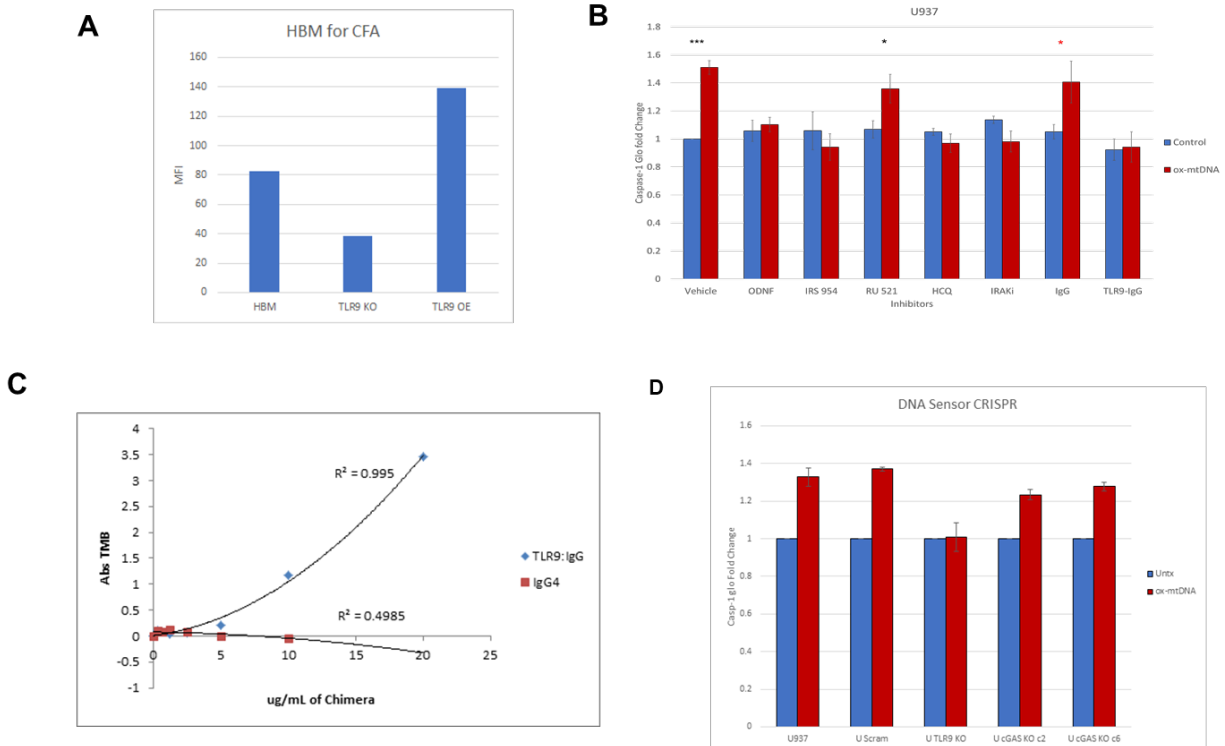
A) Flow cytometric TLR9 expression analysis after transfection in primary healthy BM-MNC transfected with lentiviral vectors. B) Experiment as in Figure 34C showing IFM activation of U937 cells treated with ox-mtDNA in the presence or absence of TLR9-linked inhibitors as shown. C) Sandwich ELISA to assess the relative efficacy of TLR9-IgG and control IgG for binding ox-mtDNA. D) cGAS KO does not abrogate ox-mtDNA induced IFM induction assessed by caspase-1 activation. Ox-mtDNA induced Caspase-1 cleavage is unchanged by cGAS CRISPR KO.

Discussion

Ox-mtDNA is a novel diagnostic biomarker (Ward et al., 2021) that may represent a therapeutic target for MDS and potentially other chronic inflammatory conditions. Here we demonstrate the important role that the diagnostically evident excess of ox-mtDNA plays in hematopoietic potential by inducing the overexpression and engagement of TLR9. Our findings identify it as a key DAMP contributing to both medullary HSPC pyroptosis and propagation of sterile inflammation in MDS.

We show that incubation with ox-mtDNA provides a secondary signal that is sufficient to induce activation of the canonical NLRP3 inflammasome pathway and pyroptotic cell death, as evidenced by cleavage of caspase-1 and IL-1β, and ASC speck formation and release. Our studies also suggest that strategies that effectively neutralize extracellular ox-mtDNA/TLR9 may suppress DNA-sensor-directed inflammation in the bone marrow niche and possibly improve hematopoiesis. Indeed, strategies that mitigate mitochondrial membrane depolarization, through activation of the Nrf2-antioxidant pathway, or the binding of ox-mtDNA to its cognate TLR9 receptor may offer promising therapeutic potential (Sekheri, El Kebir, Edner, & Filep, 2020; C. Zhang, Hao, Chang, Geng, & Wang, 2019). Moreover, these findings may be extended to other disorders in which ox-mtDNA has been implicated in innate immune activation (Lindqvist et al., 2016; Mehta et al., 2017; Pinti et al., 2014; Q. Zhang et al., 2010).

The important role that pyroptosis plays in the development of the phenotypic anemia of MDS was initially demonstrated by us and has become a landmark work to showcase the involvement of the innate immune microenvironment at inducing HSPC death and providing the pressure for selection of malignant/defective cells (Basiorka et

al., 2016; X. Chen et al., 2013a). The role of this axis in the evolution of malignancy is supported by the fact that TLR9 excessive expression in MDS is lost after transformation, when the biological pressure for survival and evolution is no longer needed (Kuninaka et al., 2010). Our investigation demonstrates that MDS HSPC translocate TLR9 to the plasma membrane where it, and ER-resident receptors, can engage nucleic acid-based DAMPs, such as ox-mtDNA, further enhancing pyroptosis and reinforcing surface TLR9 translocation. In this way we expect that ox-mtDNA, below the initial activation of pyroptosis, contributes to accelerating the death of healthy HSPC and selection of increasingly aggressive clones that can transform to AML. Hence, another potential consequence of ox-mtDNA/TLR9 targeting is to prevent the evolution towards leukemia and a persuasive argument of its therapeutic potential to release this selective pressure.

Earlier in the MDS disease phenotype, pyroptosis-induced abundance of ox-mtDNA in MDS plasma reinforces surface TLR9 translocation and, through engagement, activates this axis to initiate transcription of ISGs, inflammatory cytokines, and further induction of IFM activation of neighboring HSPC. Considering that in 2006, Pellagati *et al.* demonstrated that interferon stimulated gene (ISG) transcription is the most upregulated pathway in MDS (Pellagatti et al., 2006); our research suggests that this could be a result of ox-mtDNA/TLR9 pathway activation. IFM activation then results in both cell death and cell proliferation via β-catenin activation (Basiorka et al., 2016; L. Huang et al., 2020) and IL-1β which has been implicated in immuno-senescence and myeloid skewing of HSPC with aging (reviewed in (Mantovani, Dinarello, Molgora, & Garlanda, 2019)). This activation also results in degradation of the erythroid lineage

transcription factor GATA1, through caspase-1 activation (Tyrkalska et al., 2019), changing the ratio between GATA1 and the myeloid transcription factor PU.1, which governs lineage commitment, favoring myeloid commitment, maturation arrest & anemia (De Maria et al., 1999; Tyrkalska et al., 2019). Additionally, chronic TLR activation in HSC causes loss of quiescence with recruitment into the cell cycle and HSC depletion (Esplin et al., 2011; Holl & Kelsoe, 2006; D. E. Kennedy & Knight, 2017; O'Hagan-Wong et al., 2016). Having established the importance of ox-mtDNA/TLR9 in MDS, a next step will be to understand the contribution of this axis to the overall phenotype, ISG over expression, myeloid skewing induction, immune-senescence, and bone marrow failure.

Recent publications have found a novel role for Red Blood Cells (RBCs) as an anti-inflammatory sink for mtDNA (Akilesh et al., 2019; Darbonne et al., 1991; Hotz et al., 2018; Lam et al., 2021). MDS is especially sensitive to the loss of this natural ox-mtDNA removal system due to the disease's characteristic HSPC pyroptosis. Pyroptosis that not only contributes to the inflammatory milieu of the BM with high ox-mtDNA, but also leads to pan-cytopenias. In this manner, the loss of RBCs coupled with the increased ox-mtDNA results in further HSPC death and feedforward bone marrow failure.

Importantly, we also demonstrate that TLR9 is indispensable for ox-mtDNA initiated IFM activation that is proportionate to cellular TLR9 density highlighting the viability of therapeutically targeting this ligand/receptor interaction. Importantly, we showcase that use of TLR9 agonists, or use of a chimeric TLR9 ectodomain IgG decoy developed by us, to trap excess ox-mtDNA thus successfully improving hematopoietic potential in MDS BM explants through the reduction of IFM activity. However,

considering that other nucleic acid-based DAMPs are released through pyroptosis it would be important to understand the contribution of other DAMPs to this phenotype to assess the hierarchy of this axis in the pathogenesis of MDS. However, some of our data demonstrate that TLR9 is critical and so the use of a soluble chimeric ectodomain of TLR9 could well be beneficial at clearing other potential DAMPs that use TLR9 for signaling. Similarly, specifically neutralizing TLR9 activation could be beneficial although the fact that ox-mtDNA has specific activation of TLR9 through IRF7, but further research is needed to assess the global impact on BM. Therefore, our work demonstrates a novel, therapeutically targetable axis that can be explored clinically in the future.

Chapter 5: Oxidized Mitochondrial DNA is a Biomarker and Catalyst of Pyroptotic Cell Death in Myelodysplastic Syndromes

The results of this dissertation have established a novel biomarker for medullary pyroptosis in MDS and from that Danger Associated Molecular Pattern signaling pathway was discovered a therapeutically targetable axis.

Ox-mtDNA is abundant in the plasma of MDS patients, and is a sensitive, specific, and biologically relevant biomarker of inflammasome activation. Ox-mtDNA is especially elevated in Lower risk MDS and is a diagnostic biomarker for MDS compared to other BM failure diseases. The oxDNA ELISA is a user friendly, quick, and scalable way to quantify pyroptosis patient peripheral blood plasma, hopefully allowing for earlier detection and less painful bone marrow biopsy. Further research is needed to evaluate the impact of increased mitochondrial stress on HSPCs, corresponding changes in metabolism, and loss of effective mitophagy in MDS and transformation pressure.

Ox-mtDNA is a potent activator of the NLRP3 inflammasome and pyroptosis, but intracellular mtDNA is dispensable for inflammasome activation. Given the elevated levels in MDS plasma, ox-mtDNA is a contributing factor in the inflammatory nature of the MDS BM microenvironment.

MDS HSPC translocate TLR9 to the plasma membrane where it and ER-resident receptors can engage CpG-rich DNA, such ox-mtDNA. Ox-mtDNA is abundant in MDS

plasma as a result of extensive medullary pyroptosis that in turn reinforces surface TLR9 translocation. Ox-mtDNA engages and activates the TLR9 axis to initiate transcription of interferon stimulated genes, inflammatory cytokines, and inflammasome activation. TLR9 is indispensable for ox-mtDNA initiated inflammasome activation that is proportionate to cellular TLR9 density; ox-mtDNA dictates hematopoietic failure via the TLR9-MyD88-NLRP3 pyroptotic axis. The activation of this pathway may account for overactivation of type 1 interferons and Interferon stimulated genes in MDS. Targeting the ox-mtDNA/TLR9 signaling pathway restores normal hematopoiesis in MDS HSPCs. Future studies need to assess the impact of TLR9 inhibitors on MDS animal models and clinical trial.

We establish the following model for MDS feed-forward bone marrow failure (**Figure 36**). MDS chronic medullary inflammation and constitutive innate immune activation is directed in part by the NLRP3 inflammasome. This pyroptosis not only contributes to the inflammatory milieu of the BM with high ox-mtDNA, but also leads to pan-cytopenias. The MDS bone marrow is especially sensitive to molecular effects of anemia, loss of the TLR9 RBC anti-inflammatory sink for mtDNA. Thus, more cell free ox-mtDNA propagates increased TLR9 expression, pyroptosis, HSPC death, and feedforward bone marrow failure.

Figure 36: Feed-Forward Bone Marrow Failure
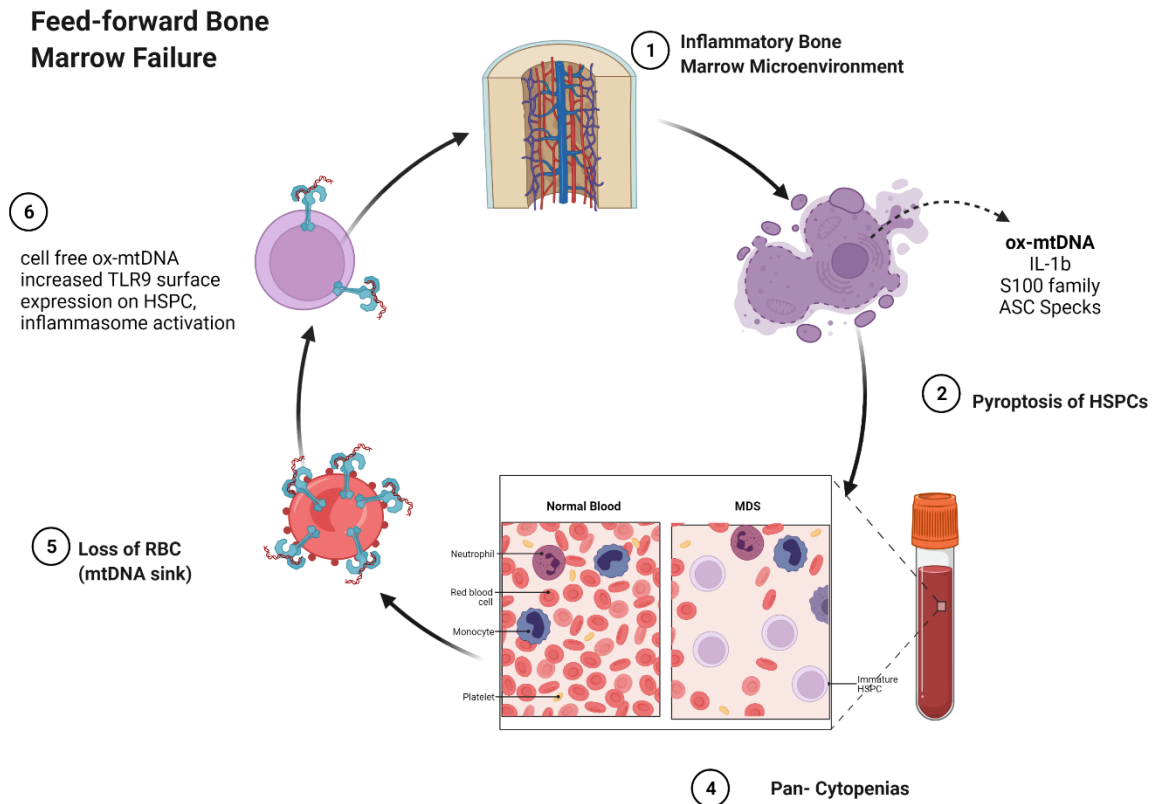
Our collaborations with the Mehta lab (NIH/NHLBI) found that ox-mtDNA is elevated in psoriatic arthritis and associated with immune dysfunction and lipid dysfunction [unpublished]. These promising results suggest that more research is needed into the ox-mtDNA/TLR9/NLRP3 axis in other inflammatory contexts such as autoimmune diseases, systemic inflammatory response syndrome, other inflammatory cancers, and diseases with poor autophagy and mitophagy (Parkinson's disease, Huntington's disease, Alzheimer's disease, Crohn's disease, Paget disease, various muscular atrophy diseases, several types of cancer and many other pathologies (Levine & Kroemer, 2008).

Literature Cited

Aarreberg, L. D., Esser-Nobis, K., Driscoll, C., Shuvarikov, A., Roby, J. A., & Gale, M., Jr. (2019). Interleukin-1beta Induces mtDNA Release to Activate Innate Immune Signaling via cGAS-STING. *Mol Cell, 74*(4), 801-815 e806. doi:10.1016/j.molcel.2019.02.038

Albitar, M., Manshouri, T., Shen, Y., Liu, D., Beran, M., Kantarjian, H. M., . . . Estey, E. H. (2002). Myelodysplastic syndrome is not merely "preleukemia". *Blood, 100*(3), 791-798. doi:10.1182/blood.v100.3.791

Alexandrakis, M. G., Passam, F. H., Kyriakou, D. S., Dambaki, C., Katrinakis, G., Tsirakis, G., . . . Stathopoulos, E. N. (2004). Expression of the proliferation-associated nuclear protein MIB-1 and its relationship with microvascular density in bone marrow biopsies of patients with myelodysplastic syndromes. *J Mol Histol, 35*(8-9), 857-863. doi:10.1007/s10735-004-2341-0

Basiorka, A. A., McGraw, K. L., Abbas-Aghababazadeh, F., McLemore, A. F., Vincelette, N. D., Ward, G. A., . . . List, A. F. (2018). Assessment of ASC specks as a putative biomarker of pyroptosis in myelodysplastic syndromes: an observational cohort study. *The Lancet Haematology, 5*(9), e393-e402. doi:10.1016/s2352-3026(18)30109-1

Basiorka, A. A., McGraw, K. L., Abbas-Aghababazadeh, F., McLemore, A. F., Vincelette, N. D., Ward, G. A., . . . List, A. F. (2018). Assessment of ASC specks

as a putative biomarker of pyroptosis in myelodysplastic syndromes: an observational cohort study. *Lancet Haematol, 5*(9), e393-e402. doi:10.1016/S2352-3026(18)30109-1

Basiorka, A. A., McGraw, K. L., Eksioglu, E. A., Chen, X., Johnson, J., Zhang, L., . . . List, A. F. (2016). The NLRP3 inflammasome functions as a driver of the myelodysplastic syndrome phenotype. *Blood, 128*(25), 2960-2975. doi:10.1182/blood-2016-07-730556

Bejar, R. (2017). CHIP, ICUS, CCUS and other four-letter words. *Leukemia, 31*(9), 1869-1871. doi:10.1038/leu.2017.181

Ben-Ezra, J. M., Trinh, K., Harris, A. C., & Kornstein, M. J. (1998). Ploidy Analysis and Ki-67 Expression in Myelodysplastic Syndromes. *Hematology, 3*(3), 215-222. doi:10.1080/10245332.1998.11746393

Cavallini, C., Chignola, R., Dando, I., Perbellini, O., Mimiola, E., Lovato, O., . . . Scupoli, M. T. (2018). Low catalase expression confers redox hypersensitivity and identifies an indolent clinical behavior in CLL. *Blood, 131*(17), 1942-1954. doi:10.1182/blood-2017-08-800466

Chen, G. Y., & Nunez, G. (2010). Sterile inflammation: sensing and reacting to damage. *Nat Rev Immunol, 10*(12), 826-837. doi:10.1038/nri2873

Chen, X., Eksioglu, E. A., Zhou, J., Zhang, L., Djeu, J., Fortenbery, N., . . . Wei, S. (2013). Induction of myelodysplasia by myeloid-derived suppressor cells. *J Clin Invest, 123*(11), 4595-4611. doi:10.1172/JCI67580

Chuang, M. K., Chiu, Y. C., Chou, W. C., Hou, H. A., Chuang, E. Y., & Tien, H. F. (2015). A 3-microRNA scoring system for prognostication in de novo acute

myeloid leukemia patients. *Leukemia, 29*(5), 1051-1059.
doi:10.1038/leu.2014.333

Cogle, C. R. (2015). Incidence and Burden of the Myelodysplastic Syndromes. *Curr Hematol Malig Rep, 10*(3), 272-281. doi:10.1007/s11899-015-0269-y

Collado, R., Ivars, D., Oliver, I., Tormos, C., Egea, M., Miguel, A., . . . Carbonell, F. (2014). Increased oxidative damage associated with unfavorable cytogenetic subgroups in chronic lymphocytic leukemia. *Biomed Res Int, 2014*, 686392. doi:10.1155/2014/686392

Collins, L. V., Hajizadeh, S., Holme, E., Jonsson, I. M., & Tarkowski, A. (2004). Endogenously oxidized mitochondrial DNA induces in vivo and in vitro inflammatory responses. *J Leukoc Biol, 75*(6), 995-1000. doi:10.1189/jlb.0703328

Durrani, J., & Maciejewski, J. P. (2019). Idiopathic aplastic anemia vs hypocellular myelodysplastic syndrome. *Hematology Am Soc Hematol Educ Program, 2019*(1), 97-104. doi:10.1182/hematology.2019000019

Estey, E. (2007). Acute myeloid leukemia and myelodysplastic syndromes in older patients. *J Clin Oncol, 25*(14), 1908-1915. Retrieved from http://www.ncbi.nlm.nih.gov/entrez/query.fcgi?cmd=Retrieve&db=PubMed&dopt=Citation&list_uids=17488990

Fenaux, P., Haase, D., Santini, V., Sanz, G. F., Platzbecker, U., Mey, U., & Committee, E. G. (2020). Myelodysplastic syndromes: ESMO Clinical Practice Guidelines for diagnosis, treatment and follow-up. *Ann Oncol*. doi:10.1016/j.annonc.2020.11.002

Fernandes-Alnemri, T., Wu, J., Yu, J. W., Datta, P., Miller, B., Jankowski, W., . . .
Alnemri, E. S. (2007). The pyroptosome: a supramolecular assembly of ASC
dimers mediating inflammatory cell death via caspase-1 activation. *Cell Death
Differ, 14*(9), 1590-1604. doi:10.1038/sj.cdd.4402194

Gaidt, M. M., Ebert, T. S., Chauhan, D., Schmidt, T., Schmid-Burgk, J. L., Rapino, F., . .
. Hornung, V. (2016). Human Monocytes Engage an Alternative Inflammasome
Pathway. *Immunity, 44*(4), 833-846. doi:10.1016/j.immuni.2016.01.012

Garcia-Martinez, I., Santoro, N., Chen, Y., Hoque, R., Ouyang, X., Caprio, S., . . .
Mehal, W. Z. (2016). Hepatocyte mitochondrial DNA drives nonalcoholic
steatohepatitis by activation of TLR9. *J Clin Invest, 126*(3), 859-864.
doi:10.1172/JCI83885

Giles, B. M., & Boackle, S. A. (2013). Linking complement and anti-dsDNA antibodies in
the pathogenesis of systemic lupus erythematosus. *Immunol Res, 55*(1-3), 10-
21. doi:10.1007/s12026-012-8345-z

Glauser, T. A., Sagatys, E. M., Williamson, J. C., Burton, B. S., Berger, C., Merwin, P., .
. . Bennett, J. M. (2013). Current pathology practices in and barriers to MDS
diagnosis. *Leuk Res, 37*(12), 1656-1661. doi:10.1016/j.leukres.2013.10.007

Grazioli, S., & Pugin, J. (2018). Mitochondrial Damage-Associated Molecular Patterns:
From Inflammatory Signaling to Human Diseases. *Front Immunol, 9*, 832.
doi:10.3389/fimmu.2018.00832

Grishman, E. K., White, P. C., & Savani, R. C. (2012). Toll-like receptors, the NLRP3
inflammasome, and interleukin-1beta in the development and progression of type
1 diabetes. *Pediatr Res, 71*(6), 626-632. doi:10.1038/pr.2012.24

Hajizadeh, S., DeGroot, J., TeKoppele, J. M., Tarkowski, A., & Collins, L. V. (2003). Extracellular mitochondrial DNA and oxidatively damaged DNA in synovial fluid of patients with rheumatoid arthritis. *Arthritis Res Ther, 5*(5), R234-240. doi:10.1186/ar787

Heckl, D., Kowalczyk, M. S., Yudovich, D., Belizaire, R., Puram, R. V., McConkey, M. E., . . . Ebert, B. L. (2014). Generation of mouse models of myeloid malignancy with combinatorial genetic lesions using CRISPR-Cas9 genome editing. *Nat Biotechnol, 32*(9), 941-946. doi:10.1038/nbt.2951

Huang, L. S., Hong, Z., Wu, W., Xiong, S., Zhong, M., Gao, X., . . . Malik, A. B. (2020). mtDNA Activates cGAS Signaling and Suppresses the YAP-Mediated Endothelial Cell Proliferation Program to Promote Inflammatory Injury. *Immunity, 52*(3), 475-486 e475. doi:10.1016/j.immuni.2020.02.002

Jeong, J. J., Gu, X., Nie, J., Sundaravel, S., Liu, H., Kuo, W.-L., . . . Wickrema, A. (2019). Cytokine-Regulated Phosphorylation and Activation of TET2 by JAK2 in Hematopoiesis. *Cancer Discovery, 9*(6), 778-795. doi:10.1158/2159-8290.cd-18-1138

Jitschin, R., Hofmann, A. D., Bruns, H., Giessl, A., Bricks, J., Berger, J., . . . Mougiakakos, D. (2014). Mitochondrial metabolism contributes to oxidative stress and reveals therapeutic targets in chronic lymphocytic leukemia. *Blood, 123*(17), 2663-2672. doi:10.1182/blood-2013-10-532200

Jorgensen, I., Zhang, Y., Krantz, B. A., & Miao, E. A. (2016). Pyroptosis triggers pore-induced intracellular traps (PITs) that capture bacteria and lead to their clearance by efferocytosis. *J Exp Med, 213*(10), 2113-2128. doi:10.1084/jem.20151613

Kang, D., Kim, S. H., & Hamasaki, N. (2007). Mitochondrial transcription factor A
(TFAM): roles in maintenance of mtDNA and cellular functions. *Mitochondrion,
7*(1-2), 39-44. doi:10.1016/j.mito.2006.11.017

Kim, E., Ilagan, J. O., Liang, Y., Daubner, G. M., Lee, S. C., Ramakrishnan, A., . . .
Abdel-Wahab, O. (2015). SRSF2 Mutations Contribute to Myelodysplasia by
Mutant-Specific Effects on Exon Recognition. *Cancer Cell, 27*(5), 617-630.
doi:10.1016/j.ccell.2015.04.006

King, M. P., & Attardi, G. (1989). Human cells lacking mtDNA: repopulation with
exogenous mitochondria by complementation. *Science, 246*(4929), 500-503.
Retrieved from http://www.ncbi.nlm.nih.gov/pubmed/2814477

Ko, M., Bandukwala, H. S., An, J., Lamperti, E. D., Thompson, E. C., Hastie, R., . . .
Rao, A. (2011). Ten-Eleven-Translocation 2 (TET2) negatively regulates
homeostasis and differentiation of hematopoietic stem cells in mice. *Proc Natl
Acad Sci U S A, 108*(35), 14566-14571. doi:10.1073/pnas.1112317108

Lee, H. M., Kim, J. J., Kim, H. J., Shong, M., Ku, B. J., & Jo, E. K. (2013). Upregulated
NLRP3 inflammasome activation in patients with type 2 diabetes. *Diabetes,
62*(1), 194-204. doi:10.2337/db12-0420

Lin, C. W., Manshouri, T., Jilani, I., Neuberg, D., Patel, K., Kantarjian, H., . . . Albitar, M.
(2002). Proliferation and apoptosis in acute and chronic leukemias and
myelodysplastic syndrome. *Leuk Res, 26*(6), 551-559. doi:10.1016/s0145-
2126(01)00170-9

Lindqvist, D., Fernstrom, J., Grudet, C., Ljunggren, L., Traskman-Bendz, L., Ohlsson, L.,
& Westrin, A. (2016). Increased plasma levels of circulating cell-free

mitochondrial DNA in suicide attempters: associations with HPA-axis hyperactivity. *Transl Psychiatry, 6*(12), e971. doi:10.1038/tp.2016.236

Liu, L., Mao, Y., Xu, B., Zhang, X., Fang, C., Ma, Y., . . . Wei, X. (2019). Induction of neutrophil extracellular traps during tissue injury: Involvement of STING and Toll-like receptor 9 pathways. *Cell Prolif*, e12579. doi:10.1111/cpr.12579

Look, A. T. (2005). Molecular Pathogenesis of MDS. *Hematology Am Soc Hematol Educ Program*, 156-160. doi:2005/1/156 [pii] 10.1182/asheducation-2005.1.156

Lotze, M. T., Zeh, H. J., Rubartelli, A., Sparvero, L. J., Amoscato, A. A., Washburn, N. R., . . . Billiar, T. (2007). The grateful dead: damage-associated molecular pattern molecules and reduction/oxidation regulate immunity. *Immunol Rev, 220*, 60-81. doi:10.1111/j.1600-065X.2007.00579.x

Mehta, N. N., Teague, H. L., Swindell, W. R., Baumer, Y., Ward, N. L., Xing, X., . . . Gudjonsson, J. E. (2017). IFN-gamma and TNF-alpha synergism may provide a link between psoriasis and inflammatory atherogenesis. *Sci Rep, 7*(1), 13831. doi:10.1038/s41598-017-14365-1

Mohammad, A. A. (2018). Myelodysplastic syndrome from theoretical review to clinical application view. *Oncol Rev, 12*(2), 397. doi:10.4081/oncol.2018.397

Montalban-Bravo, G., & Garcia-Manero, G. (2018). Myelodysplastic syndromes: 2018 update on diagnosis, risk-stratification and management. *Am J Hematol, 93*(1), 129-147. doi:10.1002/ajh.24930

Nelson, B. P., Gupta, R., Dewald, G. W., Paternoster, S. F., Rosen, S. T., & Peterson, L. C. (2007). Chronic lymphocytic leukemia FISH panel: impact on diagnosis. *Am J Clin Pathol, 128*(2), 323-332. doi:10.1309/21TN2RUWKR827UW2

Nimer, S. D. (2008). Myelodysplastic syndromes. *Blood, 111*(10), 4841-4851.

doi:111/10/4841 [pii]

10.1182/blood-2007-08-078139

Ojeda, D. S., Grasso, D., Urquiza, J., Till, A., Vaccaro, M. I., & Quarleri, J. (2018). Cell

Death Is Counteracted by Mitophagy in HIV-Productively Infected Astrocytes but

Is Promoted by Inflammasome Activation Among Non-productively Infected

Cells. *Front Immunol, 9*, 2633. doi:10.3389/fimmu.2018.02633

Paludan, S. R. (2015). Activation and regulation of DNA-driven immune responses.

Microbiol Mol Biol Rev, 79(2), 225-241. doi:10.1128/MMBR.00061-14

Pellagatti, A., Cazzola, M., Giagounidis, A. A., Malcovati, L., Porta, M. G., Killick, S., . . .

Boultwood, J. (2006). Gene expression profiles of CD34+ cells in myelodysplastic

syndromes: involvement of interferon-stimulated genes and correlation to FAB

subtype and karyotype. *Blood, 108*(1), 337-345. doi:10.1182/blood-2005-12-4769

Perregaux, D., & Gabel, C. A. (1994). Interleukin-1 beta maturation and release in

response to ATP and nigericin. Evidence that potassium depletion mediated by

these agents is a necessary and common feature of their activity. *J Biol Chem,

269*(21), 15195-15203. Retrieved from

http://www.ncbi.nlm.nih.gov/pubmed/8195155

Picou, F., Vignon, C., Debeissat, C., Lachot, S., Kosmider, O., Gallay, N., . . . Herault,

O. (2019). Bone marrow oxidative stress and specific antioxidant signatures in

myelodysplastic syndromes. *Blood Adv, 3*(24), 4271-4279.

doi:10.1182/bloodadvances.2019000677

Pinti, M., Cevenini, E., Nasi, M., De Biasi, S., Salvioli, S., Monti, D., . . . Cossarizza, A. (2014). Circulating mitochondrial DNA increases with age and is a familiar trait: Implications for "inflamm-aging". *Eur J Immunol, 44*(5), 1552-1562. doi:10.1002/eji.201343921

Plesa, A., Chelghoum, Y., Mattei, E., Labussiere, H., Elhamri, M., Cannas, G., . . . Thomas, X. (2013). Mobilization of CD34(+)CD38(-) hematopoietic stem cells after priming in acute myeloid leukemia. *World J Stem Cells, 5*(4), 196-204. doi:10.4252/wjsc.v5.i4.196

Schneider, R. K., Schenone, M., Ferreira, M. V., Kramann, R., Joyce, C. E., Hartigan, C., . . . Ebert, B. L. (2016). Rps14 haploinsufficiency causes a block in erythroid differentiation mediated by S100A8 and S100A9. *Nat Med, 22*(3), 288-297. doi:10.1038/nm.4047

Sekheri, M., El Kebir, D., Edner, N., & Filep, J. G. (2020). 15-Epi-LXA4 and 17-epi-RvD1 restore TLR9-mediated impaired neutrophil phagocytosis and accelerate resolution of lung inflammation. *Proc Natl Acad Sci U S A, 117*(14), 7971-7980. doi:10.1073/pnas.1920193117

Shi, J., Zhao, Y., Wang, K., Shi, X., Wang, Y., Huang, H., . . . Shao, F. (2015). Cleavage of GSDMD by inflammatory caspases determines pyroptotic cell death. *Nature, 526*(7575), 660-665. doi:10.1038/nature15514

Shimada, K., Crother, T. R., Karlin, J., Dagvadorj, J., Chiba, N., Chen, S., . . . Arditi, M. (2012). Oxidized mitochondrial DNA activates the NLRP3 inflammasome during apoptosis. *Immunity, 36*(3), 401-414. doi:10.1016/j.immuni.2012.01.009

Simard, J. C., Cesaro, A., Chapeton-Montes, J., Tardif, M., Antoine, F., Girard, D., & Tessier, P. A. (2013). S100A8 and S100A9 induce cytokine expression and regulate the NLRP3 inflammasome via ROS-dependent activation of NF-kappaB(1.). *PLoS One, 8*(8), e72138. doi:10.1371/journal.pone.0072138

Smeets, M. F., Tan, S. Y., Xu, J. J., Anande, G., Unnikrishnan, A., Chalk, A. M., . . . Walkley, C. R. (2018). Srsf2(P95H) initiates myeloid bias and myelodysplastic/myeloproliferative syndrome from hemopoietic stem cells. *Blood, 132*(6), 608-621. doi:10.1182/blood-2018-04-845602

Steensma, D. P., Bejar, R., Jaiswal, S., Lindsley, R. C., Sekeres, M. A., Hasserjian, R. P., & Ebert, B. L. (2015). Clonal hematopoiesis of indeterminate potential and its distinction from myelodysplastic syndromes. *Blood, 126*(1), 9-16. doi:10.1182/blood-2015-03-631747

Tanaka, T. N., & Bejar, R. (2019). MDS overlap disorders and diagnostic boundaries. *Blood, 133*(10), 1086-1095. doi:10.1182/blood-2018-10-844670

Tarrago-Litvak, L., Viratelle, O., Darriet, D., Dalibart, R., Graves, P. V., & Litvak, S. (1978). The inhibition of mitochondrial DNA polymerase gamma from animal cells by intercalating drugs. *Nucleic Acids Res, 5*(6), 2197-2210. doi:10.1093/nar/5.6.2197

Valent, P. (2019). ICUS, IDUS, CHIP and CCUS: Diagnostic Criteria, Separation from MDS and Clinical Implications. *Pathobiology, 86*(1), 30-38. doi:10.1159/000489042

Valent, P., Orazi, A., Steensma, D. P., Ebert, B. L., Haase, D., Malcovati, L., . . . Bennett, J. M. (2017). Proposed minimal diagnostic criteria for myelodysplastic

syndromes (MDS) and potential pre-MDS conditions. *Oncotarget, 8*(43), 73483-73500. doi:10.18632/oncotarget.19008

Vogl, T., Tenbrock, K., Ludwig, S., Leukert, N., Ehrhardt, C., van Zoelen, M. A., . . . Roth, J. (2007). Mrp8 and Mrp14 are endogenous activators of Toll-like receptor 4, promoting lethal, endotoxin-induced shock. *Nat Med, 13*(9), 1042-1049. doi:10.1038/nm1638

Vollmer, J., Weeratna, R. D., Jurk, M., Samulowitz, U., McCluskie, M. J., Payette, P., ... Krieg, A. M. (2004). Oligodeoxynucleotides lacking CpG dinucleotides mediate Toll-like receptor 9 dependent T helper type 2 biased immune stimulation. *Immunology, 113*(2), 212-223. doi:10.1111/j.1365-2567.2004.01962.x

Ward, G. A., McGraw, K. L., Abbas-Aghababazadeh, F., Meyer, B. S., McLemore, A. F., Vincelette, N. D., . . . List, A. F. (2021). Oxidized mitochondrial DNA released after inflammasome activation is a disease biomarker for myelodysplastic syndromes. *Blood Adv, 5*(8), 2216-2228. doi:10.1182/bloodadvances.2020003475

Yu, J., Nagasu, H., Murakami, T., Hoang, H., Broderick, L., Hoffman, H. M., & Horng, T. (2014). Inflammasome activation leads to Caspase-1-dependent mitochondrial damage and block of mitophagy. *Proc Natl Acad Sci U S A, 111*(43), 15514-15519. doi:10.1073/pnas.1414859111

Zambetti, N. A., Ping, Z., Chen, S., Kenswil, K. J., Mylona, M. A., Sanders, M. A., . . . Raaijmakers, M. H. (2016). Mesenchymal Inflammation Drives Genotoxic Stress in Hematopoietic Stem Cells and Predicts Disease Evolution in Human Pre-leukemia. *Cell Stem Cell, 19*(5), 613-627. doi:10.1016/j.stem.2016.08.021

Zhang, C., Hao, X., Chang, J., Geng, Z., & Wang, Z. (2019). Mn-TAT PTD-Ngb
attenuates oxidative injury by an enhanced ROS scavenging ability and the
regulation of redox signaling pathway. *Sci Rep, 9*(1), 20103. doi:10.1038/s41598-
019-56595-5

Zhang, Q., Raoof, M., Chen, Y., Sumi, Y., Sursal, T., Junger, W., . . . Hauser, C. J.
(2010). Circulating mitochondrial DAMPs cause inflammatory responses to injury.
Nature, 464(7285), 104-107. doi:10.1038/nature08780

Zhong, Z., Liang, S., Sanchez-Lopez, E., He, F., Shalapour, S., Lin, X.-j., . . . Karin, M.
(2018). New mitochondrial DNA synthesis enables NLRP3 inflammasome
activation. *Nature, 560*(7717), 198-203. doi:10.1038/s41586-018-0372-z

Zhong, Z., Liang, S., Sanchez-Lopez, E., He, F., Shalapour, S., Lin, X. J., . . . Karin, M.
(2018). New mitochondrial DNA synthesis enables NLRP3 inflammasome
activation. *Nature, 560*(7717), 198-203. doi:10.1038/s41586-018-0372-z

Appendix A: Copyright Permission

Chapter 3 of this research was originally published in Blood Advances.

Grace A. Ward, Kathy L. McGraw, Farnoosh Abbas-Aghababazadeh, Benjamin S. Meyer, Amy F. McLemore, Nicole D. Vincelette, Nghi B. Lam, Amy L. Aldrich, Najla H. Al Ali, Eric Padron, Javier Pinilla-Ibarz, Erico Masala, Valeria Santini, Olivier Kosmider, Michaela Fontenay, Pierre Fenaux, Joseph Johnson, Brooke L. Fridley, Alan F. List; Oxidized mitochondrial DNA released after inflammasome activation is a disease biomarker for myelodysplastic syndromes. Blood Adv 2021; 5 (8): 2216–2228. doi: https://doi.org/10.1182/bloodadvances.2020003475

The visual abstracts were created using BioRender.

Rights and Permissions

Material published in *Blood Advances* is covered by copyright. All rights reserved. No part of the publication may be reproduced (see exception below), stored in a retrieval system, translated, or transmitted in any form or by any means now or hereafter known, electronic or mechanical, without permission in writing from the publisher, The American Society of Hematology (ASH).

The copyright owner consents that copies of articles may be made for personal or internal use, or for the personal or internal use of specific clients, for those registered with the Copyright Clearance Center Inc. This consent is given on the condition that the copier pay the stated per-copy fees through the Copyright Clearance Center, Inc., for copying beyond that permitted by Sections 107 and 108 of the US Copyright Law (Fair Use). This consent does not extend to other kinds of copying, such as copying for general distribution, for advertising or for promotional purposes, for creating new collective works, or for resale. For those kinds of purposes, permission must be sought from the publisher using the following guidelines. If you have any questions regarding our rights and permissions policies please contact *Blood Advances* Permissions.

Republication Requests

Authors reusing their own material
Authors have permission to share their article in the following ways after it has been published in *Blood Advances*:

- With students or colleagues for their personal use in presentations and other educational endeavors.
- On the authors' institutional repositories.
- On the authors' personal websites.
- As a link to the article on the journal's website anywhere at any time.
- Publicly on non-commercial platforms.

The author must include the following citation when citing material that appeared in *Blood Advances*:

"This research was originally published in *Blood Advances*. Author(s). Title. *Blood Adv*. Year;Vol:pp-pp. © the American Society of Hematology."

Specific examples of acceptable author reuse and sharing include:

- Reprinting the article in print collections of the author's own writing.
- Reusing figures and tables created by the author in future works.
- Reproducing the article for use in courses the author is teaching. If the author is employed by an academic institution, that institution may also reproduce the article for course teaching.
- Distributing photocopies of the article to colleagues, but only for non-commercial purposes.
- Posting a copy of the article on the author's personal website, departmental website, and/or the university intranet. A hyperlink to the article on the *Blood* website must be included.
- Presenting the work orally in its entirety.
- Using the article in theses and/or dissertation.

Authors reusing their own material in the above ways must include appropriate attribution and do not need to contact *Blood Advances* for permission.

For all other uses, the author must request permission from ASH by visiting the Copyright Clearance Center.